AN ABSTRACT OF THE THESIS OF

Richard P. Jenks for the degree of Master of Science

in Nuclear Engineering presented on December 15, 1982

Title: Direct Shear Testing of UO_2 Sphere-Pac Nuclear Reactor Fuel

Abstract approved: Redacted for Privacy

K. L. Peddicord

The design, development, and utilization of a direct shear test apparatus is presented in this thesis. The effectiveness of the device for determining the friction angle stress state parameter is studied. Two materials, alumina and uranium dioxide, were tested.

Alumina microspheres were employed in the initial experiments to simulate the behavior of the sphere-pac material. The results of the initial tests justified the use of the mechanism to study the shear strength of uranium dioxide microspheres.

Experimental results for the alumina were compared with independent test results and found to be comparable for a similar method of data reduction. However, a preferred method of data reduction is presented which shows a more conservative friction angle value for extrapolation purposes.

The experimental results for uranium dioxide are presented and confirmed the adaptability of the direct shear device for friction angle determination.

Direct Shear Testing of UO_2 Sphere-Pac Nuclear Reactor Fuel

by

Richard P. Jenks

A Thesis

submitted to

Oregon State University

in partial fulfillment of
the requirements for the
degree of
Master of Science

Completed December 15, 1982

Commencement June 1983

APPROVED:

Redacted for Privacy

Professor of Nuclear Engineering in charge of major

Redacted for Privacy

Head of Department of Nuclear Engineering

Redacted for Privacy

Dean of Graduate School

Date thesis is presented December 15, 1982

Typed by Richard P. Jenks for Richard P. Jenks

Acknowledgments

Special thanks go to my major professor, Dr. K. L. Peddicord, for his encouragement and recommendations. To my committee members, Dr. S. E. Binney, Dr. J. Arthur, and Dr. T. K. Plant, I also express my earnest gratitude.

In addition, my work could not have been completed without the help of Dr. T. Kennedy and Dr. T. George, who provided a wealth of information in solid mechanics. Also, a debt is owed to all my fellow graduate students, too many to mention, who bestowed their knowledge upon me freely throughout the course of this work. Especially to Dr. B. Nassersharif do I extend this acknowledgment for his friendly support, his expertise and direction, and his sense of humor.

Most importantly, I thank you, Kathy, for your love and understanding this past year. With such a steadfast partner my work and my life are much more enjoyable.

TABLE OF CONTENTS

Section | Page

LIST OF FIGURES

LIST OF TABLES

Direct Shear Testing of UO_2 Sphere-Pac Nuclear Reactor Fuel

1. INTRODUCTION

1.1 Background

Since the advent of nuclear reactors for power generation, engineers have been confronted with a myriad of material behavior issues which needed to be analyzed and explained in order to effectively predict and understand the performance of nuclear fuel. The goal has been economical production of energy as well as safe containment of radioactivity.

Such behavior as fission-product migration, fuel-cladding mechanical interaction (FCMI), and fuel swelling have been actively described and investigated over the past several years (1,2,3,4,5,6). This investigation has considerably expanded our knowledge and understanding of in-core fuel performance.

The subject of thermal-mechanical properties of nuclear fuels has become increasingly important in recent years with the imposition of stricter safeguarding measures. These measures, in the form of government policy, have attempted to reduce the threat of horizontal nuclear proliferation (7). With higher burnup fuel,

it was reasoned that fewer reloads would be necessary over the life of a reactor, and hence, there would be less opportunity for diversion in the "back end" of the fuel cycle.

Furthermore, fuel performance affects the overall economy of power production. From the size of the reactor needed to the amount of the natural resource mined, economic considerations provide additional motivation for understanding fuel performance.

All of these factors, plus uncertainty over fuel cycle costs, and the incorporation of fast breeder reactors into the power production portfolio, have created considerable interest in the high ("extended") burnup fuels.

The present generation of standard fuels, uranium dioxide and uranium carbide, are subject to various thermal and mechanical behavior problems. In attempting to push these fuels to their physical limits for higher burnup, alternative fuels may be needed to circumvent the current thermal and mechanical difficulties. This has provided the motivation for the investigation of sphere-pac fuel as a possible candidate for extended burnup applications.

1.2 Motivation for the Experiment

Recent computer models of the solid mechanical behavior of sphere-pac fuel incorporate the friction angle as an important input parameter (8). This parameter is a measure of the relationship between shearing force and compressive normal force for a bed of

particles.

Several approaches are available to obtain this quantity. Among these are the "triaxial" and the "direct shear" tests (9). The triaxial test is much more difficult to perform and interpret than the direct shear test. In addition, the triaxial test apparatus is relatively complicated and not well suited for radioactive particulates.

The friction angle can also be approximated by the angle of repose, another particle parameter. However, the method for this determination is not well defined and is subject to large experimental error. Therefore, to obtain a usable value, the current experiment was performed using a simple, inexpensive mechanism. For this experiment the direct shear test was chosen, as it was easy to perform and the results could be readily interpreted. For comparison, the angle of repose was also determined.

Research at Oregon State University has focused on the behavior analysis of sphere-pac fuel, and various studies have been completed which test and model the thermal and mechanical properties of sphere-pac particle beds.

The theory behind the direct shear experiment is presented in the following section, and the mechanism for performing the test described in section 3. The test procedure is given in section 4, followed by the results for tests of two different types of material in section 5, and conclusions in section 6. The appendices contain

an explanation of the statistical significance of the experiment and lists of experimental procedures.

2. THEORY

2.1 Introduction

Because sphere-pac fuel is granular in nature, the theory behind the experiment necessarily comes from the study of mechanics of particulate media, that is, the study of the interaction of particles (10). While it is not our objective to provide comprehensive coverage to this theory, we present the important definitions for the variables measured by the direct shear test.

2.2 Direct Shear Test

The direct shear test is commonly employed in the testing of particle samples to measure the strength and compressibility of a particle bed. The test is performed using a direct shear mechanism (11).

Figure 2.2.1 shows a sketch of an apparatus employed in soil science experiments to determine shearing stress, τ, as a function of normal stress, σ, where,

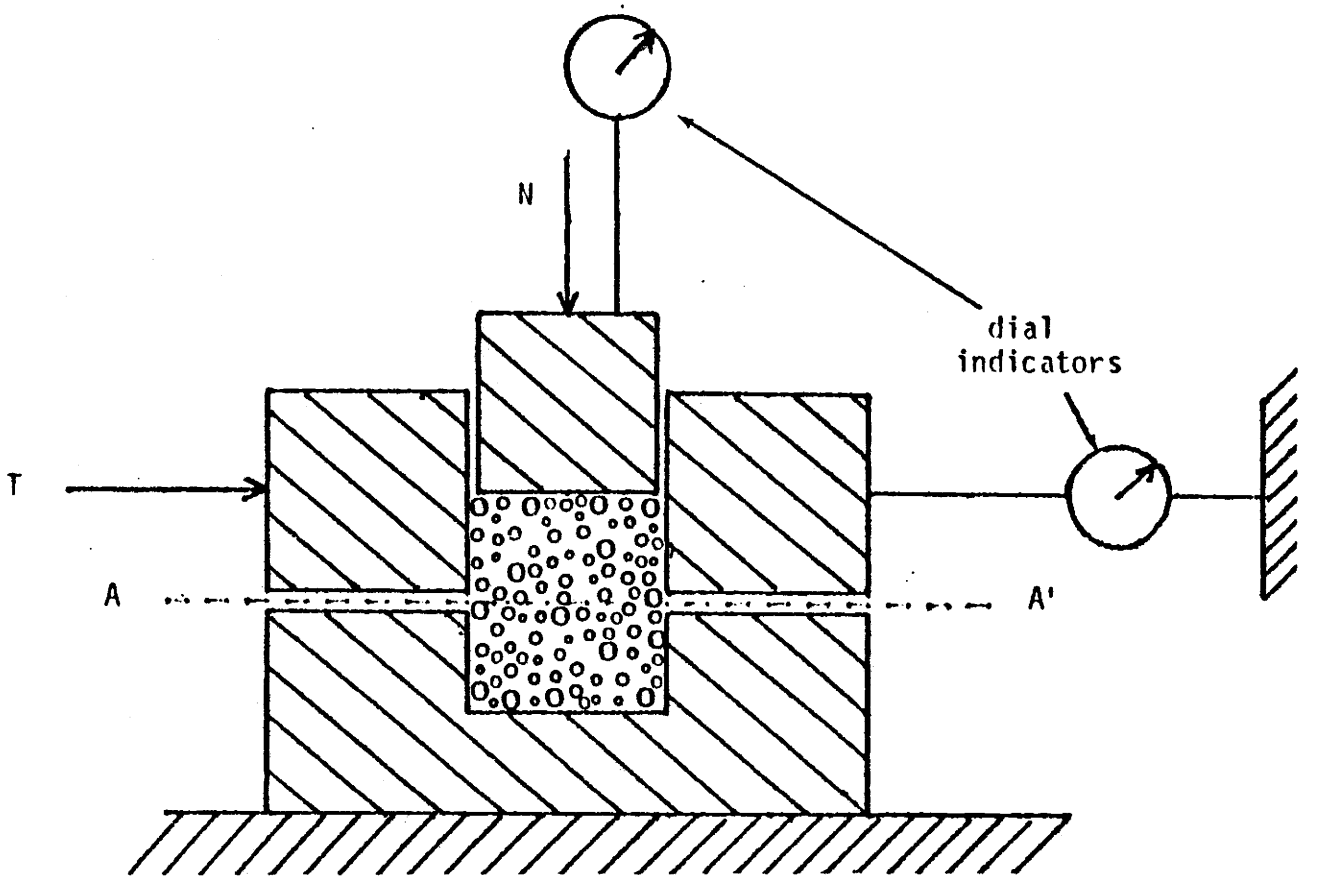

Figure 2.2.1 Sketch of Soil Science Test Device

$$\tau = \frac{T}{A} \qquad (2.2.1)$$

and

$$\sigma = \frac{N}{A} \qquad (2.2.2)$$

The variables T and N are the shearing force and the normal force respectively, and A is the nominal area of the shear plane.

The test is performed in a rigid box composed of two sections. The top section of the box is free to move, while the bottom section is fixed. A sample of the material is loaded into the device as indicated. The normal force, N, is applied to the top of the box and compresses the sample. When the tangential force, T, is applied to the top section, there is an accompanying displacement along the surface A-A'.

For a specified force, N, the shear test is performed by gradually increasing T until the material "yields." The material "yields" when there is no further change in resistance to displacement of the top section. In this context, a "failure" of the material under yielding shear stress has occurred. Dial indicators are normally used to measure displacement, both in the horizontal as well as the vertical direction.

Because of the confining nature of the mechanism, failure of the material is allowed to occur only along the surface A-A'. An example of the type of behavior that can be expected is shown in

Figure 2.2.2. The curve for shearing stress versus horizontal displacement, depicted here, does not display a sharp peak, since, after reaching the maximum shearing resistance, the shearing stress remains relatively constant with increasing displacement.

This relatively constant shearing stress is referred to as the "ultimate strength" or "ultimate resistance." It depends on the type of material and the size and shape of the particles. However, it is relatively independent of the initial void ratio or density of dry particulate material. The void ratio is defined as the ratio of the volume of voids to the volume of solids.

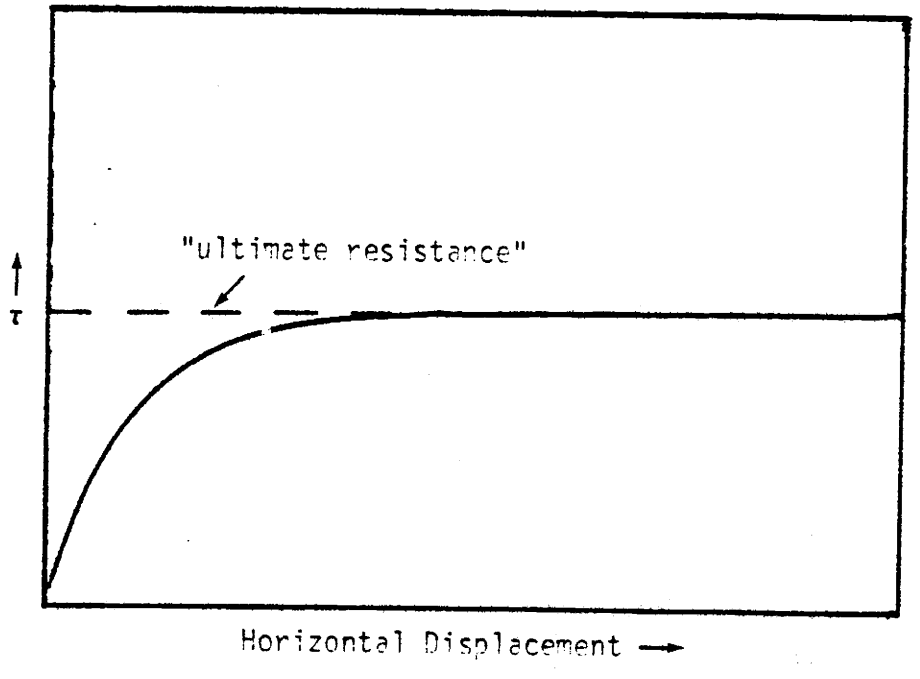

Figure 2.2.2 Shear Stress versus Horizontal Displacement

2.3 Friction Angle

For cohesionless materials, an example of the "ultimate strength envelope" which should be obtained is illustrated in Figure 2.3.1. The ultimate strength envelope is composed of the loci of points obtained by taking repeated tests of τ versus σ for the same material, but with different normal loadings, N. As shown, the envelope is approximately a straight line that passes through the origin of the coordinates.

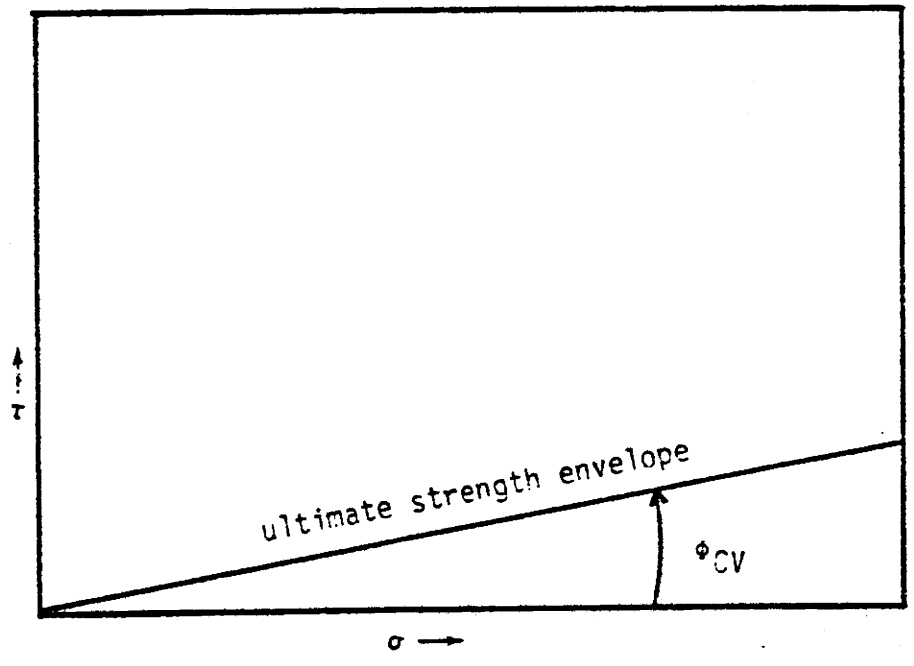

Figure 2.3.1 Ultimate Strength Envelope

The angle that the ultimate strength envelope makes with the normal stress axis is called the ultimate friction angle, Φ_{CV}, and $\tan(\Phi_{CV})$ is the slope of the curve. The ultimate strength envelope can therefore be described by

$$\tau_{failure} = \sigma_{failure} \times \tan(\Phi_{CV}) \qquad (2.3.1)$$

where $\tau_{failure}$ and $\sigma_{failure}$ are the limiting shearing and normal stresses, respectively, on the failure plane at failure. Equation 2.3.1 is sometimes referred to as the "Mohr-Coulomb failure criterion."

The ultimate strength envelope can be seen to represent a limiting condition for combined states of stress in the τ, σ plane for which failure will occur. Points falling above the envelope represent failure states. Points on or below the envelope represent states of stress equilibrium. In this context, the ultimate strength envelope is an indication of the combined states of stress in the τ, σ plane at "limiting equilibrium."

2.4 Peak Friction Angle and Dilatancy

In the previous section, the ultimate strength envelope was described for particles which are initially loose. The same envelope applies for particles that are initially densely packed. However, for the initially dense material, there is another friction angle of concern, the so-called "peak friction angle." Figure 2.4.1 shows an example of a typical plot of shearing stress versus horizontal displacement for an initially dense particle bed. Also shown, for comparison, is τ versus displacement for the initially loose material.

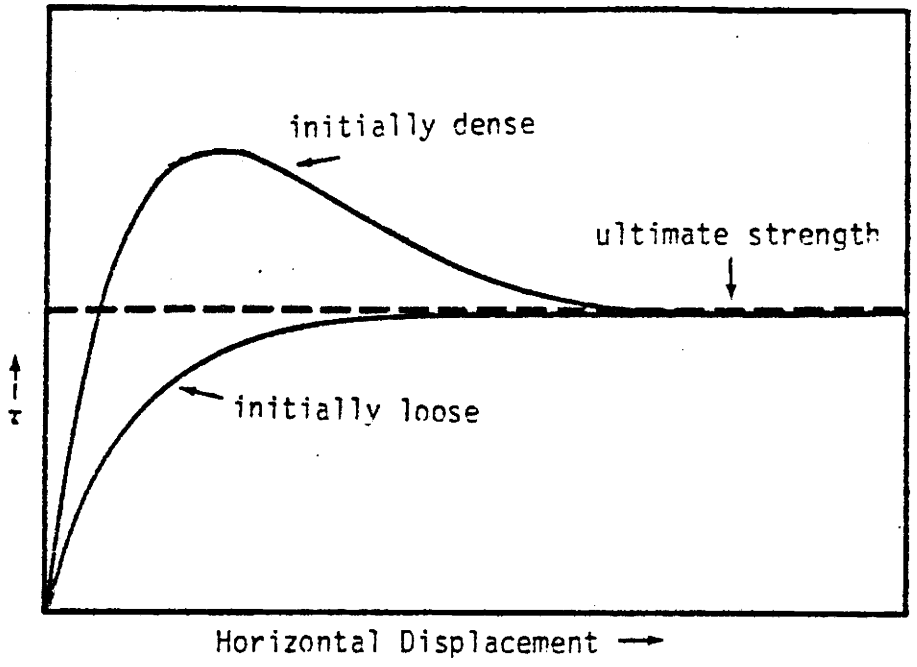

Figure 2.4.1 τ versus Displacement for Dense Bed

The initially dense particle bed exhibits a different behavior under shear than the initially loose particle bed. For the dense material, the large degree of particle interlocking is seen to cause a peak in the curve, after which less shearing stress is required to cause displacement. Ultimately, the initially dense material curve approaches the initially loose material curve.

Figure 2.4.2 displays the relative volume change during displacement for dense and loose particle beds, respectively. The dense material shows an immediate increase in volume with displacement, while the loose material exhibits an initial decrease

in volume followed by a subsequent increase.

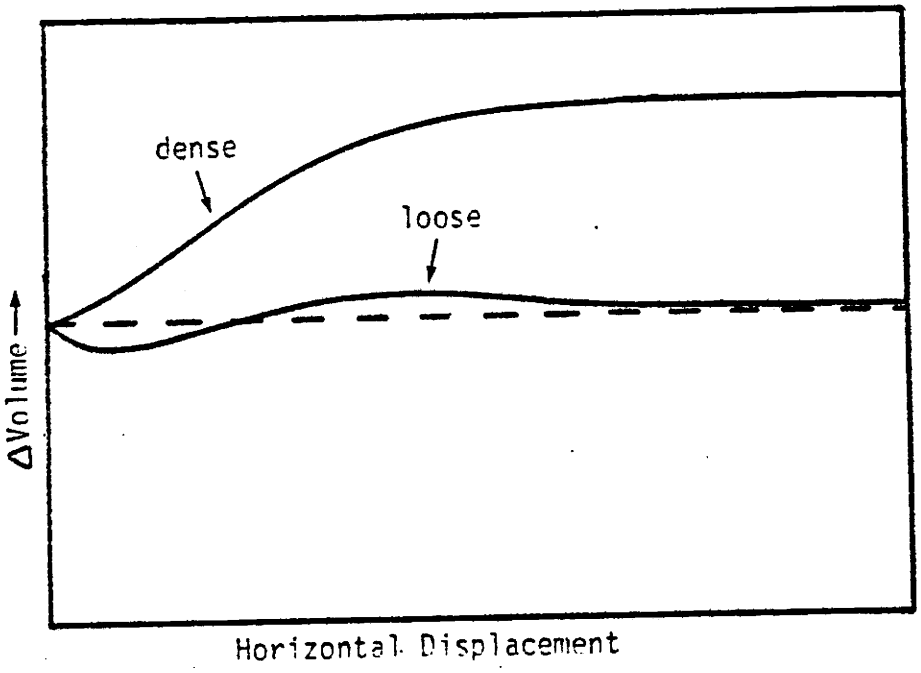

Figure 2.4.2 Relative Volume Change During Displacement of Sample

Both materials approach the same void ratio, called the critical void ratio, with large displacement. This is shown graphically in Figure 2.4.3. The critical void ratio, e_{CV}, is indicated as a horizontal line, since a sample which was initially at the critical void ratio would have almost no tendency to change volume during shear. Hence, the constant volume (CV) subscript.

The increase in volume of a sample during shear is termed "dilatancy" (12). The maximum rate of dilatation occurs in the neighborhood of the peak stress. After large displacements, both the loose and the dense materials approach the same ultimate strength and critical void ratio. As a consequence of this property

change, the material will exhibit no further dilatation and is said to have reached a state of minimum intergranular density. Some authors refer to this as the "critical state of the material" (13).

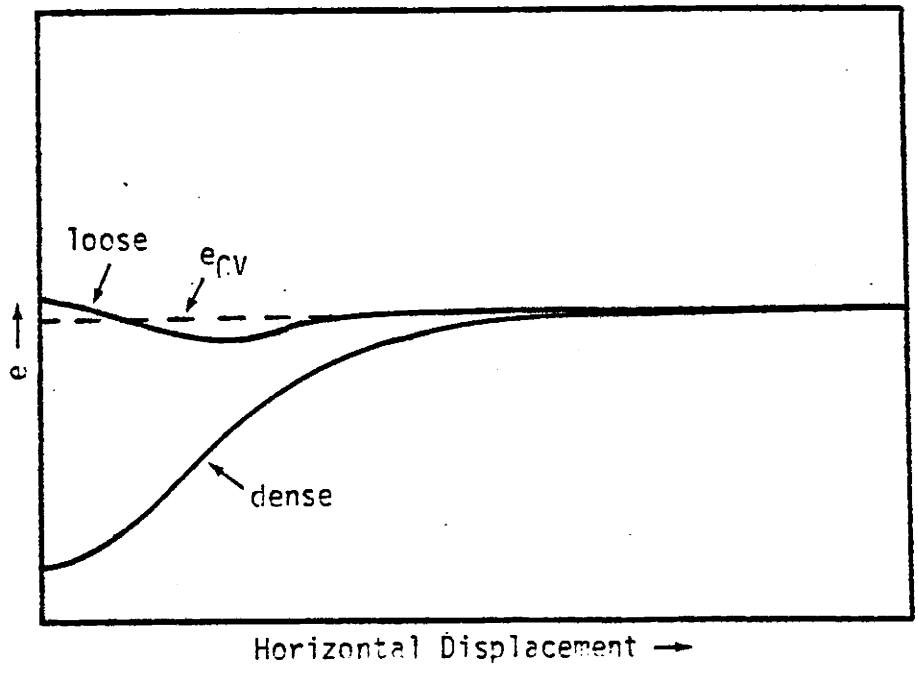

Figure 2.4.3 Critical Void Ratio versus Displacement

With equations 2.2.1, 2.2.2, and 2.3.1, the ultimate friction angle can be determined. The direct shear test allows the determination of the ultimate strength for a given normal stress. From this, the ultimate strength envelope can be developed for the sample of interest.

Before attempting to construct an apparatus for the sphere-pac direct shear research, an experiment involving direct shear testing of soil samples was reviewed (14). A schematic of the soil science test apparatus is shown in Figure 2.4.4.

In this test, certain ideal conditions are imposed on the soil sample. First of all, the failure plane is constrained to occur at the location of the shear box interface. In addition, the two forces acting on the shear box act in two perpendicular directions on the plane. These two forces when divided by the nominal area of

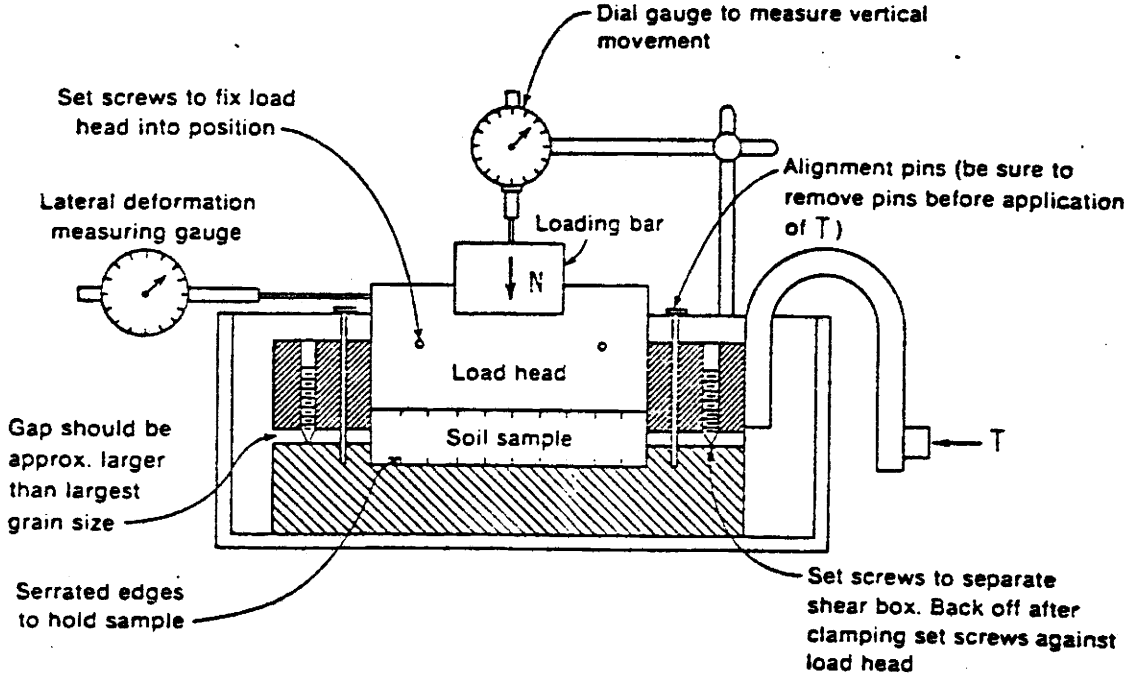

Figure 2.4.4 Schematic of Soil Science Test Apparatus

the chamber constitute the shearing stress and the normal stress defined in Section 2.2.

The criterion imposed on the stress-strain behavior is, again, the Mohr-Coulomb equation, but now we must incorporate a new parameter to account for the "cohesive" nature of soils. Restating

the Mohr-Coulomb criterion in this form gives

$$\tau = C + \sigma_N \tan(\Phi_{CV}) \qquad (2.4.1)$$

where τ, σ, and Φ_{CV} are as previously defined, and C is a parameter known as the "cohesion." Cohesion is a measure of the resistance of a material to deformation in the absence of containment.

The size, shape, composition, and moisture content of particles influence the amount of cohesion they have. For the dry, relatively uniform material of the size and shape employed in this experiment, the parameter C is relatively small, and the material is essentially cohesionless.

In the soils experiment there are two unknown quantities in Equation 2.4.1. These are C and Φ_{CV}. Hence, two measurements of τ and σ are required. This can be accomplished either by solving two simultaneous equations or by plotting the data and finding the slope and intercept of the subsequent curve. For "cohesionless" materials, on the other hand, only one data point is required, as the curve should intercept the τ axis at the origin.

The direct shear device used for the experimental determination of the ultimate friction angle will be described in Section 3.

2.5 Angle of Repose

The slope of a pile of particulate material which has been poured freely onto a surface is termed the "angle of repose" (see Figure 2.5.1). This angle represents a limiting condition for the material. As it is poured onto the pile, the pile grows in such a manner that the slope remains the same.

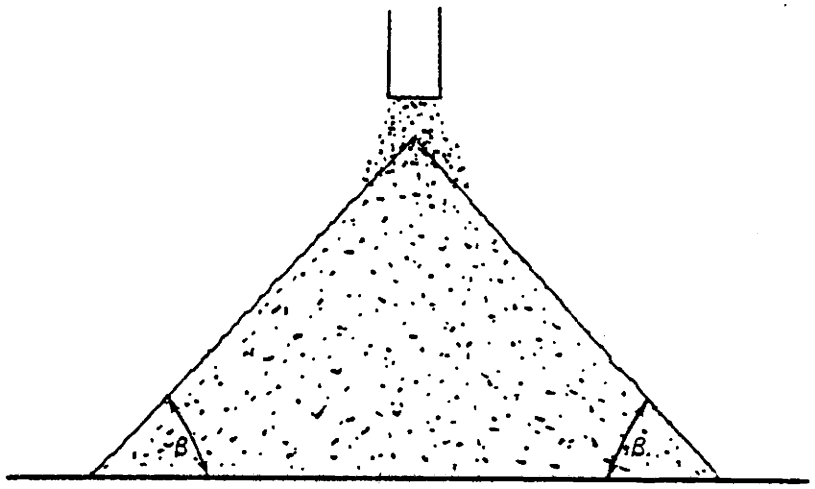

Figure 2.5.1 Angle of Repose for Particulate Material

Since the particulate material will slide when the slope of the pile becomes greater than β, we say that β is a measure of the limiting equilibrium of the material. This is similar to the friction angle, Φ_{CV}, which is also a measure of the stress equilibrium of a material. Hence, the angle of repose is often used

as an approximation for the friction angle.

If θ is defined as the angle of inclination of the container with respect to a level surface and α is defined as the angle of inclination of the material with respect to the container (see Figure 2.5.2), the angle of repose, β, can be determined by

$$\beta = \theta - \alpha \qquad (2.5.1)$$

In terms of the actual measurements this becomes

$$\beta = \arcsin\left[\frac{H}{L}\right] - \arctan\left[\frac{H'}{L'}\right] \qquad (2.5.2)$$

where H, L, H', and L' are as indicated in Figure 2.5.2c.

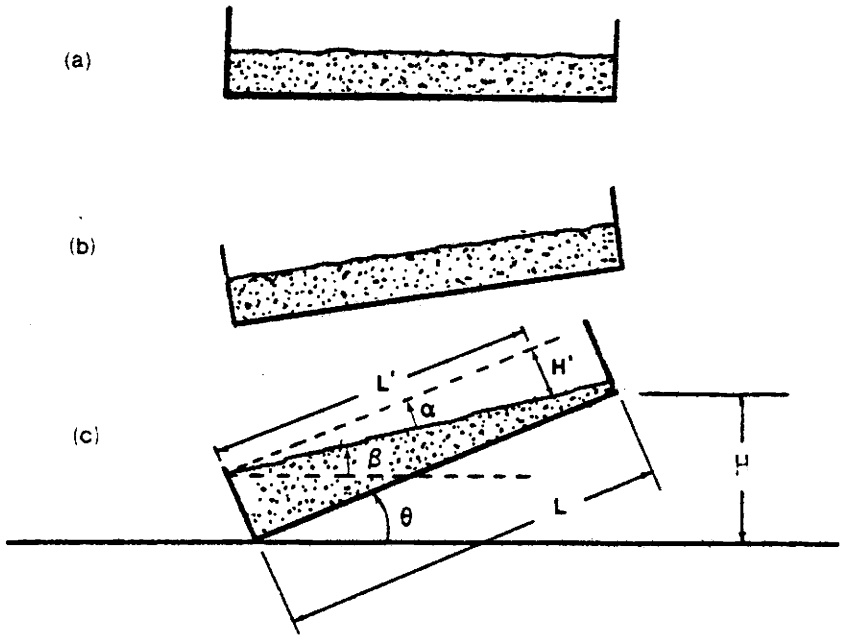

Figure 2.5.2 Repose Angle

3. MATERIALS AND EQUIPMENT

3.1 Materials to be Tested

The two materials examined with the direct shear test were alumina and uranium dioxide. Table 3.1.1 gives some useful information concerning these compounds. Although their properties differ significantly, they also have some similarities.

Table 3.1.1

Physical Properties of Alumina and UO_2

	Alumina	Uranium Dioxide
Formula	Al_2O_3	UO_2
Mol. Wt.	101.96	270.03
Density (g/cm^3)	3.5-3.9	10.96
Melting Point (^oC)	2015 $\pm$ 15	2878 $\pm$ 20
Color	White	Brown-Black

Both alumina and UO_2 are ceramic materials. Both are bi-elemental compounds of oxygen. And both can be produced in microspherical shape.

Alumina was used for the initial testing, because it could be handled without considering decontamination. Thus, the initial stages of design could be accomplished outside the confines of a hood, greatly reducing the effort required for each data point.

Most importantly, however, the radiological dose was minimized by using alumina as a "model" for uranium dioxide. This is consistent with the ALARA goals set forth by the Nuclear Regulatory Commission.

Another reason for using alumina was that it provided a second set of data which could be used for assessing computational models. In addition, previous testing of fuel clad mechanical interaction (FCMI) had similarly employed alumina, and, therefore, information concerning normal stress values was already available (15). This information, plus values of the friction angle obtained by angle of repose methods, was used for comparison purposes to help determine the feasibility of the device for testing UO_2.

The UO_2 microspheres employed in the tests were obtained from Exxon Nuclear Corporation in the three sizes shown in Table 3.1.2. Also shown in the table, are the volume fractions of the materials when they are incorporated into typical sphere-pac fuel.

Table 3.1.2

UO_2 Sphere-pac Fuel Physical Characteristics

	Coarse	Medium	Fine
Size Range (cm)	.1190-.1410	.028-.032	.0025-.0045
Average size (cm)	.13	.03	.0035
Porosity (%)	1.4	0.7	1.4
Packing Factor (%)	50.04	35.55	39.38
Smear Density of the Packed Bed (%)		86.59	
Fill Gas		Helium	

These volume fractions were used as a guide to determine the make-up of the test material.

A cross section of the "ideal" packing for the ternary mixture employed in this experiment is shown in Figure 3.1.1.

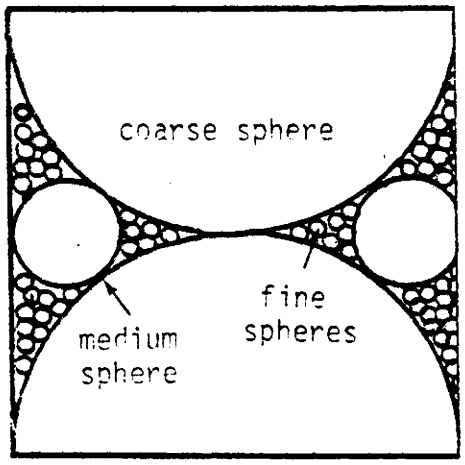

Figure 3.1.1 Cross Section of Ternary UO_2 Ideal Packing

The type of material used in the test greatly influenced the design of the testing apparatus and the procedures followed for performing the test, as will be shown in the following sections.

3.2 Equipment Design Background

Testing with the direct shear mechanism has been performed for many years in the field of soils science. This was done primarily

to measure cohesion and friction angles before the advent of the triaxial test apparatus. The sketch in Figure 2.1.1 showed the basic components of a direct shear mechanism.

The mechanism actually employed by soils engineers is somewhat more complicated, but incorporates all of the basic constituents previously mentioned:

a. Shear box (two sections)
b. Sample chamber
c. Normal loading mechanism
d. Tangential loading mechanism
e. Normal and tangential load measurement device
f. Horizontal and vertical displacement indicators

Figure 3.2.1 shows a picture of an actual direct shear test apparatus. The device is relatively large, because of the heavy stand required to support the machine and the loading mechanism. It is also very heavy since it is constructed of iron and brass.

The device used in the sphere-pac project to test shearing properties was based on the soil science direct shear testing device. However, some modifications had to be made in order to conform to the scope and limitations imposed by the project and materials involved.

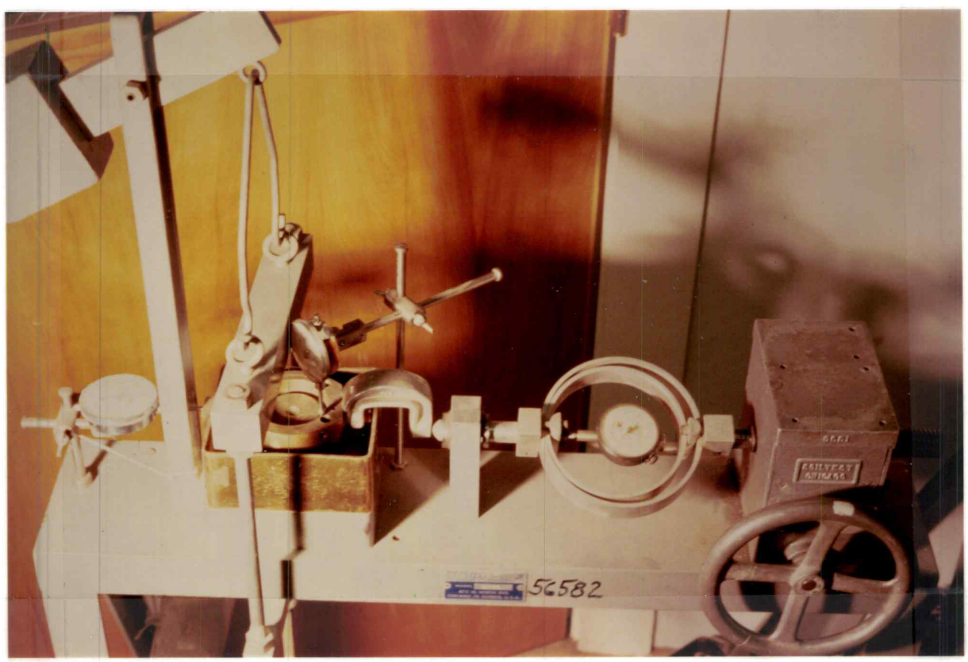

Figure 3.2.1 Actual Soils Science Direct Shear Test Apparatus

3.3 Design Constraints

While the soils science design would have been suitable for testing alumina microspheres, it was necessary to develop a different design which could also be used for testing uranium dioxide.

The device had to have several special characteristics. Some of these characteristics were:

a. Small size
b. Light weight
c. Portability
d. Ease of decontamination
e. Ability to "contain" fine particles of UO_2

The first characteristic, small size, was important, since the mechanism would eventually have to be used inside a hood, which necessarily imposed certain dimensional restrictions. Thus, before any parts or materials were ordered, a measurement was taken of the hood to be used, and the limiting dimensions were ascertained.

Since the device would be handled frequently and moved from one location within the lab or hood to another during different phases of the decontamination procedure, it was important that the entire assembly be relatively light to facilitate easy handling. However,

it had to be sufficiently strong and durable so that stresses imposed during the test would not significantly effect the structure of the device.

The first two characteristics actually imply the third, that of portability. This is important, since other experiments were ongoing during the period of time that the direct shear testing project was in progress. This meant frequent moving of the apparatus to allow other lab users access to the hood or other areas used by the direct shear mechanism.

Decontamination was an especially important consideration in the design development stage. Since a radioactive substance was to be tested after initial feasibility studies with alumina, it was necessary to design the device so as to facilitate easy clean-up.

Since fine particles of UO_2 were targeted for expermentation, the equipment had to be designed to contain this "dust-like" material. By "contain", we mean that the material had to be restricted from entering the environment outside the bounds of a laboratory hood.

These five characteristics, size, weight, portability, ease of decontamination, and containment ability, were the initial guides to constructing a device for this project.

3.4 Design Steps

Unlike the soil science machine, which was large and heavy, the sphere-pac direct shear device had to be small and portable. As a first step in the design stage a sketch of the "ideal machine" was made. Figure 3.4.1 shows how the basic soils design was modified to produce a machine with all the components above a certain level and contained on a single base plate.

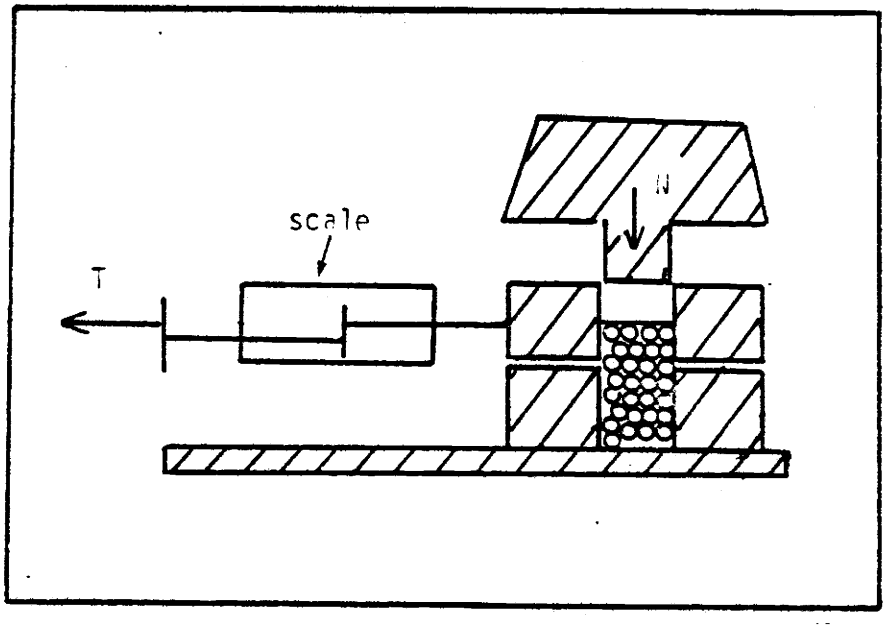

Figure 3.4.1 "Ideal Device" for Direct Shear Test

This diagramatic representation of the device shows the components necessary to apply the test. A base shear box is shown, upon which another shear box is free to slide. A chamber is included in the shear boxes to allow a place for the sample. And a piston with some weight attached is employed to provide a normal

force to the particle sample. Attached to the top shear box is a scale to measure the horizontally applied force, and on the opposite side is a dial indicator to measure the horizontal displacement.

No dial indicator is shown to measure the vertical displacement. It would require additional structural material and containment modifications which were deemed excessive considering the fact that dilatancy was not a parameter of interest for this stage of the project.

From the diagramatic representation, an initial design sketch was made which incorporated components and materials easily obtainable at modest cost. Figure 3.4.2 shows this initial sketch.

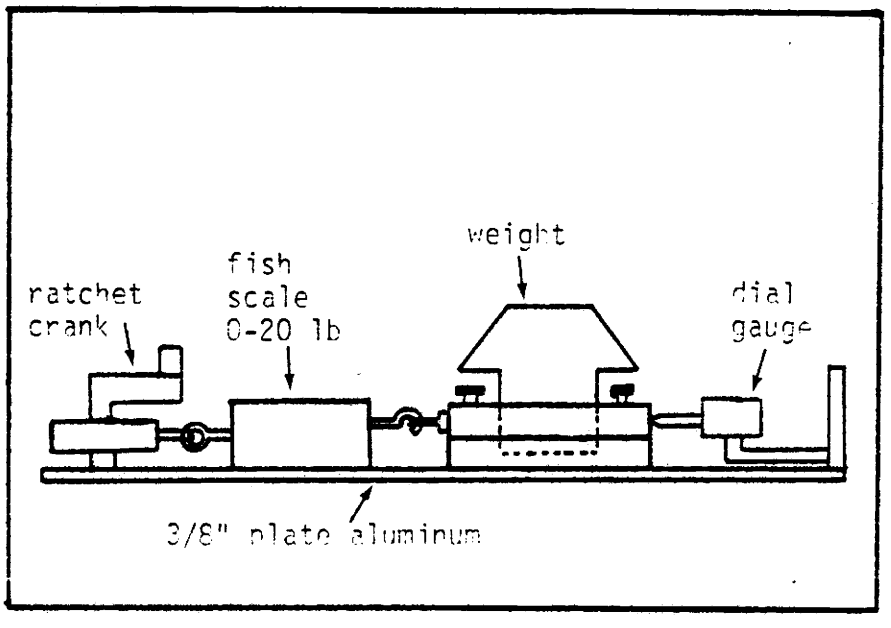

Figure 3.4.2 Initial Design Sketch of UO_2 Device

The dimensions are not shown, since only the limiting values

obtained from measuring the laboratory hood were known. The components that could be readily procured were obtained, assembled loosely on the base plate, and made to conform to the limiting dimensions. This method of design was necessary to assure modest cost not obtainable if all the components and materials are made to conform to a preconceived design with fixed dimensions.

The final product was only slightly different from the initial design sketch, the difference due mainly to cost and the availability of parts.

3.5 The Device Used for Testing Alumina

Figure 3.5.1 shows the device actually constructed and used for the direct shear testing of Alumina microspheres. The ratchet crank incorporated in the initial sketch was replaced with a less costly modified caulking gun assembly. Modified, in this instance, means that the long metal part that holds the caulking tube was removed. A regular Viking scale was employed to measure the shearing force. A containment box was made out of sheet metal to act as a pan to catch the spheres after the test was completed.

The shear box had to be fabricated at a machine shop out of block aluminum and, hence, constituted the greatest cost. Especially important in the fabrication was the tolerance between the piston and the cylinder. Since no sphere should be allowed to enter the space between the piston and the cylinder during the test,

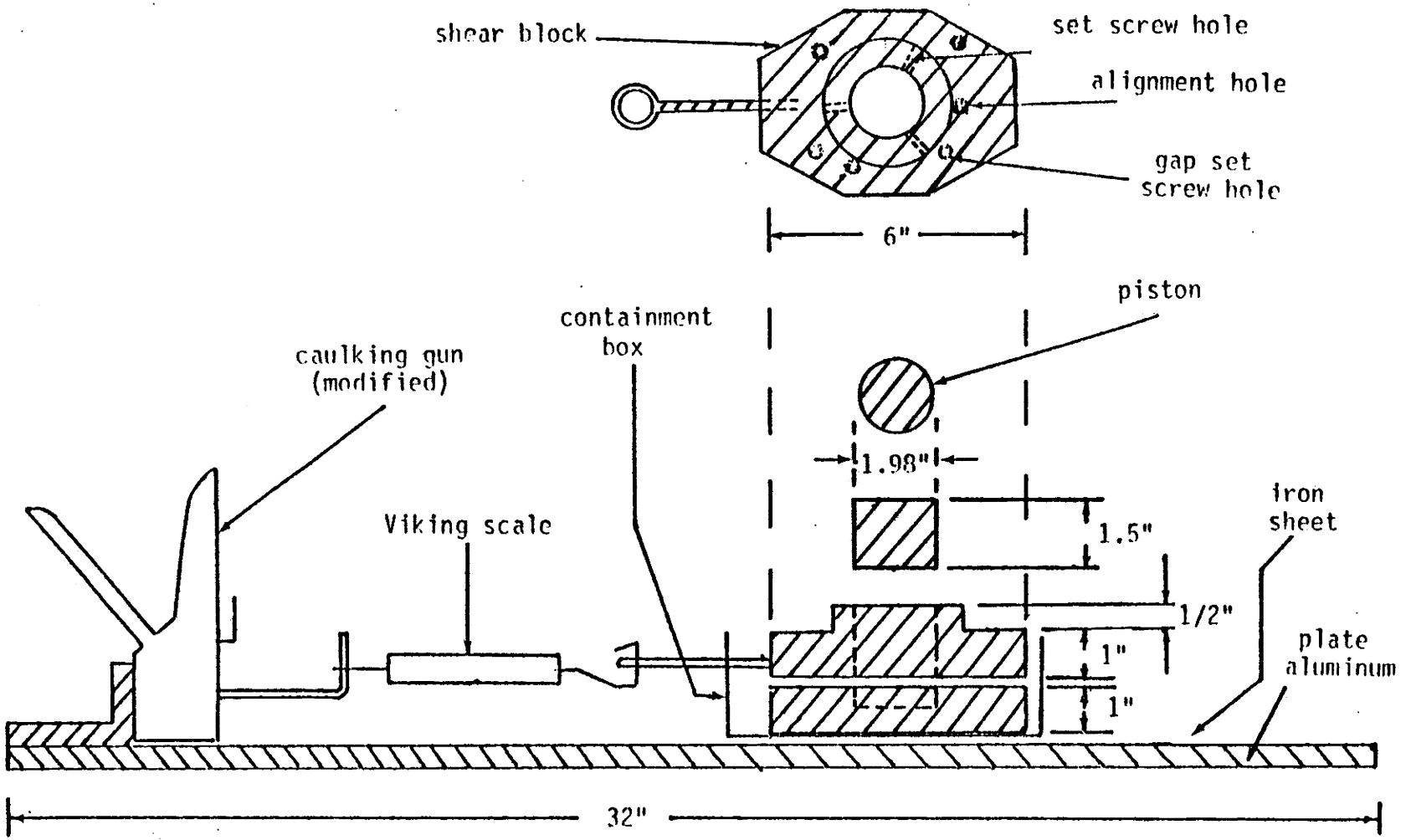

Figure 3.5.1 Test Device As Constructed

a paper disc was inserted between the piston and the sample. The disc was made out of a computer card.

The iron sheet epoxyed to the aluminum base was necessary to allow a ferrous surface upon which to place the magnetic base of the dial indicator. Such an arrangement was important to allow easy removal of the dial indicator between tests.

Alignment holes, set screw holes, and gap set threads were necessary to the application of the shear test procedure. The bolts in the caulking gun mount and the shear block assembly were used instead of welds to insure ease of disassembly for decontamination.

This design was used to evaluate the feasibility of direct shear testing of alumina microspheres. If the test was feasible, and it was deemed useful to employ the same device for uranium dioxide microspheres, some modifications would be necessary to allow for handling the radioactive material.

3.6 The Modified Device for Testing Sphere-pac Fuel

No changes of the direct shear device, itself, were needed to use it for testing uranium dioxide. However, significant modifications to the containment were necessary to meet regulations involving the use of radioactive material. For the UO_2 testing, it was necessary to incorporate a containment box to completely enclose the shear box assembly during the loading operation and during

clean-up after the test was completed.

Figure 3.6.1 shows the design modifications. The small rectangular containment box used for the alumina tests was replaced with a much larger pan of approximately 12 inches in diameter. During the clean-up phase of the experiment, a pail from which the bottom had been removed was placed over the shear box and fitted onto the pan. Over this pail was placed a funnel to which a 1000 ml Erlenmeyer flask was attached. The entire assembly was necessary to contain the UO_2 microspheres during transfer after each test.

Because the spheres tended to adhere to rough surfaces, the interior surface of the pail and funnel had to be painted with several coats of enamel paint to insure a smooth surface. In addition, contact with plastic and rubber surfaces had to be avoided because of associated static charge which inhibited the free flow of the spheres during transfer.

Two procedures were implemented for the direct shear test, depending on the material and the type of containment employed. The specific procedures will be given in the next section.

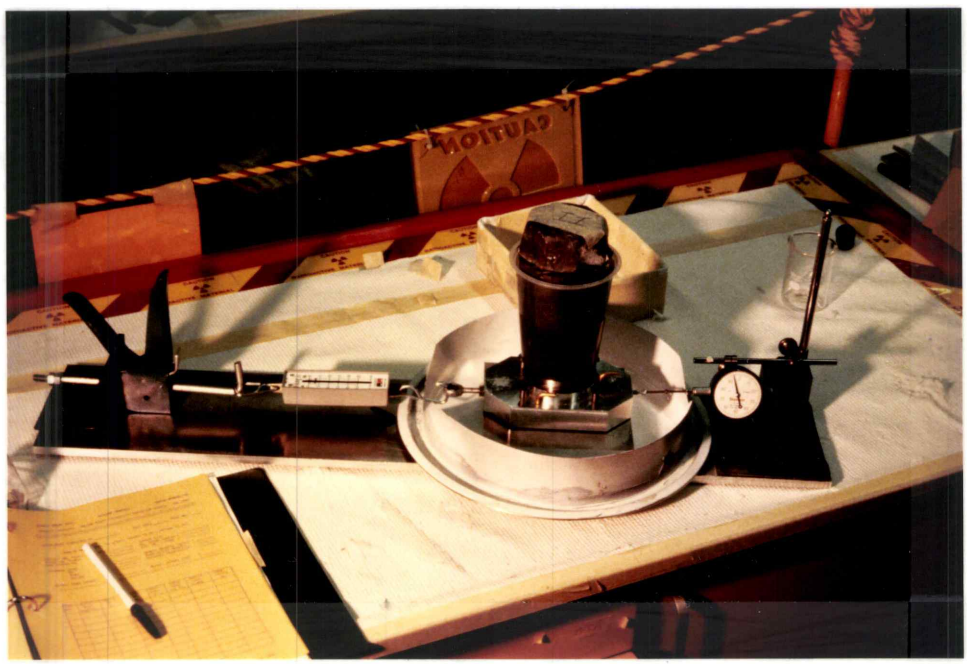

Figure 3.6.1 Modified Device for Testing Sphere-pac Fuel

4. EXPERIMENTAL PROCEDURE

4.1 Procedure for Testing Alumina Microspheres

The procedure involved is relatively straightforward and follows ASTM guidelines (14). First, the set and gap screws on the upper shear box are set to the flush position to allow the top and bottom boxes to fit tightly against each other and to allow the piston to slide freely (refer to Figure 3.5.1). With the chambers aligned and the alignment pins inserted, a sample of known weight is placed into the chamber. This is done by pouring the spheres, carefully, with a 125 ml beaker.

A paper disk is next inserted into the chamber on top of the sample followed by insertion of the aluminum piston. The paper disk is necessary to prevent spheres from becoming lodged between the piston and the cylinder walls, and causing subsequent seizing of the mechanism.

After the piston is inserted, the entire mechanism is vibrated for 1 minute while pressure is applied to the top chamber to prevent it from moving and dislodging spheres prematurely into the region between the two chambers. This region should have no gap at this stage of the test.

Once the vibration is completed, the piston is loaded with a known weight. Since the piston is free to slide within the chamber

cylinder, when the top chamber is moved upward relative to the bottom chamber, the piston and the sample remain in their initial fixed position. The upward movement of the top chamber is accomplished by turning four "gap set screws" located in the top chamber block.

By turning the gap set screws, a gap is created which allows us to measure only the resistance of the sample and not the frictional effects from the movement of the box. A precalibrated spacer device is used to measure the gap thickness. The gap necessary to allow such a measurement is slightly larger than the diameter of the alumina spheres (.05 cm).

In order to maintain the gap after the gap set screws are withdrawn, the upper box is "locked" to the piston by tightening 3 set screws. When the gap set screws are withdrawn, the sample supports not only the piston and the applied weight, but the entire upper box assembly, as well.

To insure that the upper box did, indeed, move freely during creation of the gap, a second check is made of the gap thickness after the upper box is "locked" to the piston, and the gap set screws are withdrawn. If the gap is not the same as before, the test is aborted.

For the measurement of displacement versus shearing force, incremental loadings are applied and subsequent readings of the scale and the dial indicator are recorded. First, an initial reading is taken, followed by application of 1 scale unit of force.

After 15 seconds the dial indicator reading is recorded. Subsequent applications of shearing force are made, each followed by a 15 second waiting period before the dial indicator is read.

This is repeated until the the shearing force no longer increases, and the material shows no resistance to increased applied force. Such a state is termed "failure".

After the test is performed, the material is poured into a large pan by inverting the assembly. After cleaning the surfaces to insure that there are no residual alumina microspheres, the apparatus is ready for the next sample. For a complete list of the procedure, see Appendix B.

4.2 Modified Procedure for Testing UO_2

In order to satisfy the goals of the ALARA principle, much attention was given to minimizing the exposure, or the potential exposure, to radiation. Because such exposure was to be minimized, the procedure for testing the UO_2 was changed accordingly. The procedure employed is given in Appendix C.

The part of the procedure relating to data acquisition for shearing force, displacement, normal force, density, and failure, was not altered. Only the procedures preceding and following the shear test itself, were modified to reflect the care required in handling the material. At each step in the procedure, caution was

exercised to insure that the material was contained, with minimal exposure or chance of release.

5. RESULTS

5.1 Introduction

The results for the experimentation with alumina and UO_2 microspheres will be presented in this section in two parts. The first part will pertain to alumina and the second part to UO_2. The alumina was studied first to furnish guidance in setting up the apparatus for experimentation with the radioactive material. However, the alumina statistics are also useful since this provides another set of data for modeling purposes.

5.2 Alumina Tests

The direct shear procedure as explained in section 4 yields raw data in the form shown in Figure 5.2.1. The starred entries designate measured quantities, while the other entries are consequences of subsequent calculations. See Appendix A for a discussion of the associated measurement errors.

Thirty separate tests were conducted for the alumina microspheres covering normal loadings ranging from about 40 Newtons to about 100 Newtons. This covers normal stresses in the range of about 19000 Pascals to about 48000 Pascals.

DIRECT SHEAR TEST ALUMINA SPHERES EXXON SPHERE-PAC

PROJECT LOCATION: OREGON STATE UNIV. RADIATION CENTER 754-2341

EXPERIMENT CONDUCTED BY R. Jenks TEST DATE 31Aug82 TEST NO. 22

Sample Data: (wt. in grams, length in cm., volume in cc)

Initial wt. beaker + sample = 200.47 * Sphere size = 0.05 *
Final wt. beaker = 50.18 * No. times sorted = 2 *
Net sample wt. = 150.29 Wt. / time = 0 / 60 *

Chamber diam. = 5.08 * Sample density (g/cc) = 2.35
Ht. .425 + 1.90 = 3.15 * Theoretical density = 3.96
Area = 20.268 Percent/ theoretical = 59.30
Volume = 63.84

Normal load (grams) = 8966.1 * Normal stress (pa) = 43382

TIME sec	Horiz. dial reading	Horiz. #1 in.	Metric #1 cm	Corr. area A'	Scale reading lb.	Metric shear grams	Shear stress pa
0	95.5 *		0		0.5 *		0
+15	95.0		1.27E-3		1.0		1183
	94.5		2.54E-3		2.0		3414
	93.0		6.35E-3		3.0		5645
	91.5		1.016E-2		4.0		7875
	89.0		1.651E-2		5.0		10106
	85.0		2.667E-2		5.5		11221
	78.5		4.318E-2		6.0		12336
▼	Sheared		Sheared		6.5		13452

Form 1.0 20 August 1982

Figure 5.2.1 Sample Alumina Data Sheet

5.2.1 Scale Calibration

From this set of data, the shear stress, τ, and the associated cumulative displacement, X, were calculated for each incremental tangential loading for each experiment. The dial indicator units of inches were converted directly to centimeters, while the conversion of the tangential load, T, required the use of the scale calibration curve displayed in Figure 5.2.2. Using the calibration function

$$T_{true} = A + B\ T_{scale} \qquad (5.2.1)$$

where A is -2.12239 and B is 4.52173, the lbf readingsof the scale were converted to Newtons.

5.2.2 Shear Stress-Strain Behavior of Alumina Microspheres

With the cross sectional area of the shearing plane known, the required shear stress was determined by

$$\tau = \frac{4T_{true}}{D^2} \text{ X (conversion factor)} \qquad (5.2.2)$$

where T has units of Newtons, D has the units of centimeters, and the conversion factor, 10^4 Pa per N/cm^2, transforms the dimensions to units of Pascals. Table 5.2.1 presents the resulting values for

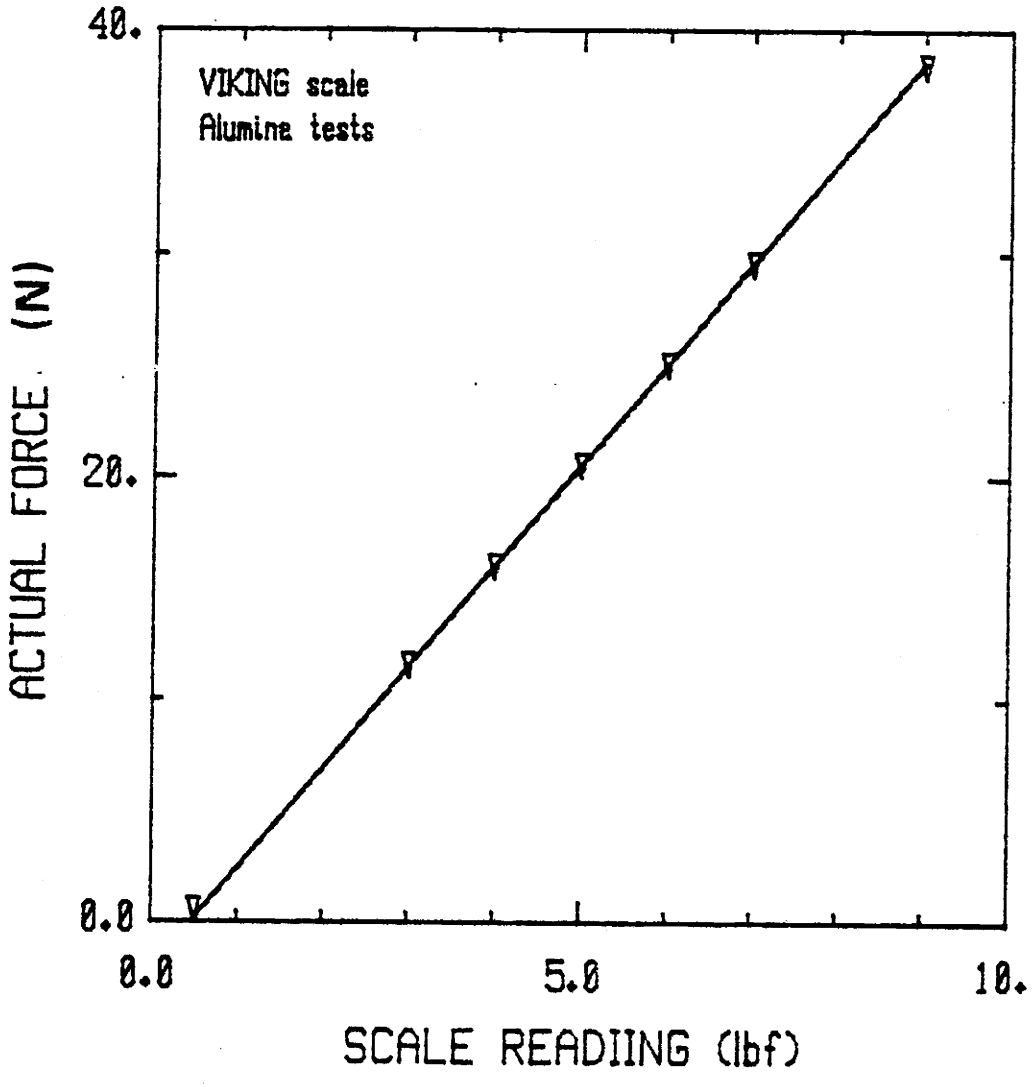

Figure 5.2.2 Alumina Scale Calibration Curve

the example data of Figure 5.2.1.

Table 5.2.1.
Example of values of displacement versus τ from test # 22

Cumulative Horizontal displacement (cm) $\pm 1.27 \times 10^{-3}$ cm	Shear stress, τ (Pa)
0.00	0
1.27×10^{-3}	1183
2.54×10^{-3}	3414
6.35×10^{-3}	5645
1.016×10^{-2}	7875
1.651×10^{-2}	10106
2.667×10^{-2}	11221
4.318×10^{-2}	12336
Sheared	13452

From these data, a graph can be constructed. Figure 5.2.3 shows a scatter plot of the data from four runs at a constant normal stress of 43382 Pa. In order to more clearly indicate the shape of the distribution of the data, the horizontal displacements were averaged over all of the tests at a given normal stress. Table 5.2.2 exhibits the values calculated for lot #6 (σ = 43382 Pa).

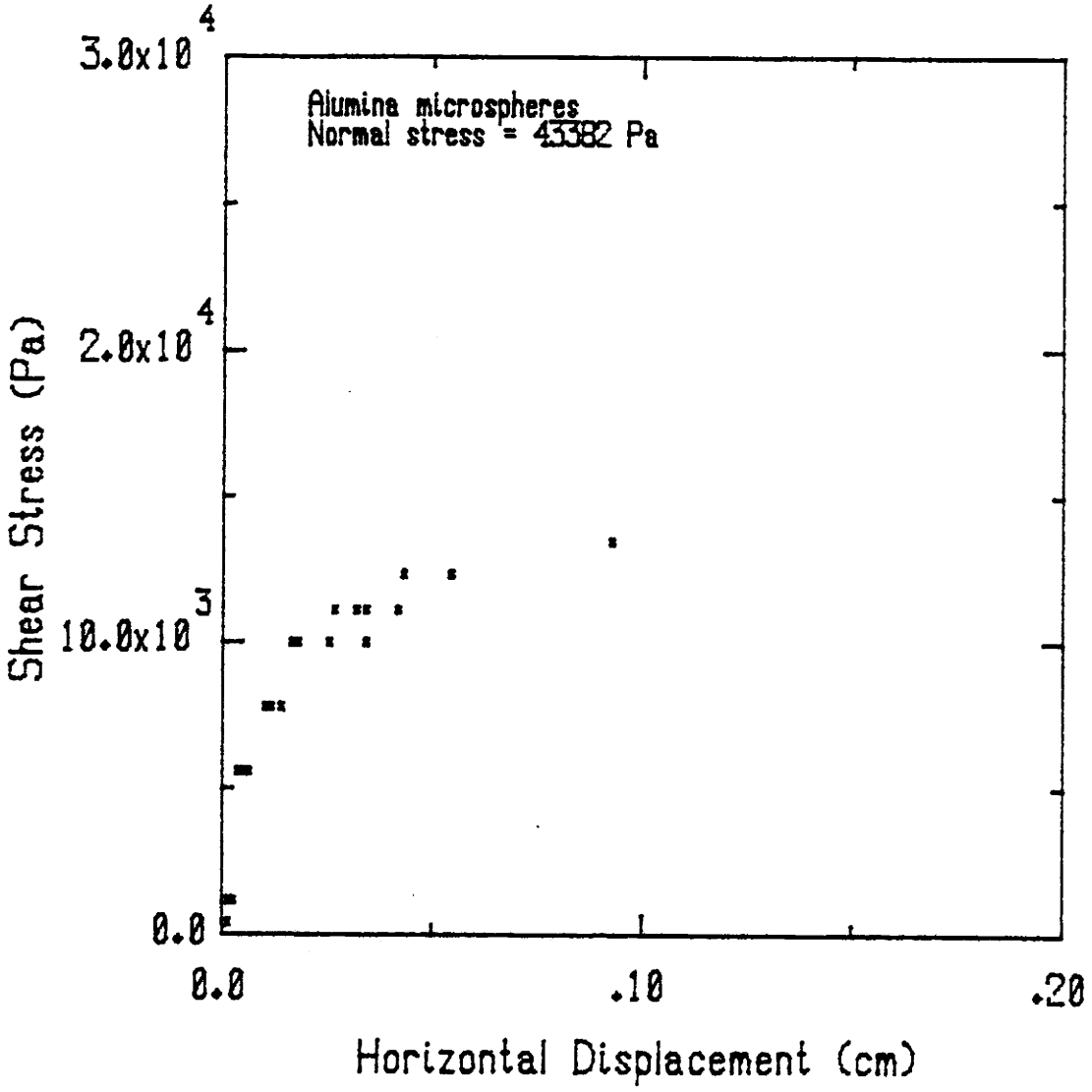

Figure 5.2.3 Scatter Plot of Alumina Data

Table 5.2.2.

Sample table to construct τ versus displacement curves

τ	horizontal displacement (cm)					
(Pa)	test 22	test 23	test 24	test 25	$\bar{X}$	S_X
0	0	0	0	0	0	0
1183	1.27E-3	0	1.27E-3	2.54E-3	1.27E-3	1.04E-3
3414	2.54E-3	1.27E-3	2.54E-3	2.54E-3	2.22E-3	6.35E-4
5645	6.35E-3	3.81E-3	5.08E-3	5.08E-3	5.08E-3	1.04E-3
7875	1.016E-2	1.397E-2	1.143E-2	1.143E-2	1.175E-2	1.60E-3
10106	1.651E-2	3.429E-2	2.540E-2	1.778E-2	2.350E-2	8.20E-3
11221	2.667E-2	4.191E-2	3.429E-2	3.175E-2	3.366E-2	6.35E-3
12336	4.318E-2	sheared	5.461E-2	5.461E-2	sheared	-------
13452	sheared	-------	9.271E-2	sheared	-------	-------

With the average displacements calculated, a graph of τ versus $\bar{X}$ can be made. Figure 5.2.4 shows the graph for the data from Table 5.2.2, with the 95% confidence intervals. In repeated runs, it would be expected that the range defined by the confidence interval would contain the "true" average value of displacement in approximately 95% of the samples (assuming independent, normally distributed samples). Here, a sample refers to a set of tests.

Another example of the experimental results is furnished in Table 5.2.3 and illustrated in Figure 5.2.5. Here the normal stress, σ is 26442 Pa. The confidence intervals have been calculated here, too. Again, this represents a confidence interval for the

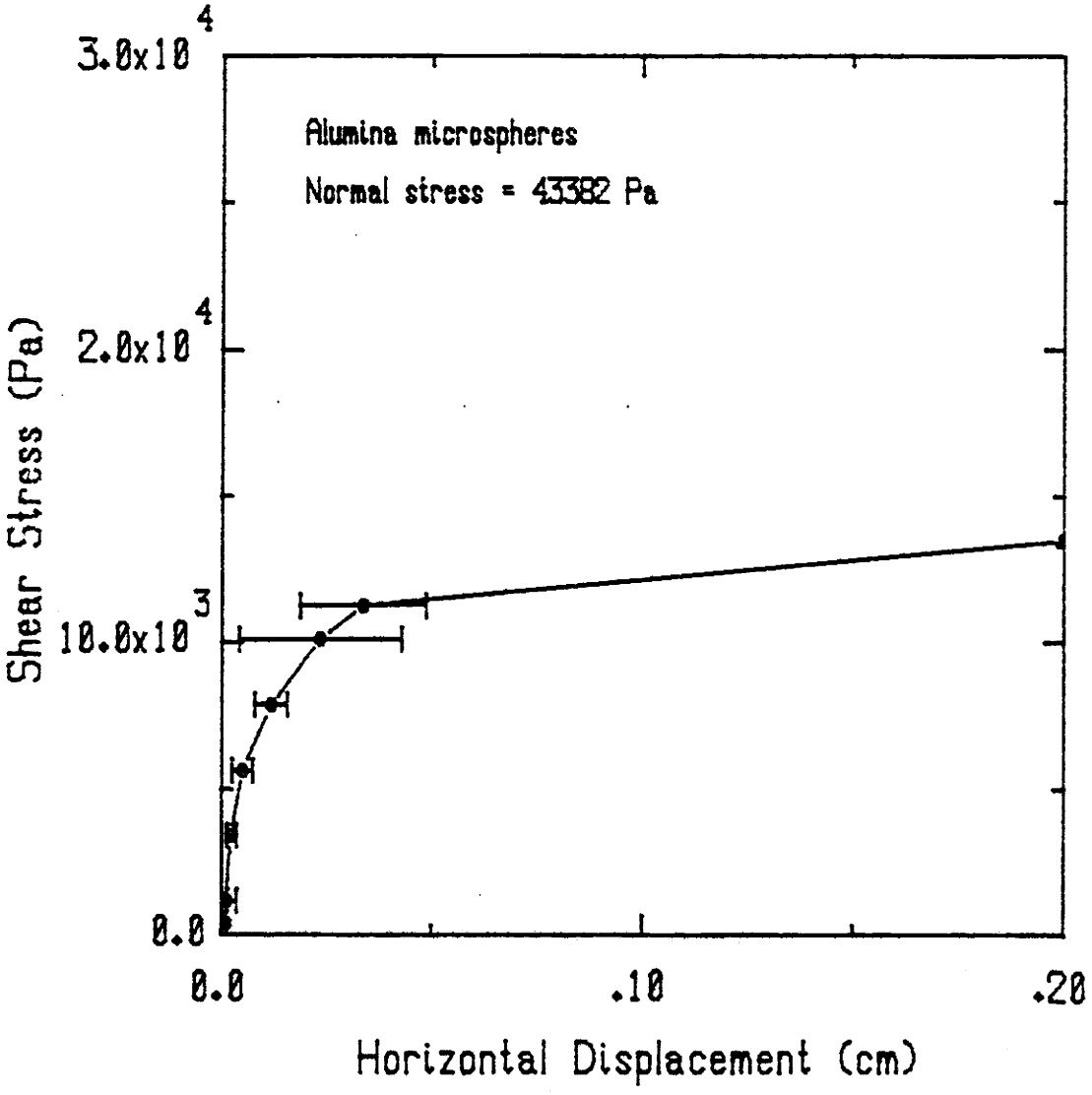

Figure 5.2.4 Shear Stress vs. Average Displacement, σ = 43382 Pa

sampling of 95%.

Table 5.2.3.
τ versus displacement for σ = 26442 Pascals

τ	horizontal displacement (cm)				
(Pa)	test 12	test 13	test 14	$\bar{X}$	S_X
0	0	0	0	0	0
1183	2.54E-3	2.54E-3	2.54E-3	2.54E-3	0
3414	1.27E-3	3.81E-3	5.08E-3	3.39E-3	1.94E-3
5645	7.62E-3	1.27E-2	1.78E-2	1.27E-2	4.31E-3
6760	2.54E-2	2.92E-2	3.30E-2	2.92E-2	3.81E-3
7875	6.985E-2	5.715E-2	5.842E-2	6.181E-2	6.99E-3
8991	8.001E-2	sheared	sheared	sheared	-------
10106	sheared	-------	-------	-------	-------

5.2.3 Friction Angle Determination for Alumina

To ascertain the friction angle, Φ_{CV}, two values were required, the scale reading at the moment the material yields and the associated normal load. These quantities were then converted to the appropriate units and graphed.

Table 5.2.4 gives the values of ultimate shear stress for each test according to lot number and normal stress. Also

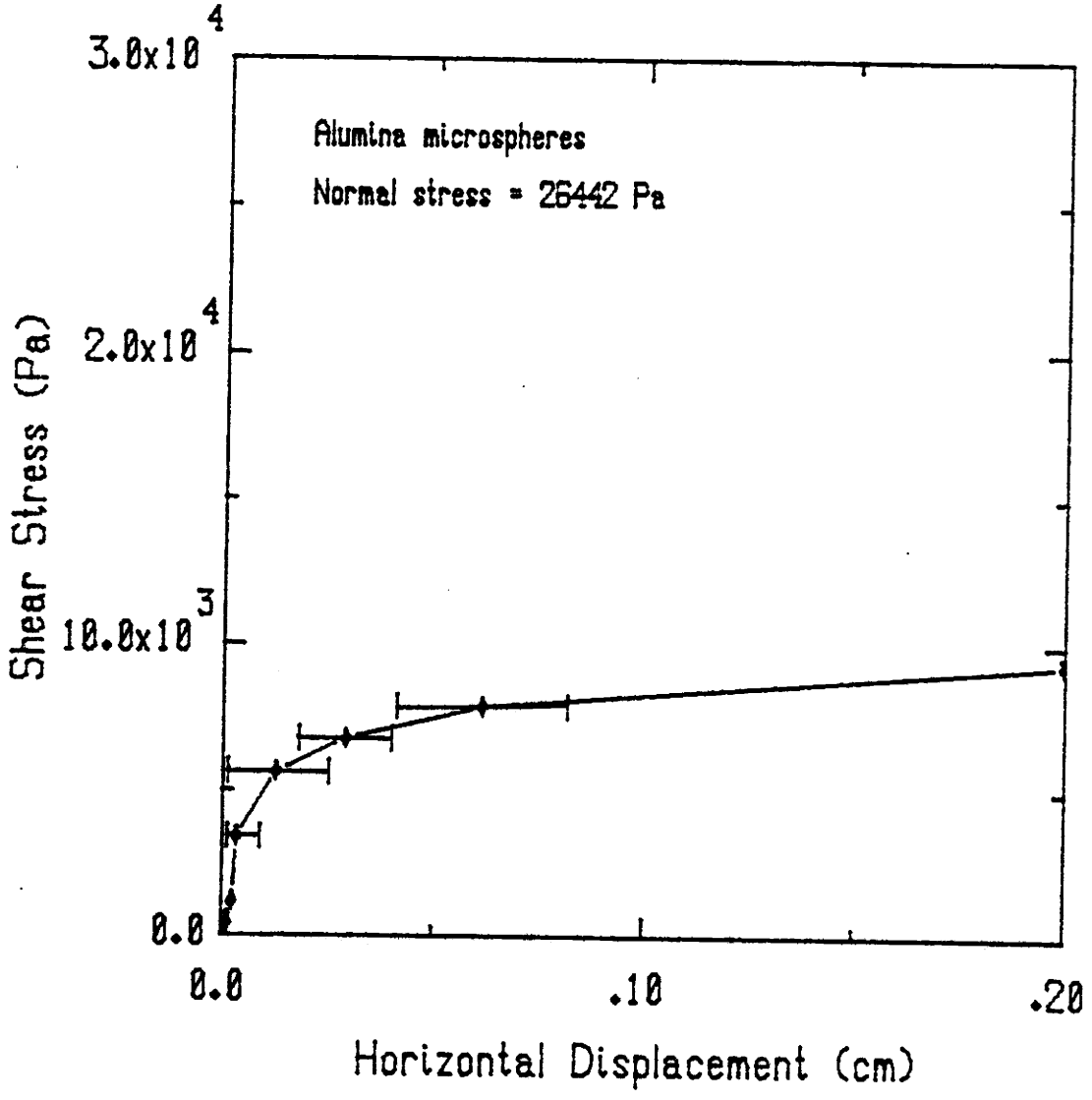

Figure 5.2.5 Shear Stress vs. Average Displacement, σ = 26442 Pa

Table 5.2.4.

Normal and ultimate stress values for alumina test runs

Lot #	Test #	σ (Pa)	τ (Pa)	$\bar{\tau}$ (Pa)	S_τ (Pa)	95% C.I. (Pa)
1	5	18545	6760			
	6	18545	6760			
	8	18545	6760	6760	0	---------
2	9	23499	8991			
	10	23499	7875			
	11	23499	8991	8619	644.3	(7018,10220)
3	12	26442	10106			
	13	26442	8991			
	14	26442	8991	9363	643.7	(7764,10962)
4	15	32702	12336			
	16	32702	11221			
	17	32702	10106	11221	1115	(8451,13991)
5	19	37370	11221			
	20	37370	11221			
	21	37370	11221	11221	0	---------
6	22	43382	13452			
	23	43382	12336			
	24	43382	14567			
	25	43382	13452	13452	910.0	(11191,15713)
7	26	48053	14567			
	28	48053	14567			
	30	48053	17913	15682	1932	(10882,20482)

indicated is the average value of the ultimate shear stress and the standard deviation for each lot.

Figure 5.2.6 illustrates the graph of the average values of the ultimate shear stress for each lot versus the corresponding normal stress. Interval estimates of ultimate strength within each lot are depicted on the graph by 95% confidence intervals.

A linear least squares regression of these data produces the following approximation

$$\tau = B\sigma + A \qquad (5.2.3)$$

where, A = 1863 and B = 0.275117.

This represents the best straight line we can draw through the points over the range of data collected. If we are interested in extrapolating the data over a large range beyond the limits of our experimental observations, the slope of the $\tau(\sigma)$ curve specified by this approximation is the best information we can use to get the friction angle, Φ_{CV}.

Since the slope of the $\tau(\sigma)$ curve is $\tan(\Phi_{CV})$, the friction angle is obtained from

$$\Phi_{CV} = \arctan(.275117)$$

$$= \underline{15.382^{o}}$$

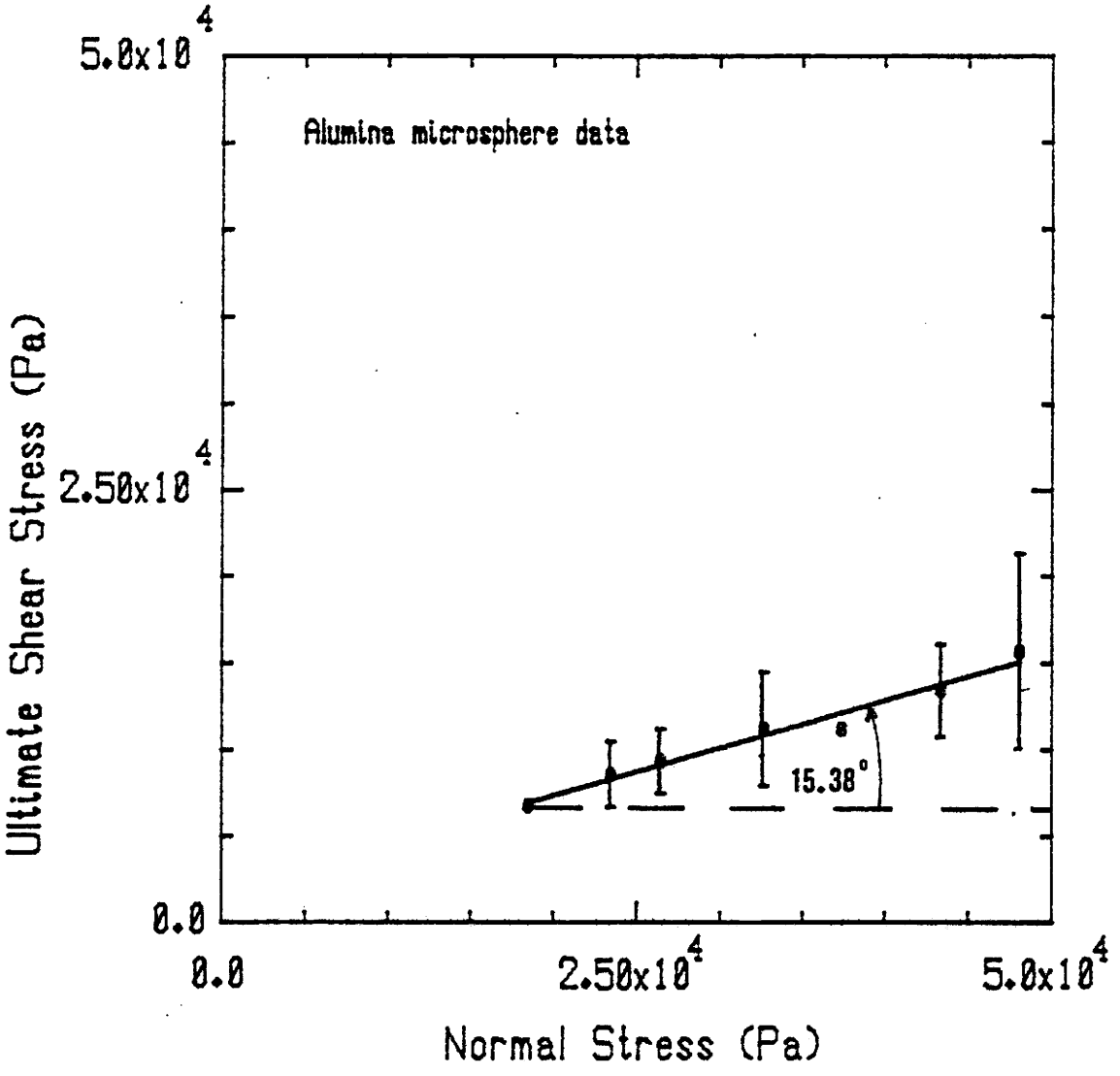

Figure 5.2.6. Linear Regression of Alumina Ultimate Shear Data

On the other hand, if we are primarily interested in extrapolating the behavior of the material back to the origin, a straight line which passes from the origin through our data would suffice. Such a line can be drawn, using a least squares polar regression of the data, which includes the origin as an assumed data point.

The expression for $\tau(\sigma)$ is then,

$$\tau = a\sigma \qquad (5.2.4)$$

where a = 0.327046981

Figure 5.2.7 gives the outcome of the polar regression of the data, where the dashed portion of the line illustrates the extrapolated range from the experimentally obtained data to the origin. The 95% confidence intervals have been included as in Figure 5.2.6. This represents the best straight line we can draw through the data points which also goes through the pseudo data point, (0,0). (Note: Polar regression constrains the model to have an intercept of zero.) Using this method, we have

$$\Phi_{CV} = \arctan(0.327046981) = \underline{18.11^{\circ}}$$

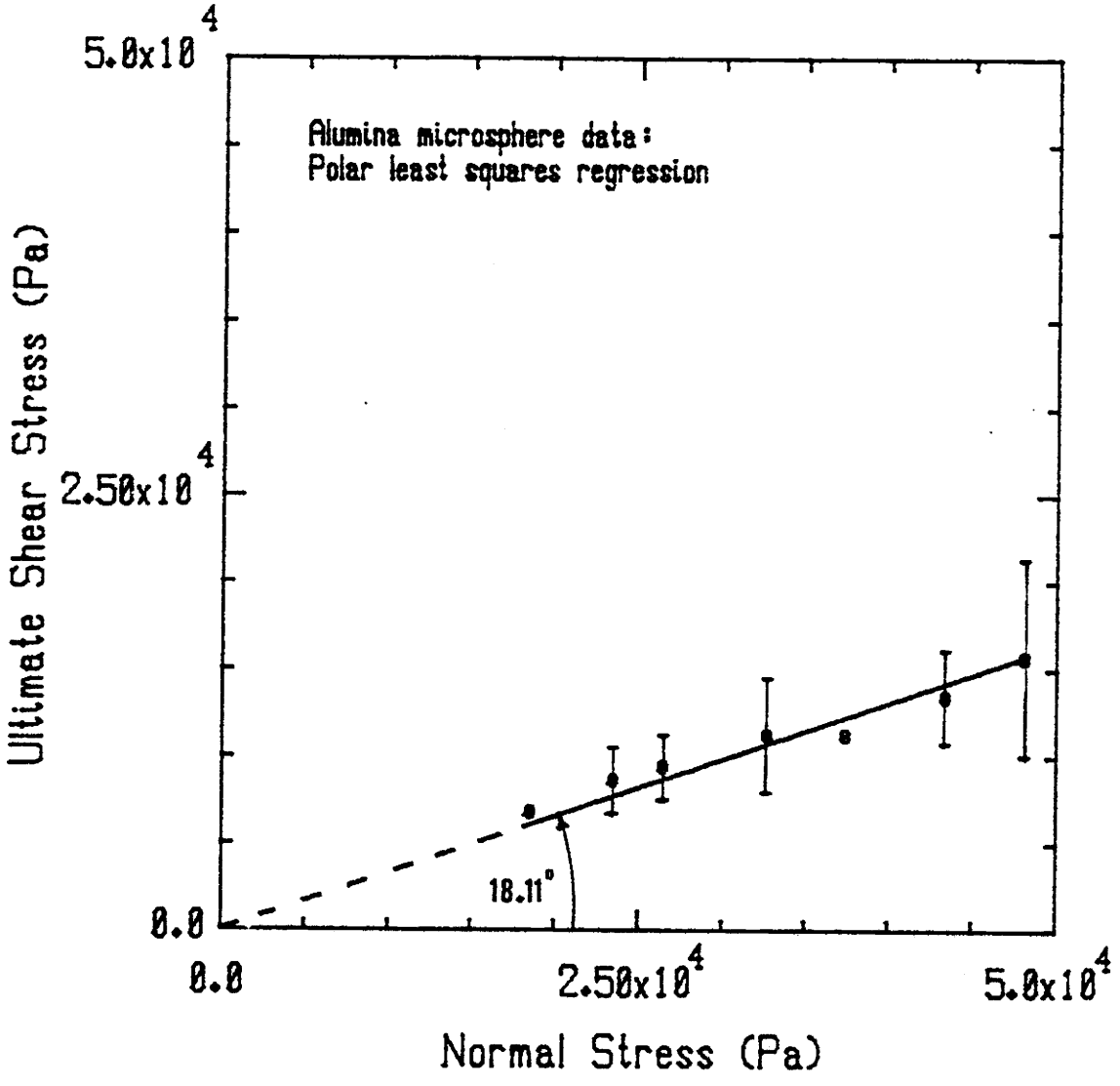

Figure 5.2.7 Polar Regression of Alumina Ultimate Shear Data

5.2.4 Angle of Repose for Alumina Microspheres

The data in Table 5.2.5 contains the measurements to determine the angle of repose. The variables H, L, H', L', θ, α, and β, correspond to the variables introduced in Section 2.5. Lengths were measured to an accuracy of $\pm$ .05 cm.

Table 5.2.5.
Experimental determination of the angle of repose

Test #	H (cm)	L (cm)	H' (cm)	L' (cm)	θ (^{o})	α (^{o})	β (^{o})
1	12.00	16.60	2.50	6.30	46.29	21.64	24.65
2	9.30	16.60	1.30	7.00	34.07	10.52	23.55
3	12.10	16.60	2.30	6.00	46.80	20.97	25.83
4	11.70	17.20	2.50	7.85	42.86	17.67	25.19
5	10.80	16.60	1.60	5.95	40.59	15.05	25.54

From these data it can be seen that the average value for the angle of repose is 24.96^o with a standard deviation of $.90^o$. Analysis of these data will be delivered in Section 6.2.

5.3 Uranium Dioxide Tests

An example of the raw data provided by the direct shear test procedure outlined in Section 4, is presented in Figure 5.3.1. Here, test 45 was performed using the UO_2 uniform ternary mixture which simulated the sphere-pac fuel mixture. The starred entries represent the measured quantities, while the other entries are derived by calculations.

Experiments were performed on the following UO_2 materials:

a. Fine fraction microspheres (.0035 cm diameter)
b. Medium " " (.03 " ")
c. Coarse " " (.13 " ")
d. Ternary (3-size) " (uniformly mixed)
e. Ternary " " (premixed)

The range of normal loadings for the twenty-seven separate tests performed, extended from 45 Newtons to 90 Newtons, corresponding to normal stresses of approximately 22000 Pa to 44000 Pa. Availability of material restricted the testing of fine fraction microspheres and uniformly mixed ternary microspheres.

DIRECT SHEAR TEST UO_2 SPHERES EXXON SPHERE-PAC

PROJECT LOCATION: OREGON STATE UNIV. RADIATION CENTER 754-2341

EXPERIMENT CONDUCTED BY R. Jenks TEST DATE 5 Nov 82 TEST NO. 45

Sample Data: (wt. in grams, length in cm., volume in cc)

Initial wt. beaker + sample = Taced
Final wt. beaker 100.07 F * = /
Net sample wt. 91.42 M * = 455.92
264.43 C *
Chamber diam. = 5.08*
Ht. 1.25+1.20 = 2.45*
Area = 20.268
Volume = 49.66

Sphere size = 3-size *
No. times sorted = New C/used F/M
Vib. Wt. / Time = 204/60 *
Sample density (g/cc) = 9.18
Theoretical density = 10.96
Percent/ theoretical = 83.77

Normal load (grams) = 9084.5*
Normal stress (pa) = 43955

TIME sec	Horiz. dial reading	Horiz. #H in.	Metric #H cm	Corr. area A'	Scale reading lb.	Metric shear grams	Shear stress pa
0	97.0*		0		0.5*		0
+15	97.0		0		1.0		1168
"	97.0		0		2.0		3377
"	96.5		1.27E-3		2.5		4481
"	87.5		2.41E-2		8.5		17731
"	84.0		3.30E-2		9.0		18835
"	81.0		4.06E-2		9.5		19939
↓	Sheared		Sheared		10.0		21043

Form 1.0 20 August 1982

Figure 5.3.1 Sample UO_2 Data Sheet

5.3.1 UO_2 Scale Calibration

Because of the time span (over 2 months) separating the alumina and the UO_2 runs, another scale calibration had to be performed. This was deemed necessary because the equipment had been moved around considerably during the modification stage. Since the calibration was important to properly convert the raw data to the correct shear stress, considerable care was taken in ascertaining the proper calibration function.

The plot of the observed scale reading versus the actual force is shown in Figure 5.3.2. The data were fitted with a least squares linear regression to the calibration function given in Equation 5.2.1. The slope and intercept parameters determined by this method were, respectively,

$$B = 4.47578$$

$$A = -2.10709$$

By this method the observed reading in pounds force was converted to S.I. units of Newtons which have been corrected to indicate the actual force.

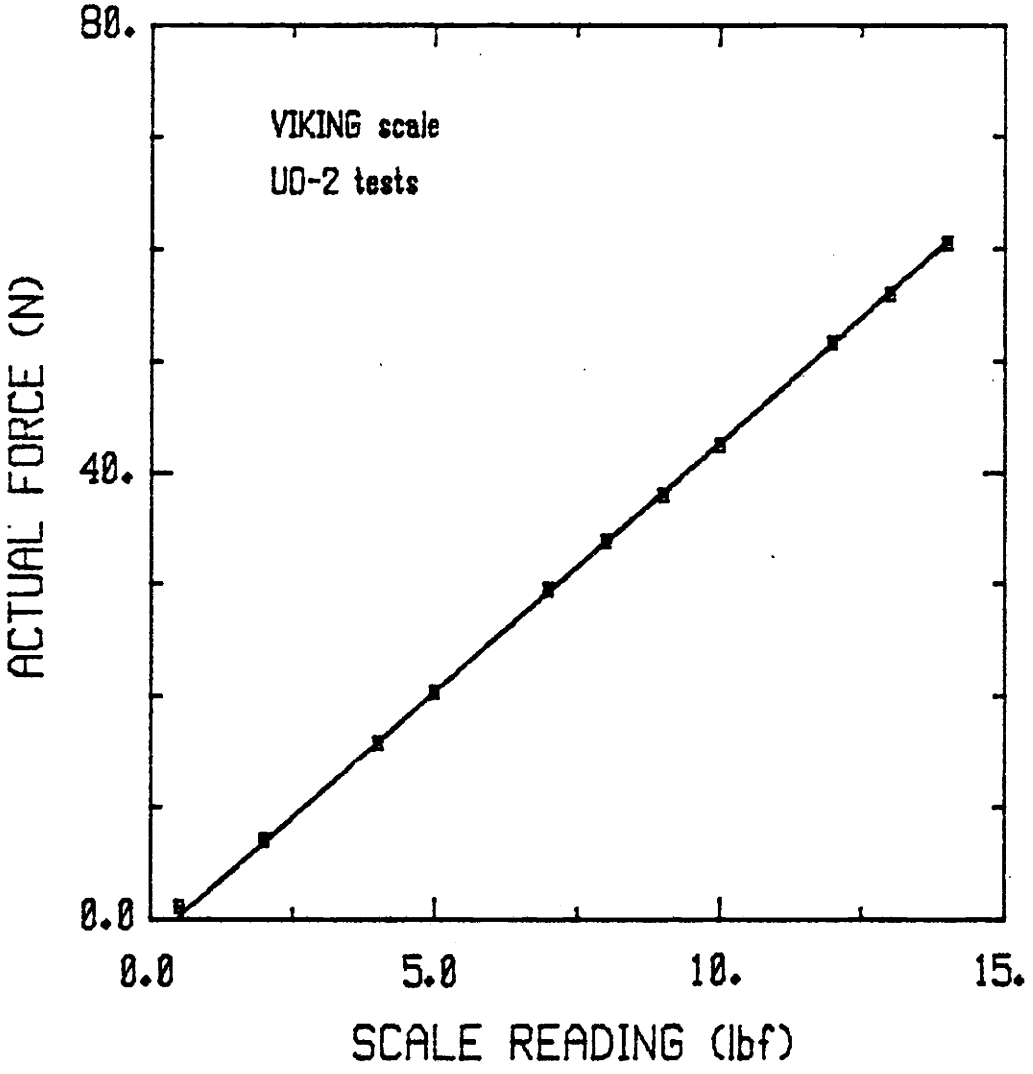

Figure 5.3.2 UO_2 Scale Calibration Curve

5.3.2 Stress-Strain Behavior of UO_2

Once the scale readings were corrected and converted to Newtons, they were divided by the nominal cross sectional area of the shearing plane (20.268 cm^2) to obtain the shear stress. A set of cumulative displacement versus shear stress tables was then produced which were subsequently plotted to show the stress-strain behavior for the material.

Table 5.3.1 gives values of cumulative displacement versus τ for the values from test #45.

Table 5.3.1.

Example of values of displacement versus τ from test # 45

Cumulative Horizontal displacement (cm) + 1.27×10^{-3} cm	Shear stress, τ (Pa)
0.00	0
0.00	1168
0.00	3377
1.27×10^{-3}	4481
1.27×10^{-3}	5585
2.54×10^{-3}	6689
3.81×10^{-3}	7794
5.08×10^{-3}	8898
5.08×10^{-3}	10002
6.35×10^{-3}	11106
7.62×10^{-3}	12210

Table 5.3.1 (continued)

1.02×10^{-2}	13314
1.23×10^{-2}	14418
1.65×10^{-2}	15523
2.03×10^{-2}	16627
2.41×10^{-2}	17731
3.30×10^{-2}	18835
4.06×10^{-2}	19939
Sheared	21043

A scatter plot was constructed from the three sets of data for the UO_2 uniform ternary mixture (tests 43, 44, and 45). Figure 5.3.3 indicates the plot of these values for a normal stress of 43955 Pa. To allow a better representation of the behavior of the material, and to provide mean values about which confidence intervals could be indicated, the horizontal displacements for the three sets were averaged. This is shown in Table 5.3.2, which displays the displacements for each experiment at discrete shear stresses, as well as the mean values and the sample standard deviations.

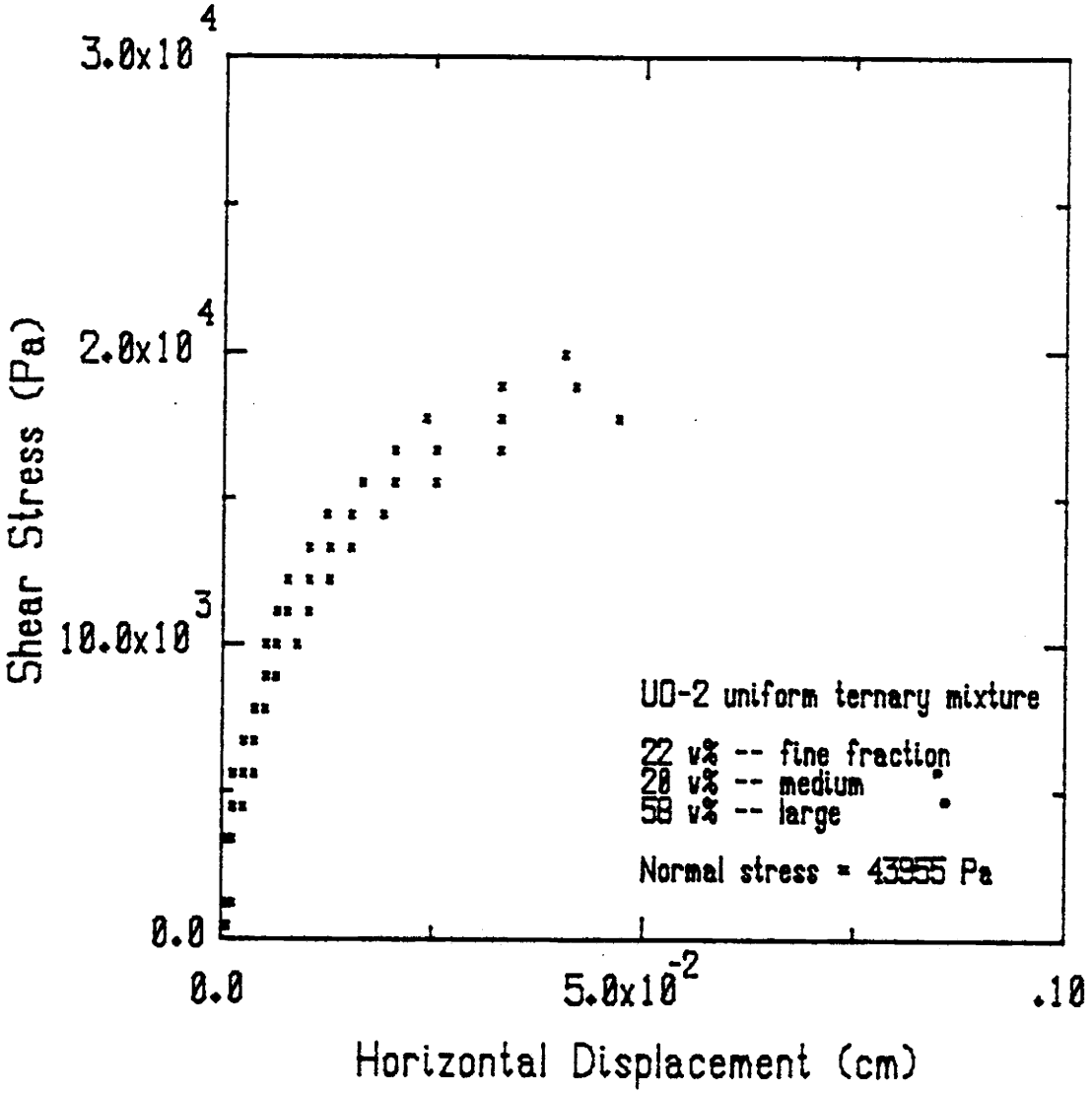

Figure 5.3.3 Scatter Plot of UO_2 Data

Table 5.3.2.

τ versus displacement for σ = 26442 Pascals

τ	horizontal displacement (cm)				
(Pa)	test 43	test 44	test 45	$\bar{X}$	S_X
0	0	0	0	0	0
1168	1.27E-3	0	0	4.23E-4	7.33E-4
3377	1.27E-3	0	0	4.23E-4	7.33E-4
4481	2.54E-3	1.27E-3	1.27E-3	1.69E-3	7.33E-4
5585	3.81E-3	2.54E-3	1.27E-3	2.54E-3	1.27E-3
6689	3.81E-3	2.54E-3	2.54E-3	2.96E-3	7.33E-4
7794	5.08E-3	3.81E-3	3.81E-3	4.23E-3	7.33E-4
8898	6.35E-3	5.08E-3	5.08E-3	5.50E-3	7.33E-4
10002	8.89E-3	6.35E-3	5.08E-3	6.77E-3	1.94E-3
11106	1.02E-2	7.62E-3	6.35E-3	8.06E-3	1.96E-3
12210	1.27E-2	1.02E-2	7.62E-3	1.02E-2	2.54E-3
13314	1.52E-2	1.27E-2	1.02E-2	1.27E-2	2.50E-3
14418	1.91E-2	1.52E-2	1.23E-2	1.55E-2	3.41E-3
15523	2.54E-2	2.03E-2	1.65E-2	2.07E-2	4.47E-3
16627	3.30E-2	2.54E-2	2.03E-2	2.62E-2	6.39E-3
17731	4.70E-2	3.30E-2	2.41E-2	3.47E-2	1.15E-2
18835	sheared	4.19E-2	3.30E-2	sheared	-------
19939	-------	sheared	4.06E-2	sheared	-------
21043	-------	-------	sheared	sheared	-------

From this table a graph of the average displacements was made and is shown in Figure 5.3.4. Also indicated is the 95% confidence interval associated with each point. This gives us an idea of where

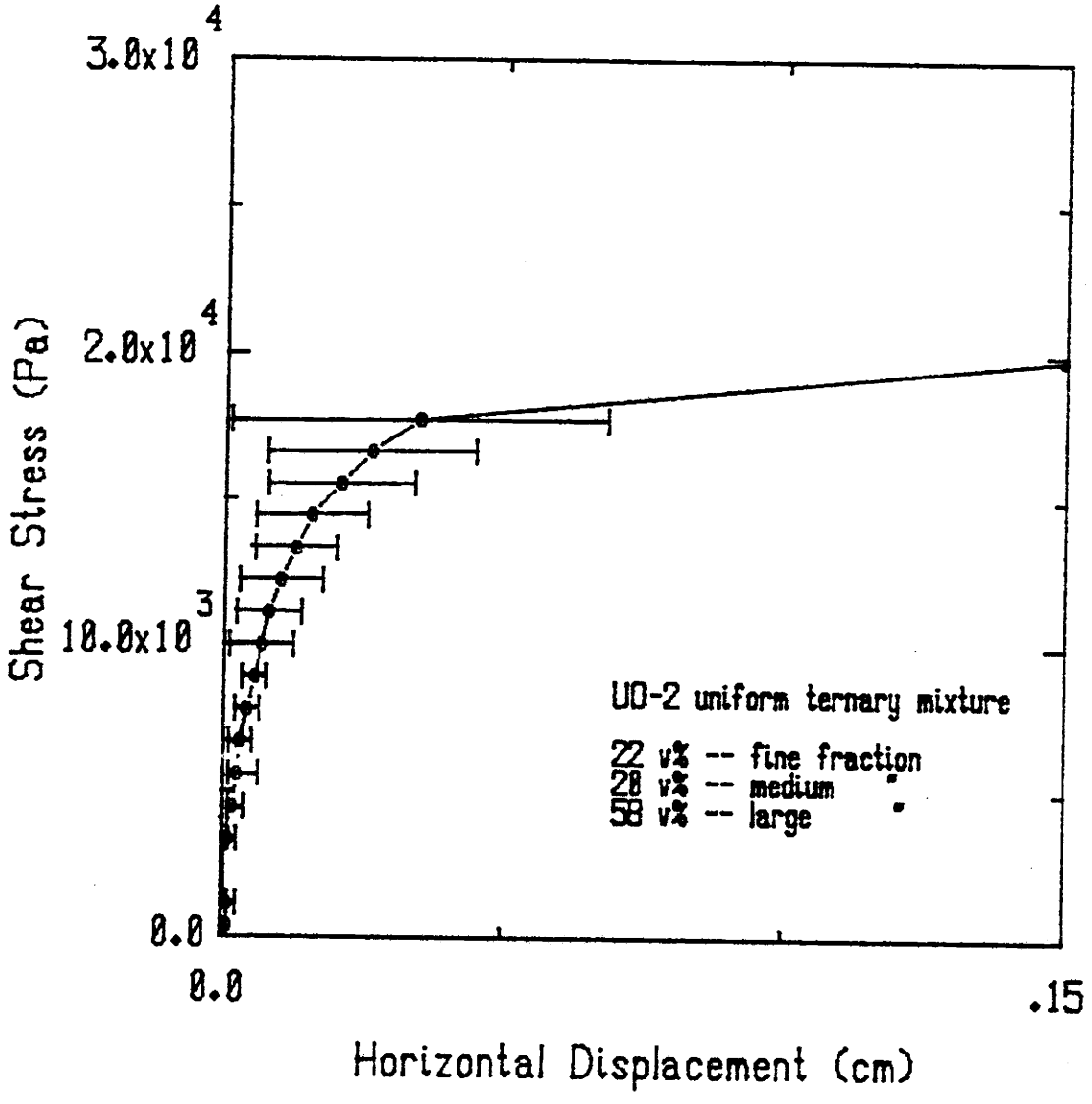

Figure 5.3.4 Shear Stress vs. Average Displacement, σ = 26442 Pa

our value is in relation to the "true" or expected value of displacement.

Additional results are illustrated in Figures 5.3.5 through 5.3.8, which indicate shear stress as a function of horizontal displacement for fine, medium, coarse, and ternary premixed UO_2 respectively. The principal difference between the uniform and the premixed UO_2 samples was the mixing techniques employed.

For the uniform ternary samples, an attempt was made to place the sample into the chamber in 3 layers. Each layer was produced by pouring the coarse fraction into the chamber with the medium fraction, stirring this mixture, and then placing the fine fraction on top with very little stirring. Once all the layers were finished, it was expected that the vibration stage of the procedure would distribute the fine fraction into a stable packing configuration which would approximate the Sphere-pac fuel mixture.

On the other hand, the premixed ternary samples were not constructed in this manner, but were simply the batch "leftovers" from the uniform ternary samples. This was done partly because of limitations on the availability of the material, and partly because it would be interesting to see if we could detect a difference in friction angle calculation between the two mixing methods.

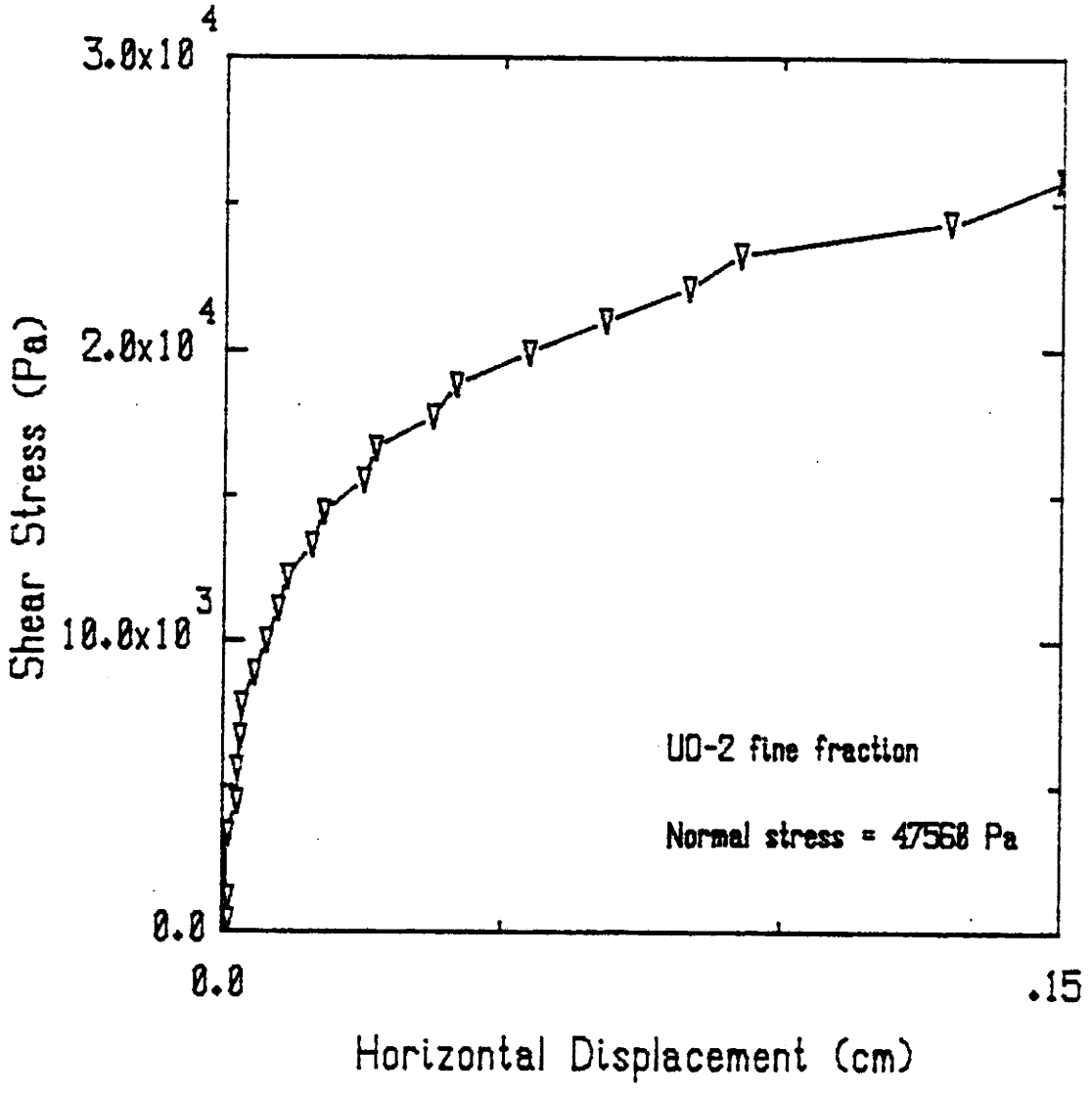

Figure 5.3.5 Shear Stress vs. Average Displacement for UO_2 Fines

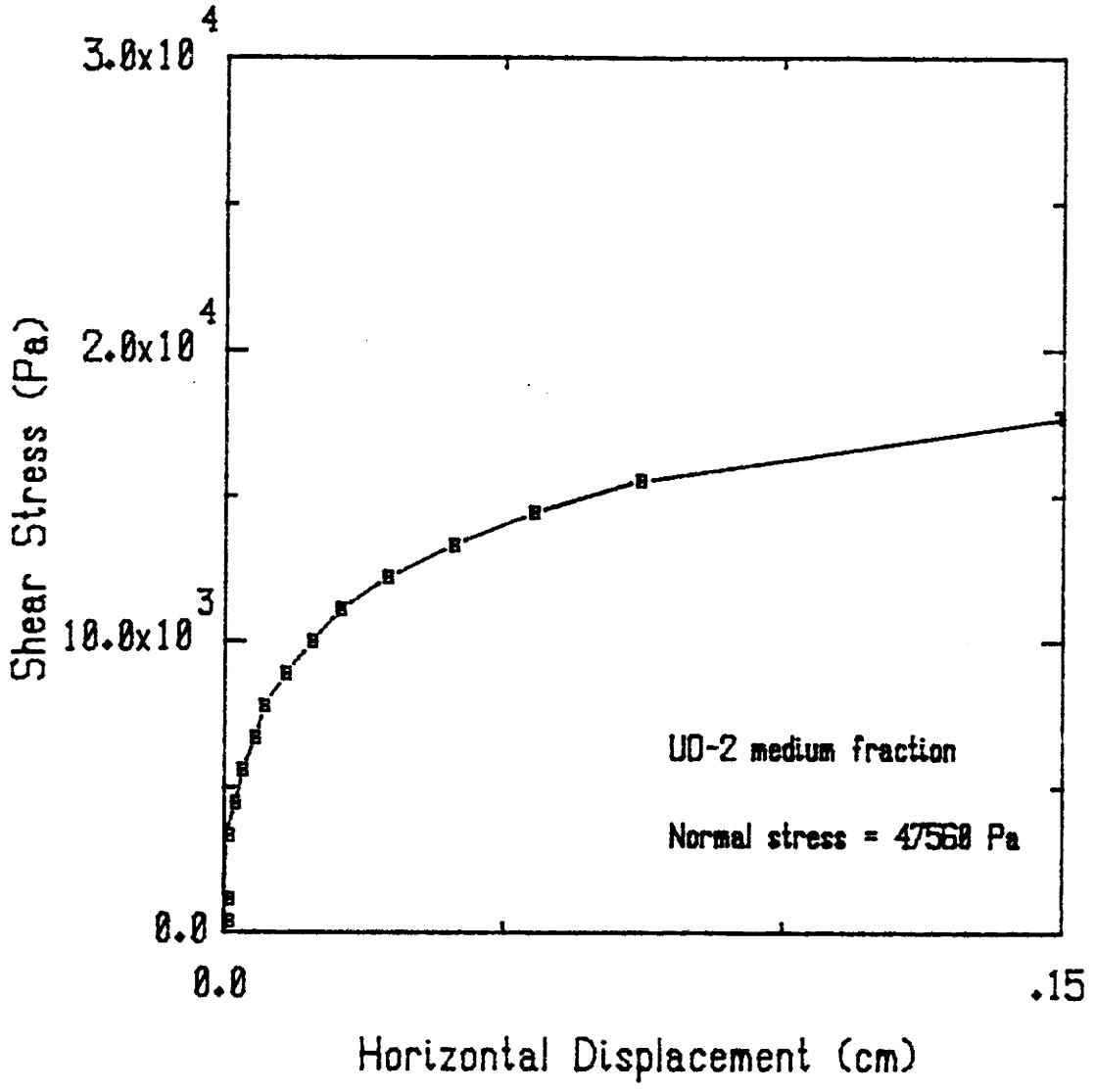

Figure 5.3.6 Shear Stress vs. Average Displacement for UO_2 Medium

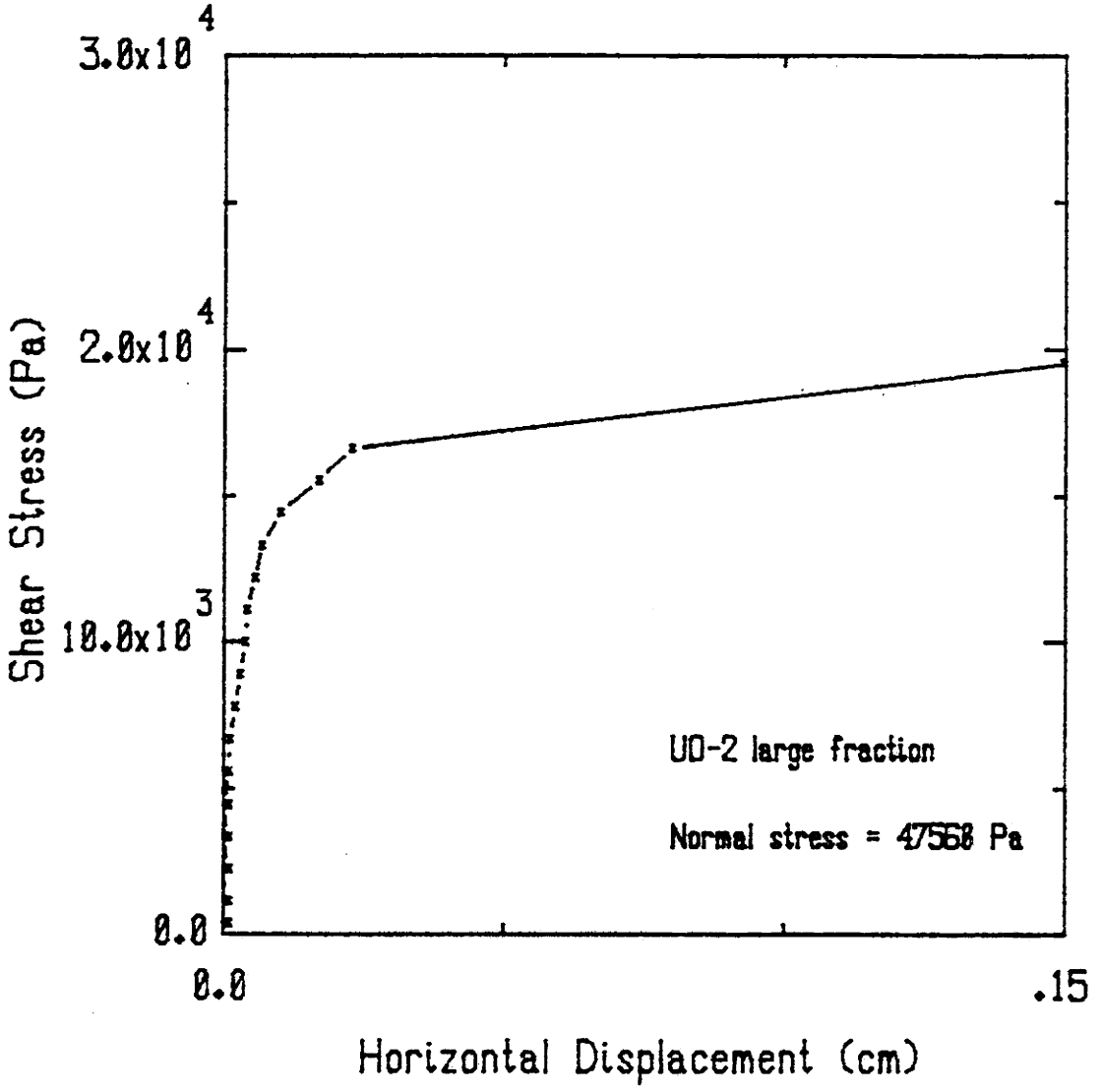

Figure 5.3.7 Shear Stress vs. Average Displacement for UO_2 Coarse

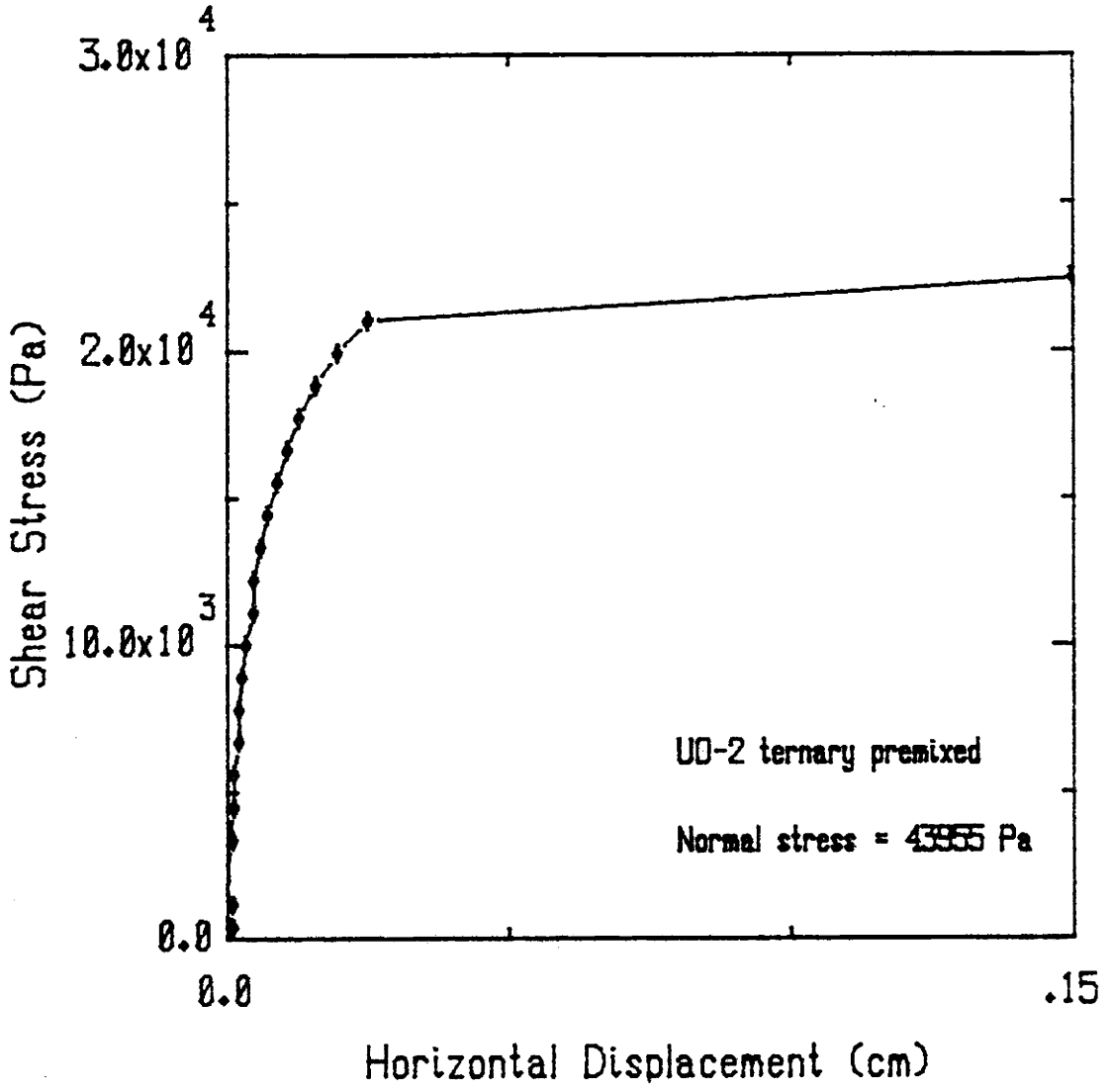

Figure 5.3.8 Shear Stress vs. Average Displacement for UO_2 Ternary

5.3.3 Elastic Behavior of UO_2

It is interesting to note that particulate material exhibits elastic behavior like most other materials. When subjected to a load and subsequently unloaded, the material has a slight tendency to return to a prestressed configuration. This indicates that some energy is stored in the particles which allows elastic behavior to exist.

Figures 5.3.9 and 5.3.10 show the results of two "unloading" experiments that were performed with the UO_2 medium and coarse fractions, respectively. These were performed by applying the tangential forces, as in the usual procedure, until the material exhibited a deformation pattern. When this stage was reached, the tangential force was reduced to zero. The test then resumed from this point, at zero shear stress, with increasing incremental loadings, until another deformation pattern developed, and so on, until the material yielded. This was only done for the medium and coarse fraction due to limitations on the availability of material.

5.3.4 Friction Angle Determination for UO_2

The friction angle was found in exactly the same manner as for the alumina microspheres, except that due to the small quantity of material obtainable and the radioactive nature of the material, fewer measurements were obtained. This meant that a linear

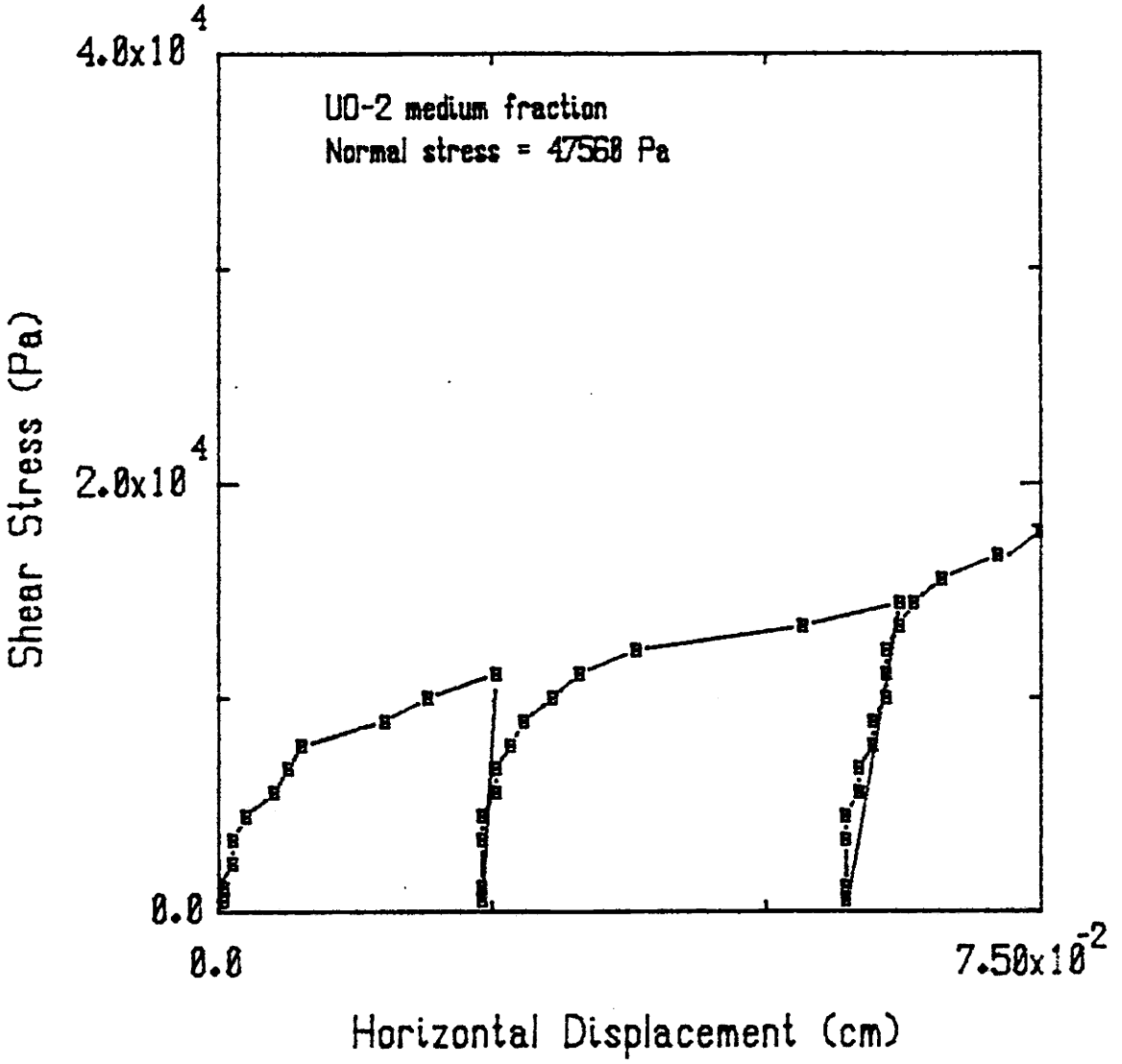

Figure 5.3.9 Medium Fraction UO_2 Unloading Data

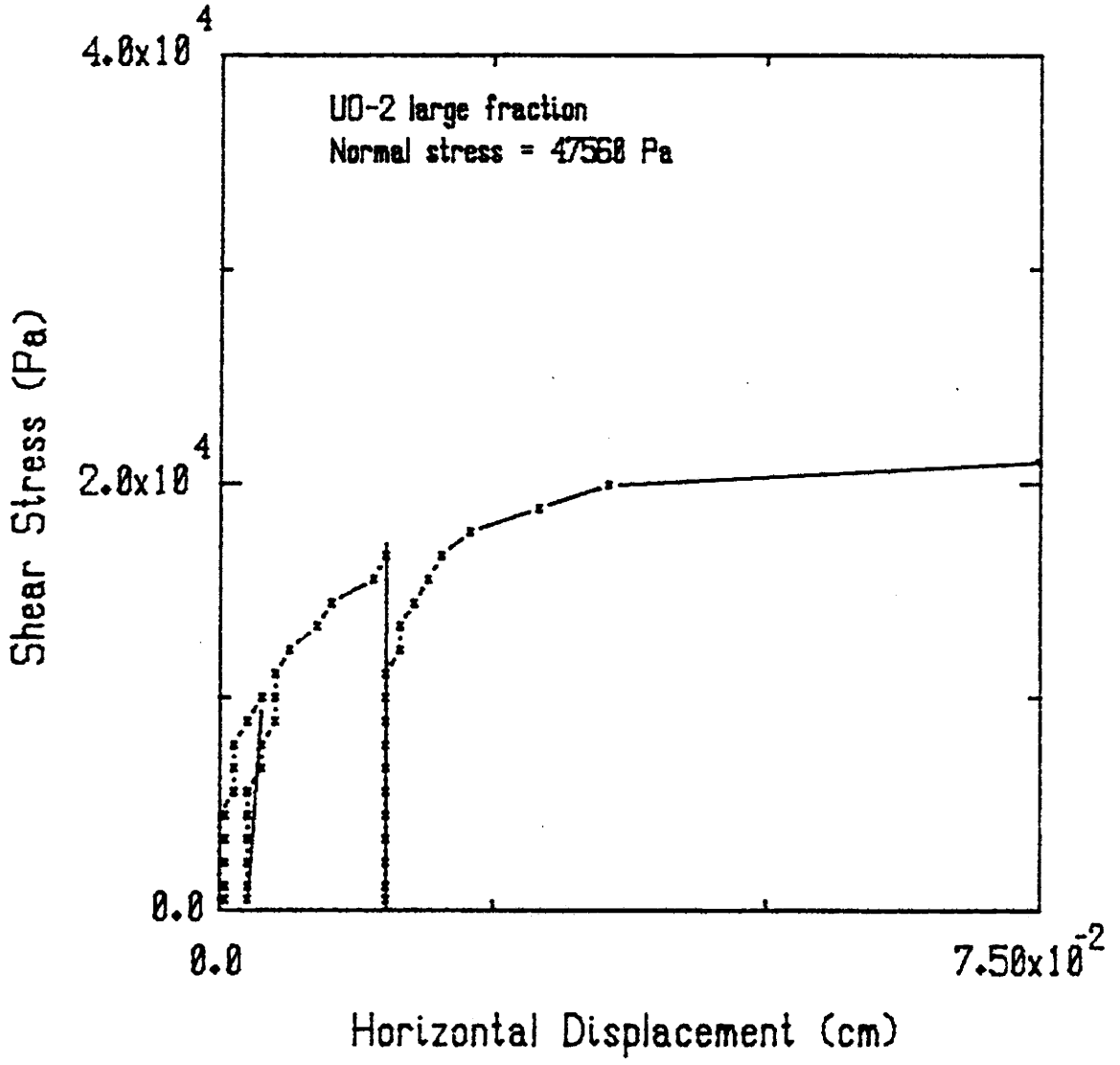

Figure 5.3.10 Coarse Fraction UO_2 Unloading Data

regression of the fine fraction and the uniform ternary data was not possible and, therefore, a polar regression had to be performed.

Nevertheless, linear regressions could be made with the measurements obtained for the medium, coarse, and premixed ternary UO_2. Table 5.3.3 summarizes the observed values necessary for calculating the friction angle.

Table 5.3.3
Normal and ultimate stress values for uranium dioxide microspheres

Material	Test	σ (Pa)	τ (Pa)	$\bar{\tau}$ (Pa)	S_τ (Pa)	95% C.I. (Pa)
Fine	31	47560	25460			
	32	47560	25460			
	33	47560	26564	25828	637.4	(24245,27411)
Medium	34	47560	16627			
	35	47560	18835			
	36	47560	17731	17731	1104	(14988,20474)
	50	22345	10002			
	51	22345	10002			
	52	22345	8898	9634	637.4	(8050,11218)
Coarse	38	47560	17731			
	39	47560	21043			
	40	47560	19939	19571	1686	(15382,23760)
	53	22345	10002			
	54	22345	10002			
	55	22345	10002	10002	0	----------
Ternary Uniform	43	43955	18835			
	44	43955	19939			
	45	43955	21043	19939	1104	(17196,22682)
Ternary Premixed	47	43955	22147			
	48	43955	23252			
	49	43955	22147	22515	638.0	(20930,24100)
	56	23345	12210			
	57	22345	11106			
	58	22345	12210	11842	637.4	(10258,13426)

Figures 5.3.11 through 5.3.15 represent graphs of the ultimate shear stress versus the normal stress for the mixtures shown in Table 5.3.3. Where a linear regression was possible, it was drawn through the points without extrapolation to the shear axis. The polar regressions are indicated as lines drawn from the origin which best fit the data using a least squares approach.

Recalling that

$$\tau = B\sigma + A$$

for a linear least squares regression and

$$\tau = a\sigma$$

for a polar least squares regression, the friction angle can be determined as the arctan of the slope of the curve. This is arctan(B) for the linear regression and arctan(a) for the polar regression. Table 5.3.4 summarizes the outcome of the friction angle calculations.

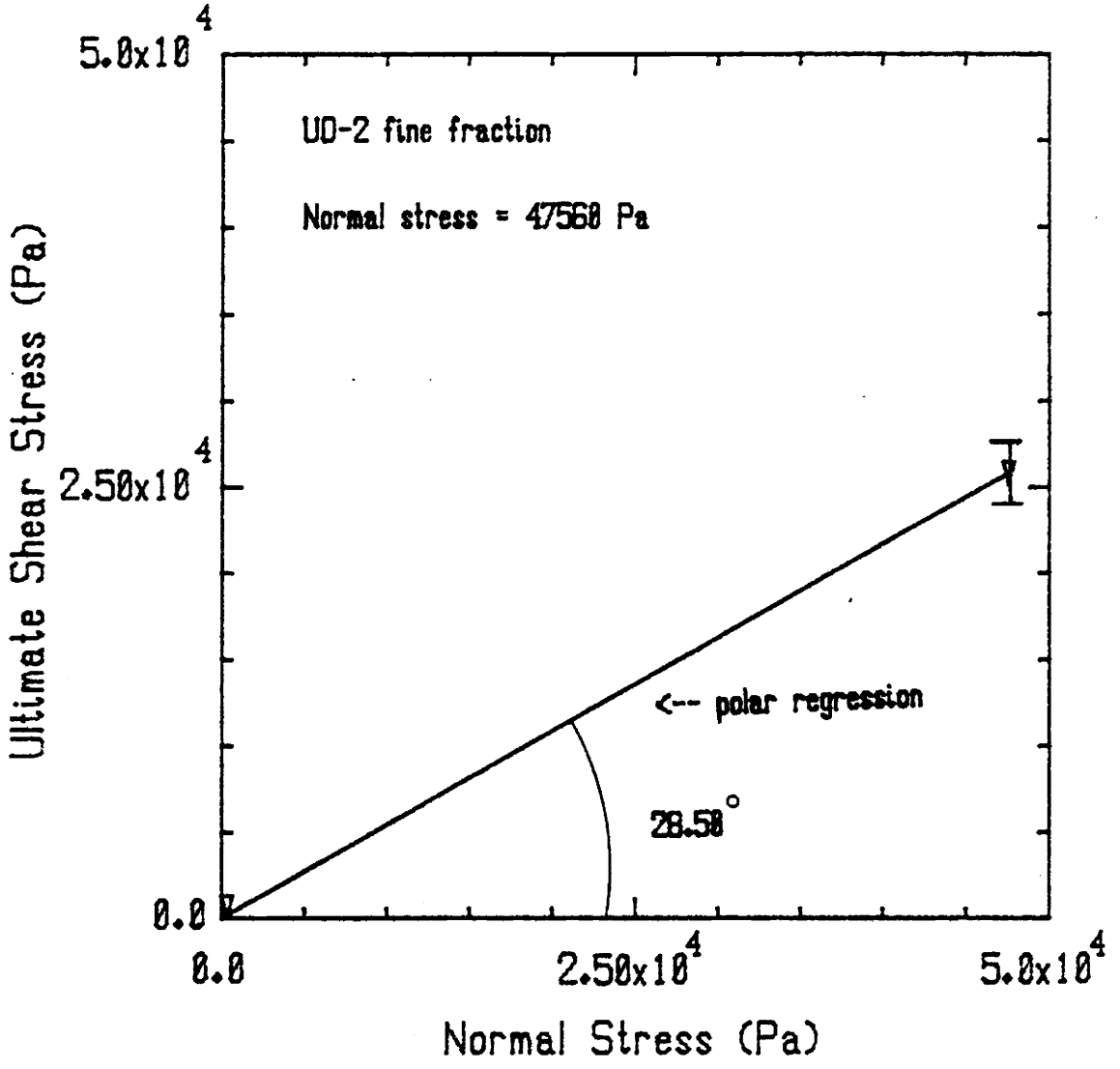

Figure 5.3.11 Polar Regression of Fine Fraction UO_2 Data

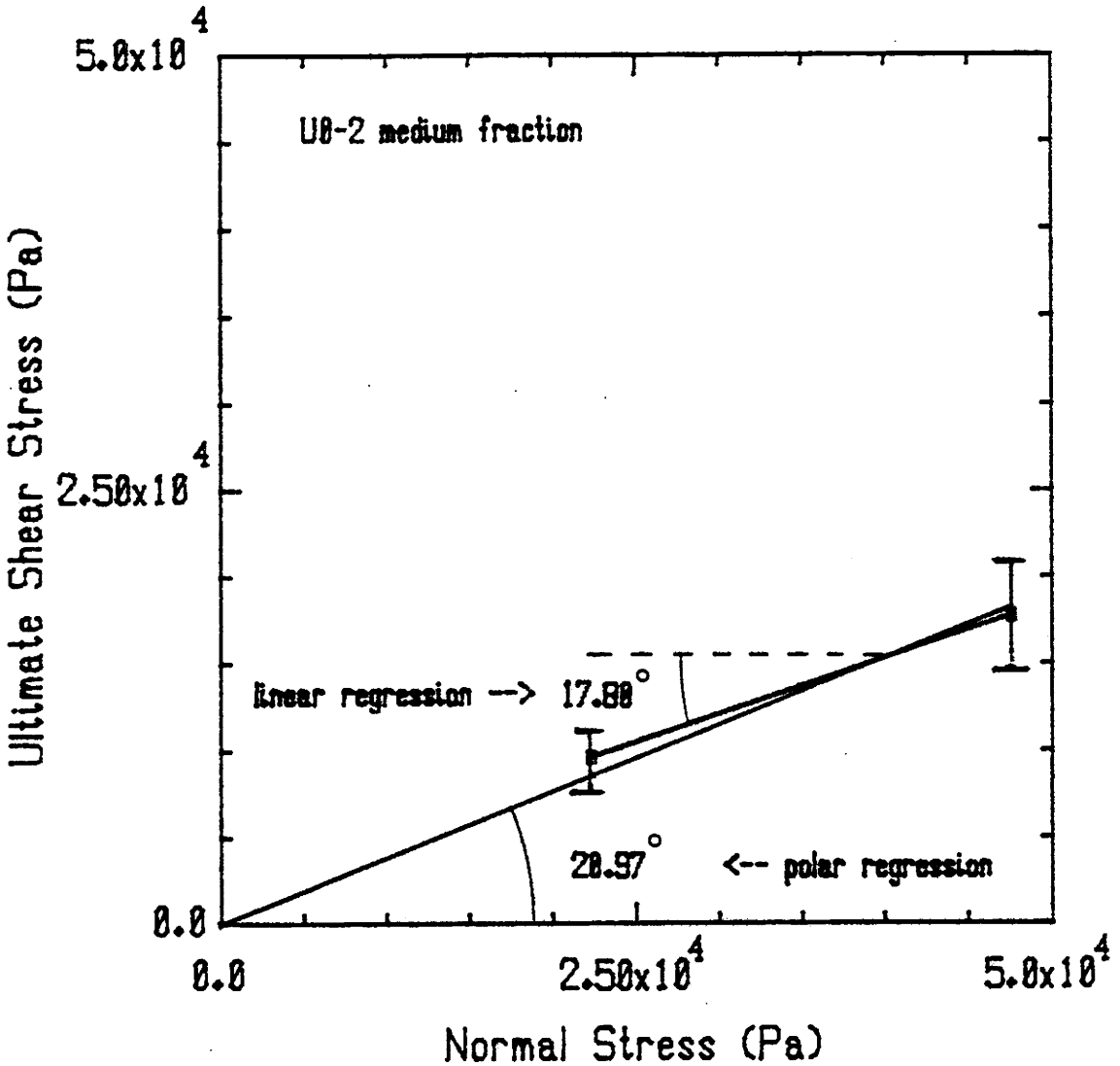

Figure 5.3.12 Polar and Linear Regressions, UO_2 Medium Fraction

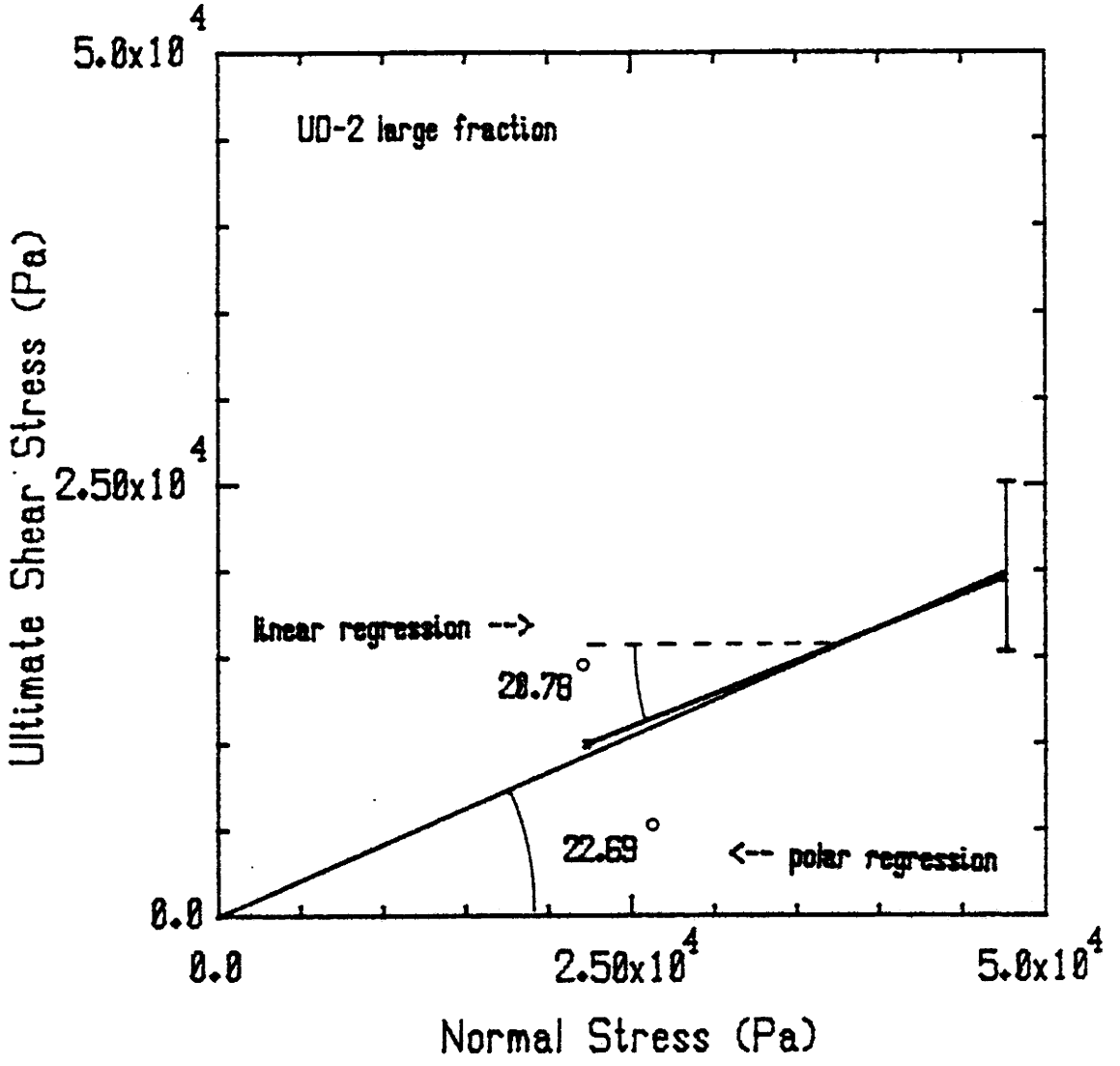

Figure 5.3.13 Polar and Linear Regressions, UO_2 Coarse Fraction

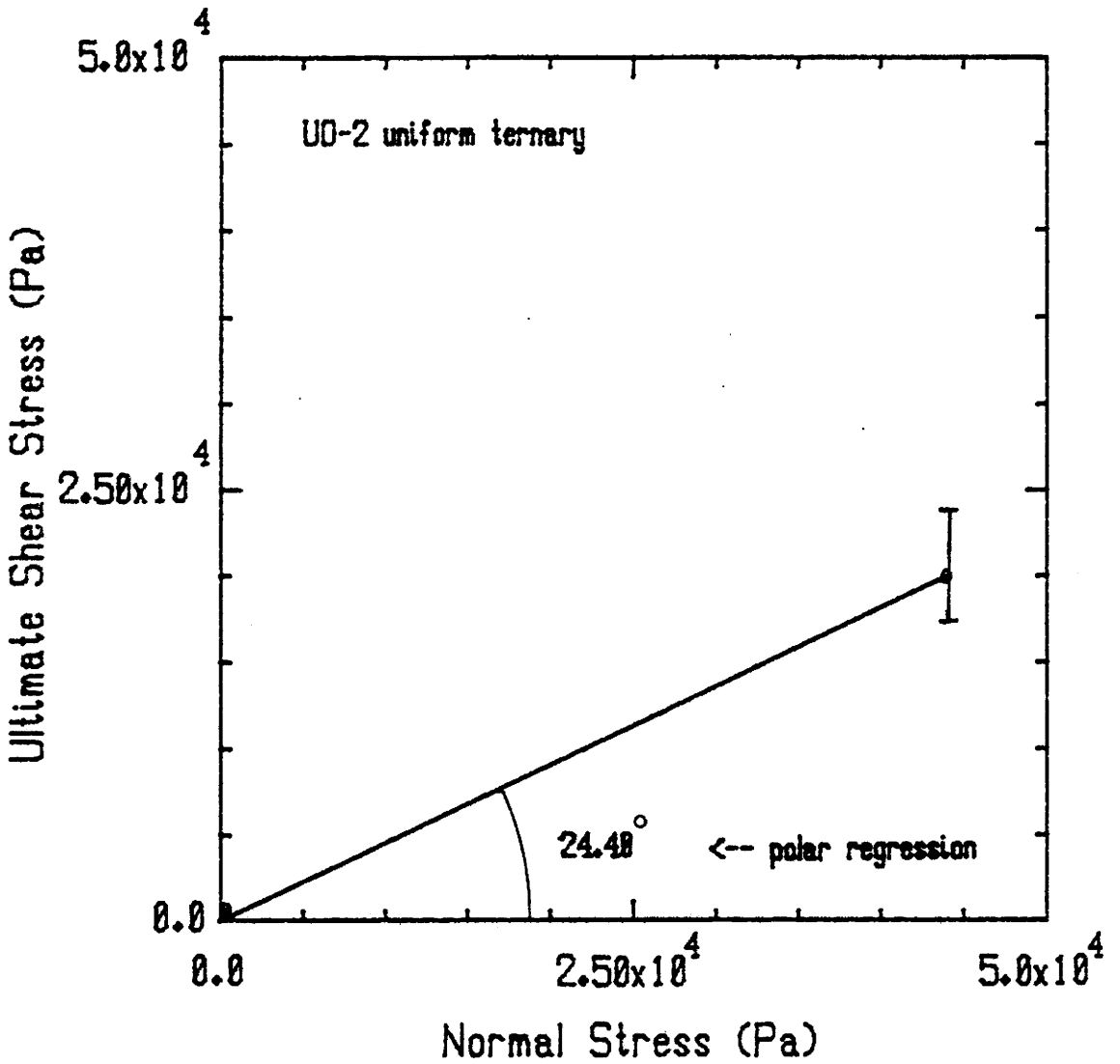

Figure 5.3.14 Polar Regression of Uniform Ternary UO_2

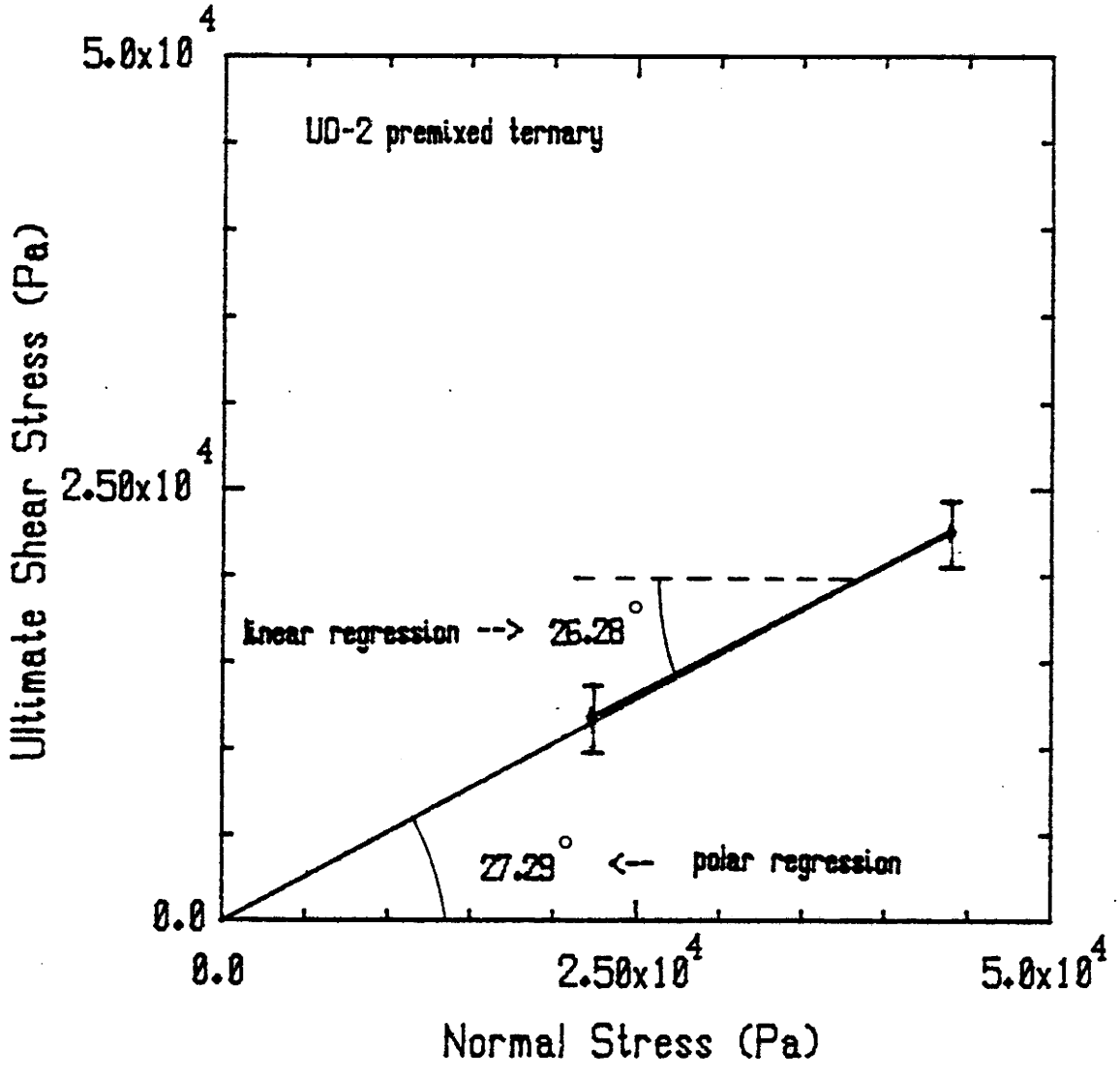

Figure 5.3.15 Polar and Linear Regressions of Premixed Ternary UO_2

Table 5.3.4

Curve parameters and friction angle for uranium dioxide

Material	Φ_{CV} from regression:				
	Linear (^{o})	Polar (^{o})	B	A (Pa)	a
Fine	------	28.50	-------	-------	0.543061
Medium	17.80	20.97	0.321119	2458.60	0.383362
Coarse	20.78	22.69	0.379496	1522.15	0.418015
Ternary (uniform)	------	24.40	-------	-------	0.453623
Ternary (premixed)	26.28	27.29	0.493892	805.978	0.515870

5.3.5 Angle of Repose for UO_2 Microspheres

Angle of repose measurements were carried out for coarse fraction and premixed ternary microspheres in the same manner as for the alumina. Limited supply of material prevented further measurements.

Table 5.3.5 contains the results of the experiment to ascertain the angle of repose for coarse fraction UO_2. The definition of the variables can be found in Section 2.5. Lengths were measured to an accuracy of $\pm$ .05 cm.

Table 5.3.5.

Determination of the angle of repose for the coarse fraction

Test #	H (cm)	L (cm)	H' (cm)	L' (cm)	θ (^{o})	α (^{o})	β (^{o})
1	10.50	16.60	1.90	7.20	39.24	14.78	24.46
2	9.40	16.60	1.05	5.15	34.49	11.52	22.97
3	9.10	16.60	0.50	5.00	33.24	5.71	27.53
4	11.50	16.60	2.00	6.20	43.85	17.88	25.97

The average angle of repose from these measurements for the coarse fraction is 25.23^o with a sample standard deviation of 1.96^o. Assuming a normal population, a 95% confidence interval for this measurement is $(22.11^o, 28.35^o)$.

For the premixed ternary material the experimental and calculational results are indicated in Table 5.3.6.

Table 5.3.6

Determination of the angle of repose for the premixed ternary

Test #	H (cm)	L (cm)	H' (cm)	L' (cm)	θ (^{o})	α (^{o})	β (^{o})
1	11.50	16.60	2.00	6.05	43.85	18.29	25.56
2	11.90	16.60	2.05	5.90	45.80	19.16	26.64
3	10.30	16.60	1.40	6.60	38.35	11.98	26.37
4	11.40	16.60	1.95	6.25	43.37	17.33	26.04

From these measurements, the average angle of repose for the premixed sample is seen to be 26.15^{o} with a sample standard deviation of 0.47^{o}. The corresponding 95% confidence interval for this measurement is $(25.40^{o}, 26.90^{o})$.

Discussion and analysis of these results will be presented in Section 6.3.

6. DISCUSSION AND CONCLUSIONS

6.1 Introduction

The primary objective of the experimental work was to find out whether or not the simple direct shear apparatus, as constructed, could provide a sufficiently accurate value for the friction angle. To accomplish this aim, alumina microspheres were tested.

The results that were obtained with alumina were presented in section 5.2. It will be shown in this section that they were significant and indeed justified using the apparatus for measurements of friction angle. Values obtained from other methods will be compared, and the errors involved in the experiment will be discussed.

Of equal concern to the goals of this work, was the accumulation of data from the direct shear testing of UO_2. The results of the UO_2 tests will be discussed in Section 6.3.

The friction angle for UO_2 microspheres has not been measured previously, and therefore no quantitative comparison with other values can be made. However, results obtained by angle of repose experiments, conducted concurrently with the UO_2 experiments, are available for discussion.

6.2 Discussion of Alumina Results

6.2.1 Stress-Displacement Behavior for Alumina Microspheres

The examples of the observed stress-displacement behavior presented in Section 5.2.2 show agreement with the expected behavior for loose cohesionless materials as described in Sections 2.2 and 2.4. That is to say, the shape of the curve through the average values of the displacements looks the same as the shape of the curve expected for such materials.

Figure 6.2.1 shows the stress-displacement behavior for all of the normal stresses used. All of the curves show a similar shape indicative of the nature of the material. There does, however, appear to be a trend toward steeper slopes near the origin as the normal stress loading is increased. This indicates that the resistance to deformation is increased with associated increase in the compressive load on the material. Of course the ultimate shear stress also increases with increasing normal stress, as is readily apparent in this plot.

One must be careful in drawing any conclusions from Figure 6.2.1, since the behavior of the material in the neighborhood of the origin is almost certainly different than the behavior that was

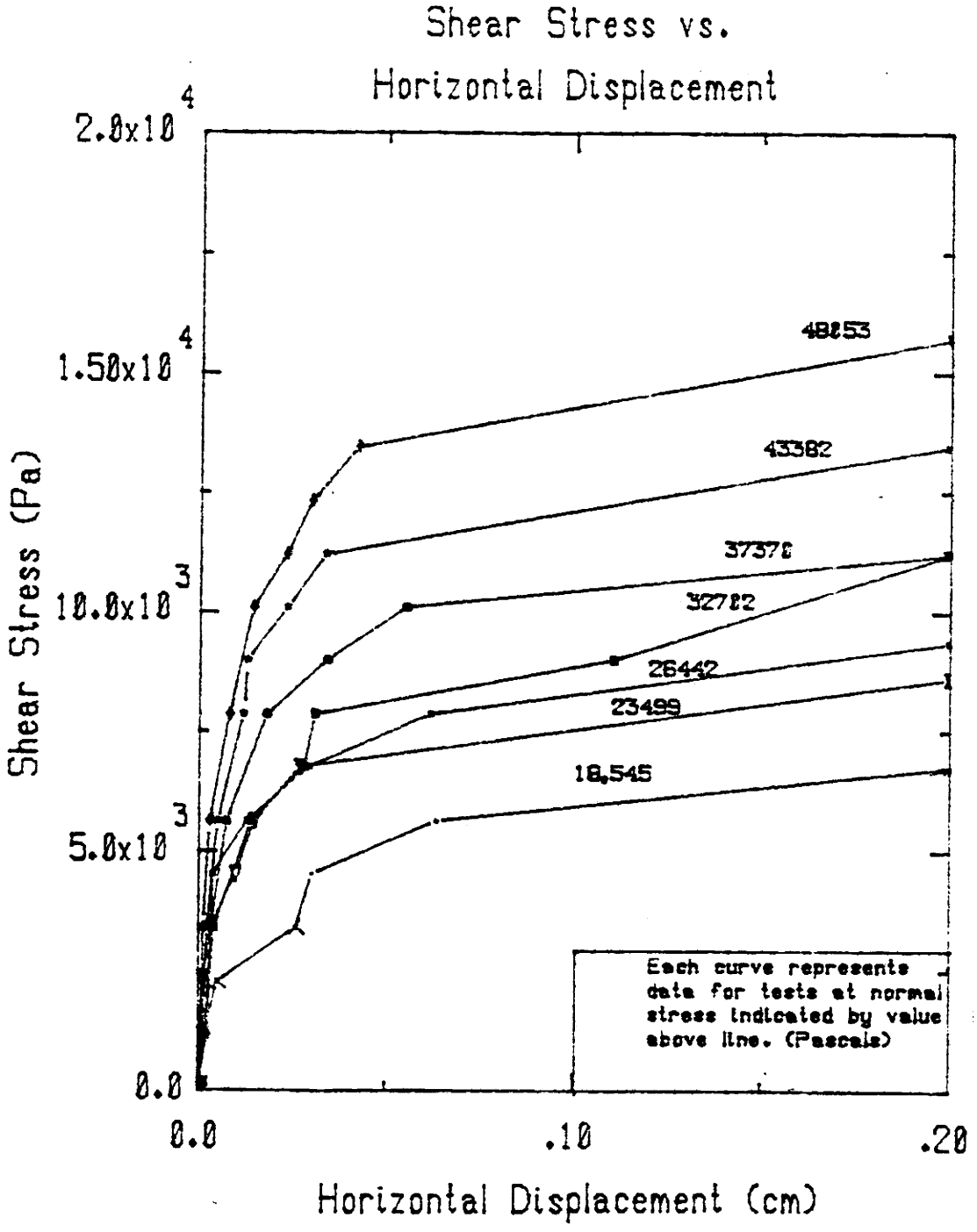

Figure 6.2.1 Alumina Stress-Displacement Behavior

observed. This is due to the fact that the error in our shear measurement was extremely large for small values and overshadows any observable behavior.

6.2.2 Friction angle for alumina microspheres

The regression of the average ultimate shear stress data and the normal stress data (see Figure 5.2.6) produced a linear equation with slope equal to .275117, which indicated a friction angle of 15.382^{o}. A similar determination (8), using a triaxial test device, was found to yield a friction angle of 18.5^{o}. This represents a difference of 16.9%.

Some of this difference may be explained by examining the methods used to determine the parameter for each case. In the current experiment, we express the friction angle as the arctan of the slope of the linear regression through the experimental data. This method incorporates the latest, actually observed, measurements. Extrapolations to larger normal and shear stresses should, therefore, be more accurate.

The method used with data from the triaxial test involved drawing a line from the origin through the data. Here, a larger friction angle is obtained, since the "pseudo" data point at the origin is not assigned equal weight statistically as the other sets of data points from the experiment. This produces a good approximation to the behavior of the material from the (0,0) stress

state to the range of values measured in the experiment (up to about (17000,50000) Pascals (τ,σ)).

When the the result of the polar regression shown in Figure 5.2.7 is compared to the friction angle determined in the triaxial experiment, the difference is less, because the method employed to determine the friction angle is similar. Here, the friction angle was found to be 18.11^{o}. This represents a difference of 2.11% from the triaxial value.

Another measure of the friction angle is the angle of repose measurements reported in Section 5.2.4, where an average value of 24.96^{o} was calculated. This parameter represents the value of the arctan of the slope of the curve at some point very close to the origin, since the angle of repose is a measure of the shear stress, normal stress behavior for the material in a pile with no external load. Therefore, only the weight of the material particles constitutes a normal stress, and the shearing force, which is just a component of the gravitational force vector, is relatively small.

Hence, the angle of repose should compare favorably for measurements of ultimate shear stress and normal stress near the origin. The lowest shear and normal stresses observed in the experiment were for the first lot. Figure 6.2.2 shows a polar regression of the data from lot #1 including the pseudo data point (0,0). For this regression the slope calculated was .364519 which gave

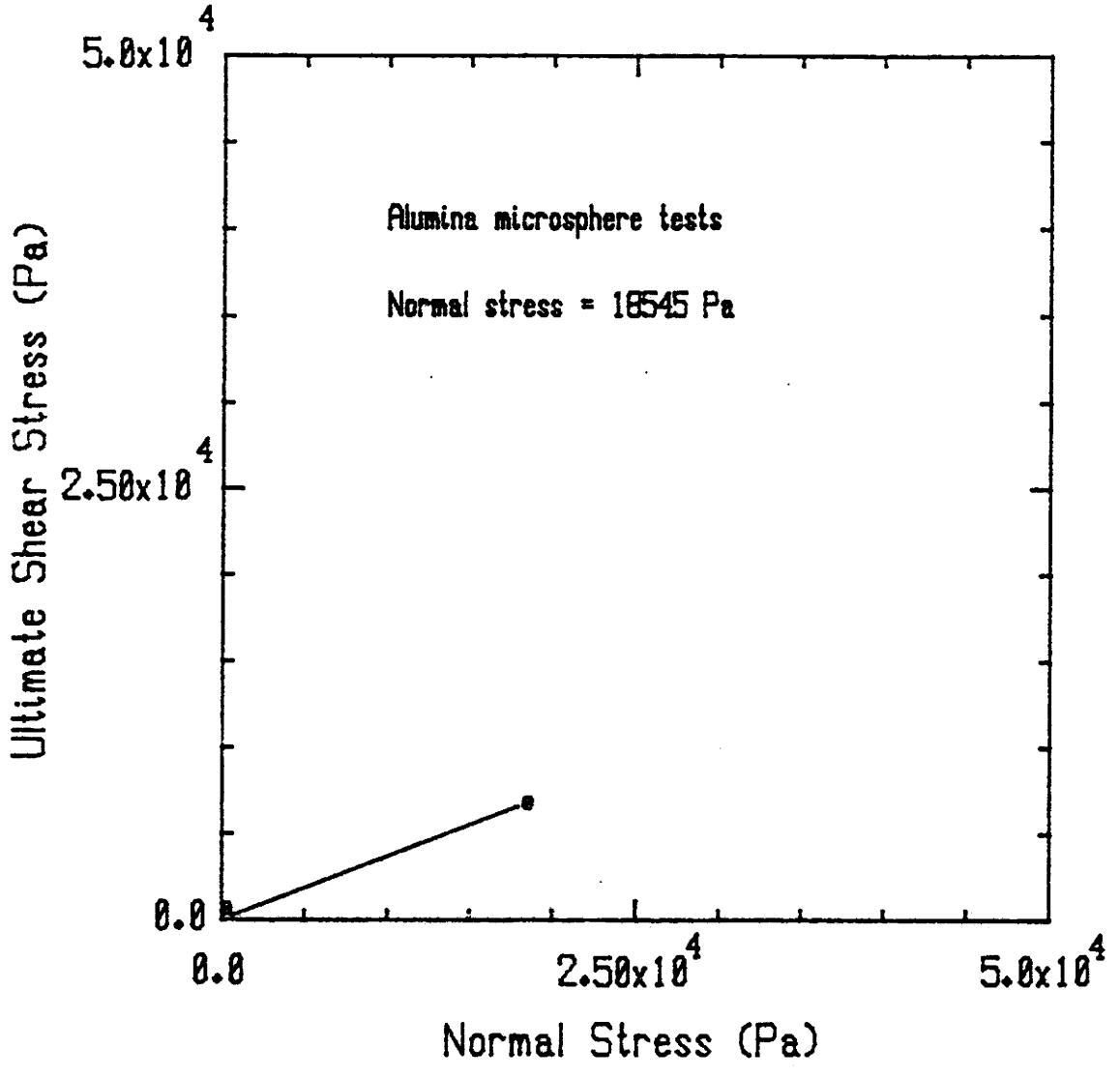

Figure 6.2.2 Polar Regression of Alumina Data Near the Origin

$$\phi_{CV} = 20.03^{o}$$

This, however, does not compare favorably with the angle of repose measurement, representing a difference of 19.75%. This indicates that the experimental observations were, indeed, sufficiently far from the origin to prevent an adequate approximation of the angle of repose.

Figure 6.2.3 shows a graph of the average ultimate shear stresses as a function of the normal stress. The purpose of this plot is to indicate the range of potential friction angles which could be obtained if only one normal stress had been used for each calculation, and the data regressed with a polar regression. This is the method suggested when using the Mohr-Coulomb failure criteria for cohesionless materials since, theoretically only one point is required.

From this discussion, it is evident that the approximation of the friction angle can be broken down into 4 regions, shown graphically in Figure 6.2.4. Region I is at or near the origin and is approximated most suitably by the angle of repose measurement 24.96^{o}. Region II is the region of extrapolation from the origin to the data and is adequately represented by the polar regression value of 18.11^{o}. Region III represents the region over which no extrapolation is required as this is the range of observed values. The linear repression in this range is good and the value of ϕ_{CV} equal to 15.38^{o} is a good indication of the failure envelope.

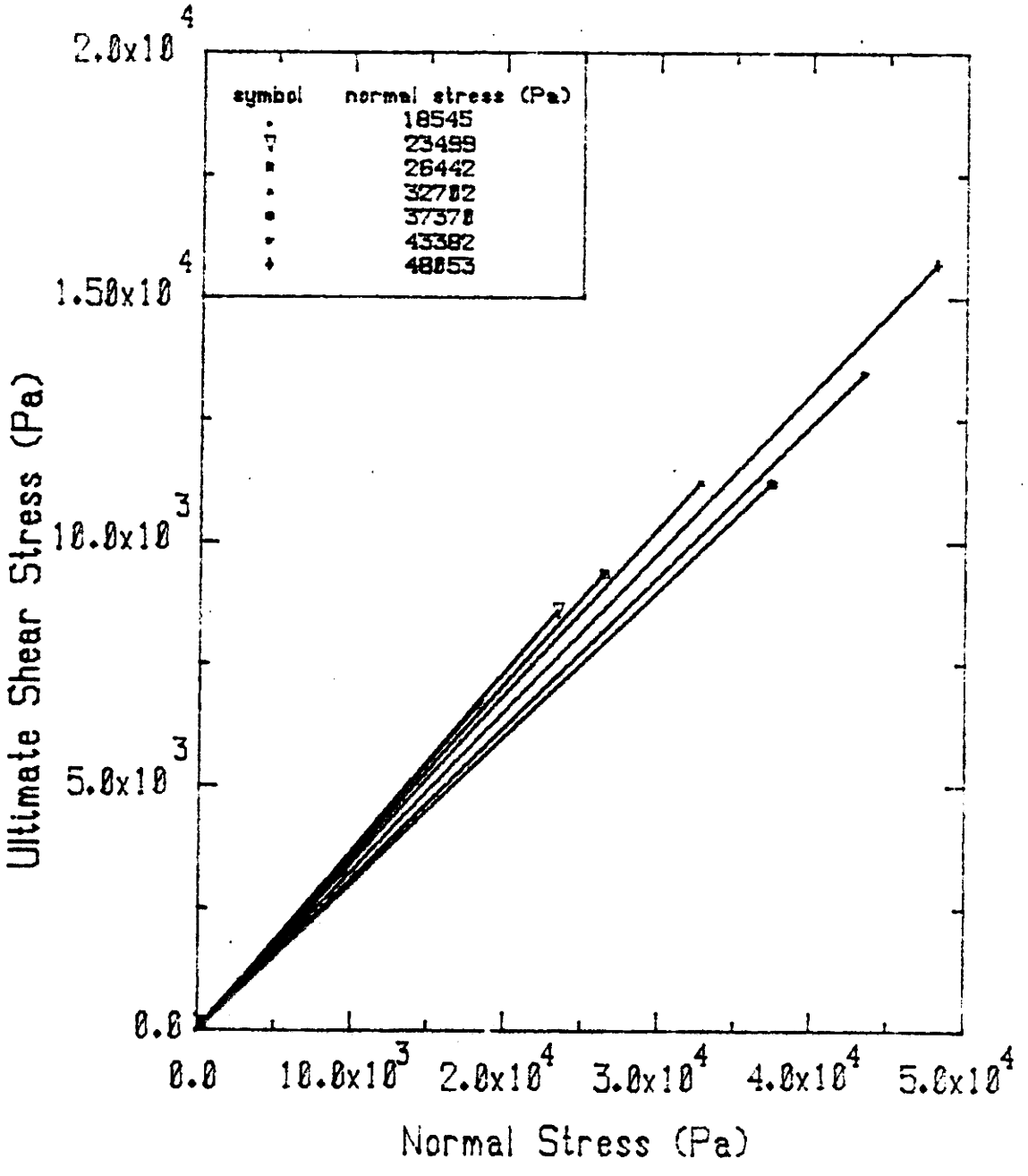

Figure 6.2.3 Average Alumina Ultimate Strength Polar Regressions

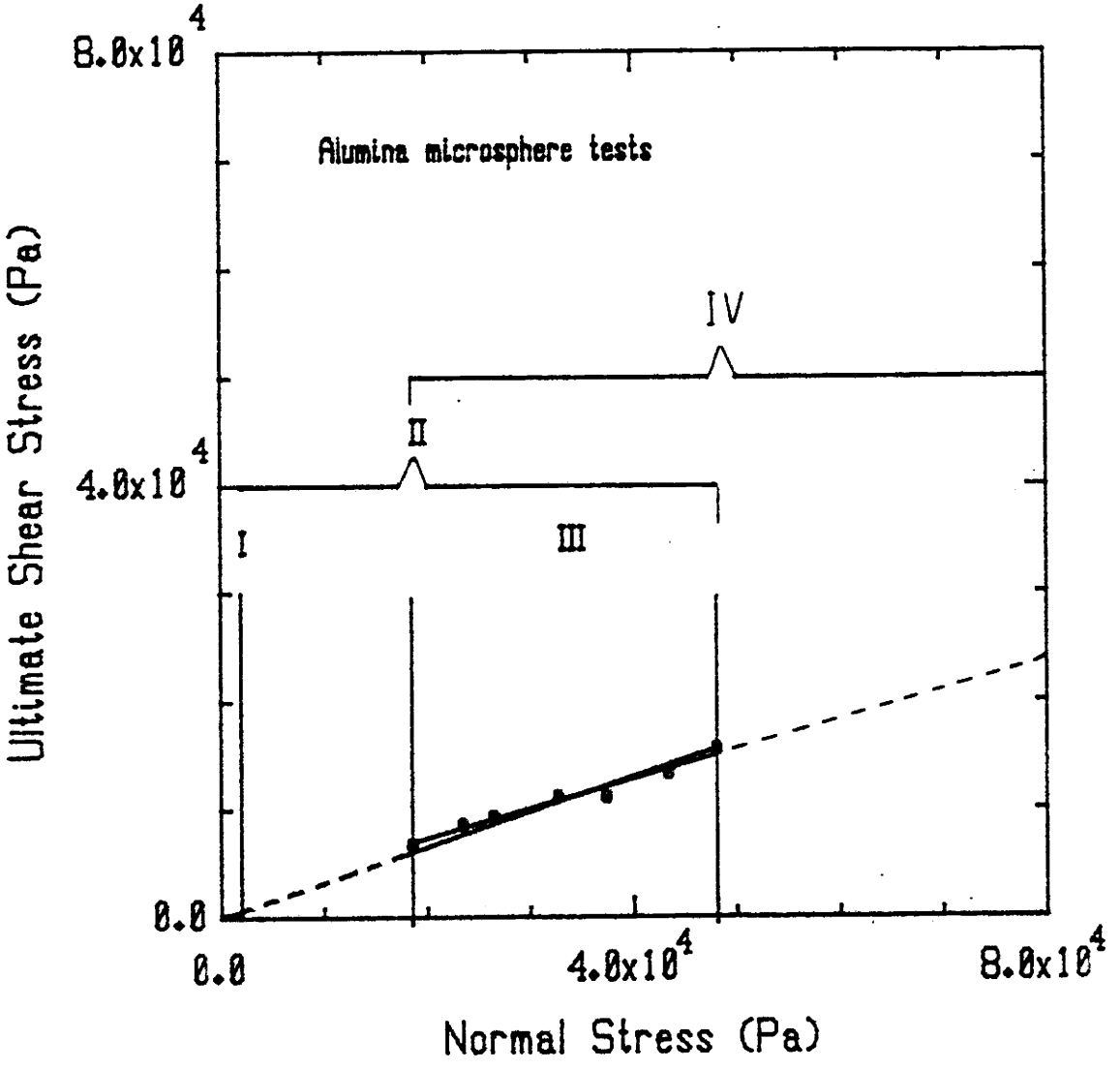

Figure 6.2.4 Friction Angle Approximation Regions

Region IV represents extrapolation beyond the range of observed data.

Here, it is evident that extrapolation of the polar regression of the data would produce a much larger expected ultimate shear for the material than extrapolation of the linear regression of the data. This is surely the case, since the linear regression gives the "latest" information regarding the behavior of the curve. Figure 6.2.5 shows the difference in the two extrapolation methods when projected to a value of normal stress of 60,000,000 Pascals. This stress is certainly possible in practice (thermal loads, for example).

With extrapolation over this range, a higher ultimate shear stress is predicted with the polar extrapolation than with the linear extrapolation. This does not represent a conservative engineering approach to modeling as far as safety considerations are concerned, since the yielding point predicted by a model employing this higher value would assume that a material is stronger than it actually is. The use of the polar extrapolation method is really only accurate over the region between the origin and the observed data.

Yet, the linear extrapolation may not accurately predict the behavior of the material, either. It represents the best estimate, nevertheless, considering the range over which the observations were made.

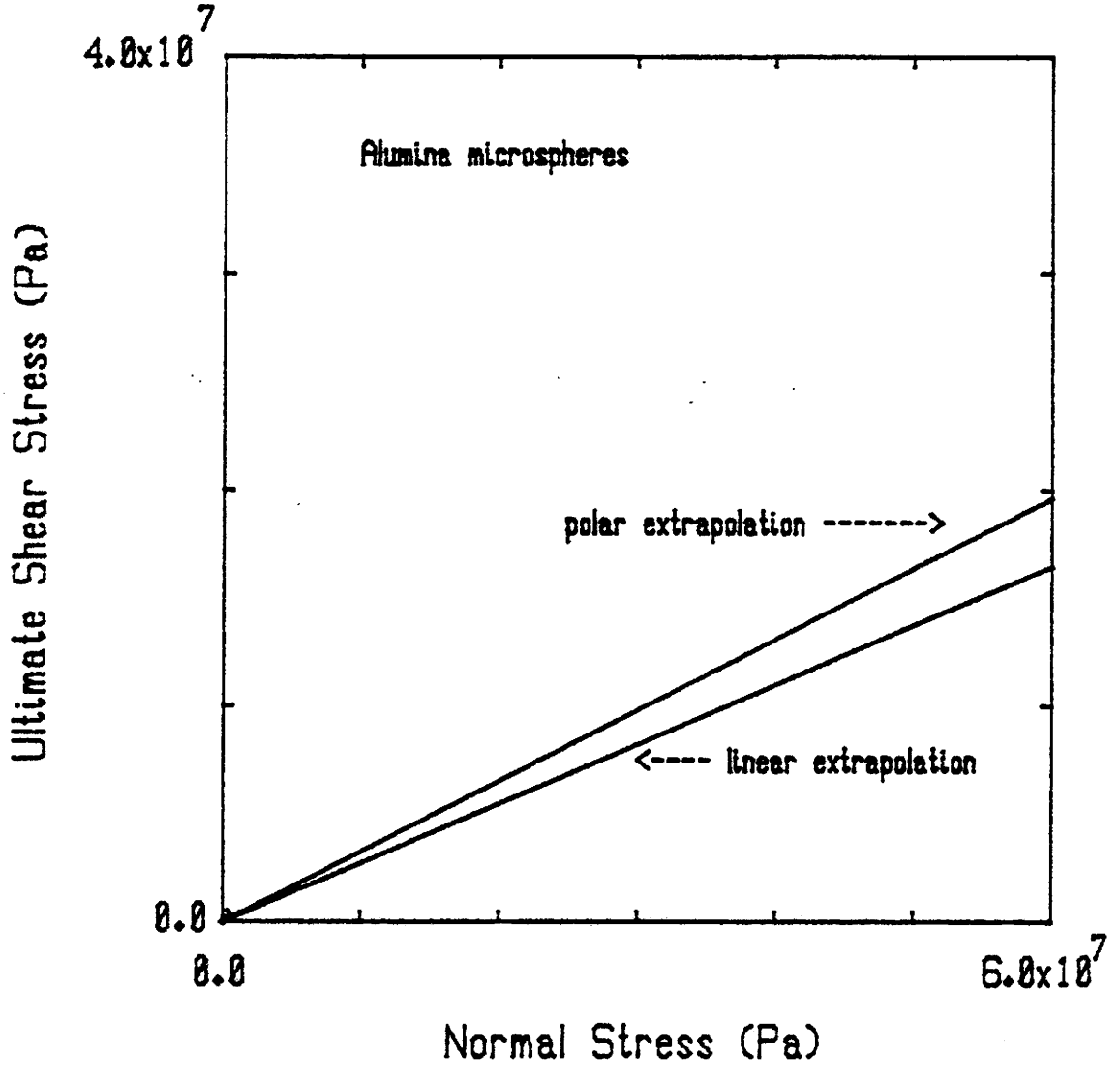

Figure 6.2.5 Potential Error with Polar Extrapolation Method

6.2.3 Feasibility of Testing UO_2

As it stands, the apparatus has proven itself to be an effective tool in the study of the mechanical behavior of alumina microspheres. Although it does not provide accurate measurements in the range of displacements close to zero, it does give acceptable results in the region of ultimate shear stress. The behavior of the material in terms of displacement under shear stress at points close to the origin, and, in fact, up to the point of failure,is of secondary concern. The determination of the friction angle is the primary consideration, here. Therefore, accuracy in predicting the friction angle should be of major importance in determining the feasibility of the direct shear device for testing sphere-pac nuclear reactor fuel.

An error analysis of the alumina friction angle (see Appendix A) shows that

$$\text{var}(\phi_{CV}) \sim \text{var}(\bar{S}) \qquad (6.3.1)$$

where $\bar{S}$ is the average of the scale readings at ultimate strength. The relative error for ϕ_{CV} is composed of the error directly attributable to measurement uncertainties (2.3%) plus error due primarily to the limited number of observations (2.01%).

While this may seem relatively high compared to the minimum

engineering standard acceptable error of 2%, it was decided, nonetheless, to proceed with testing of the UO_2 microspheres. The reason for this is that the apparatus had performed well within the confines of the hood environment required for the UO_2 tests and, thus, feasibility from the standpoint of operations had been established.

In addition, the containment system employed with the sphere-pac experiments required testing to insure that future observations, with improvements in the measurement equipment, could actually be made for the radioactive material. If the containment proved too awkward or otherwise unfeasible, it would be imprudent to make expensive design improvements in measurement equipment that would never be employed.

Observations of the stress state of UO_2 did, indeed, prove rewarding as will be explained in the next section.

6.3 Discussion of the Test Results for Sphere-Pac Material

6.3.1 Stress-Strain Behavior for UO_2 Microspheres

The stress-strain behavior of UO_2 microspheres depicted in Section 5.3.2, Figures 5.3.4 through 5.3.8, is consistent with what would be expected for loose cohesionless material and resembles the behavior exhibited by the alumina microspheres.

Figures 6.3.1 through 6.3.3 show the stress-displacement behavior for medium, coarse, and premixed ternary UO_2, respectively, for two different values of normal stress. Like alumina, the UO_2 curves show a steeper slope for higher values of normal stress, indicating increased resistance to shear stress at greater compression.

Recalling the confidence intervals of Figure 5.3.4, one can readily see that the variability, due to the shear stress and displacement error, is extremely high for all of the points from which the curve was constructed. Therefore caution should be exercised in making comparisons between the pairs of stress-strain curves. Conclusions drawn from statistics which do not show a significant difference at an acceptable confidence level are not reliable inferences, but merely speculations based on insufficient information.

With this in mind, a comparison of the stress-strain behavior

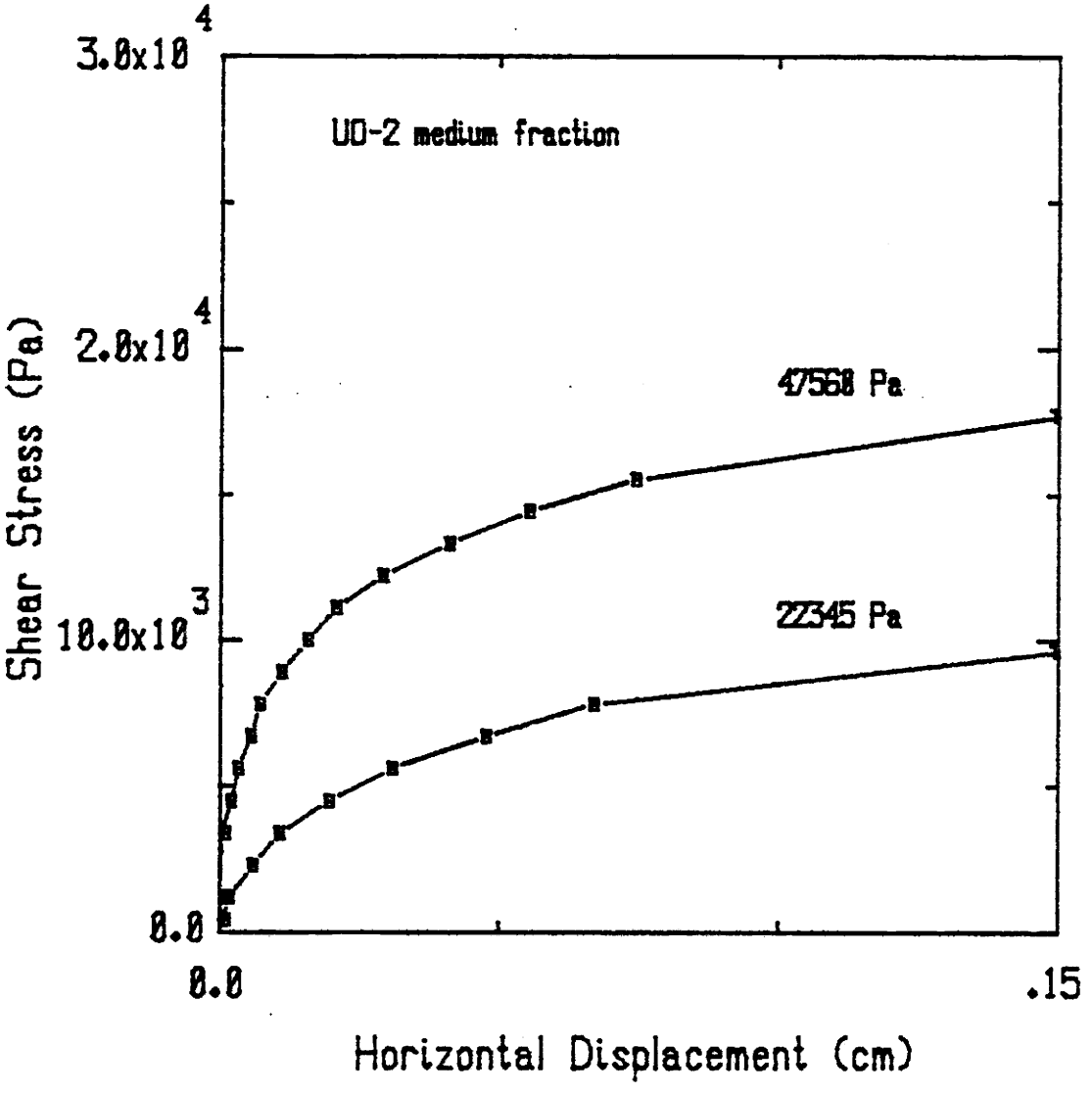

Figure 6.3.1 UO_2 Medium Fraction Stress-DIsplacement Behavior

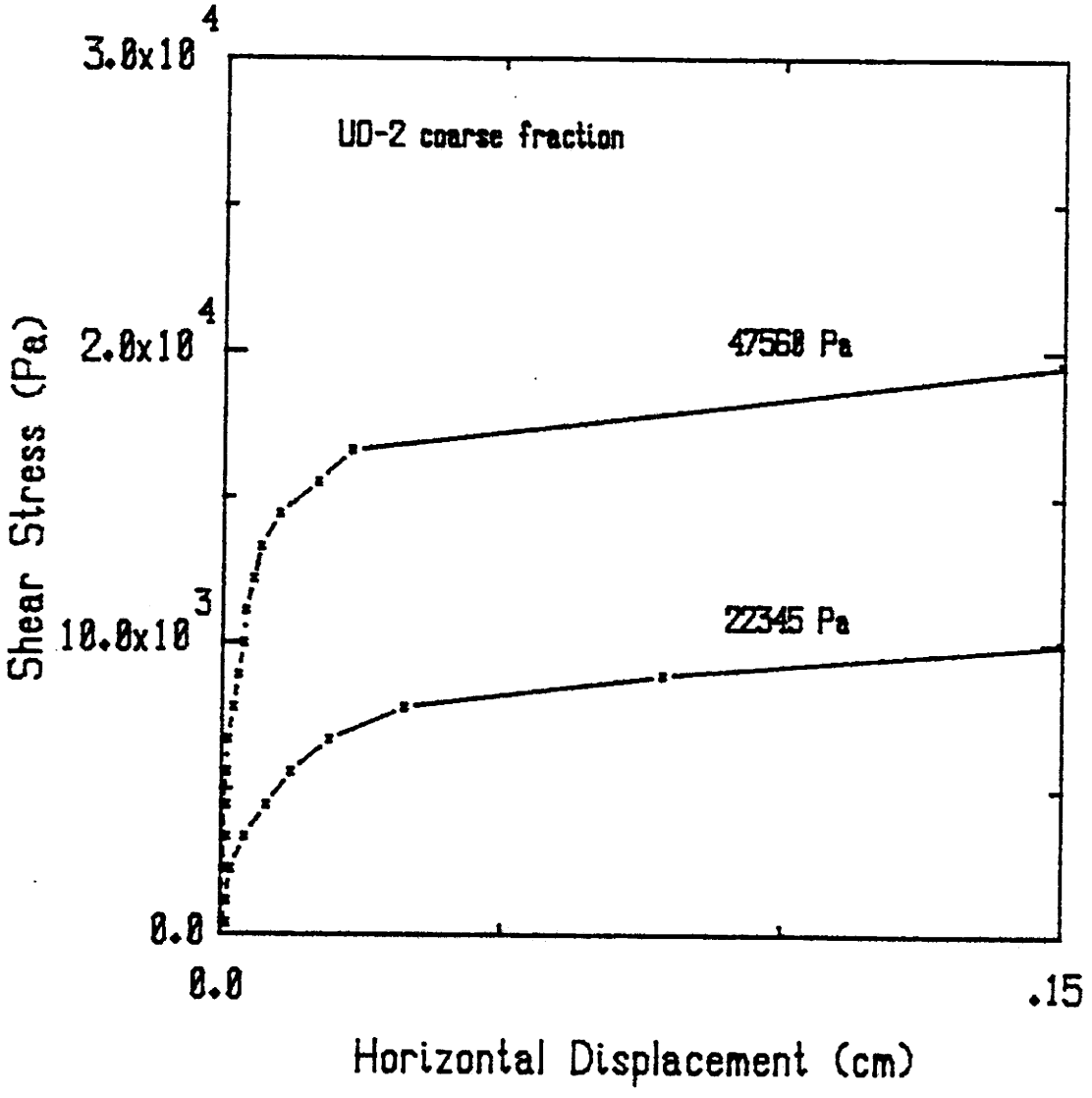

Figure 6.3.2 UO_2 Coarse Fraction Stress-Displacement Behavior

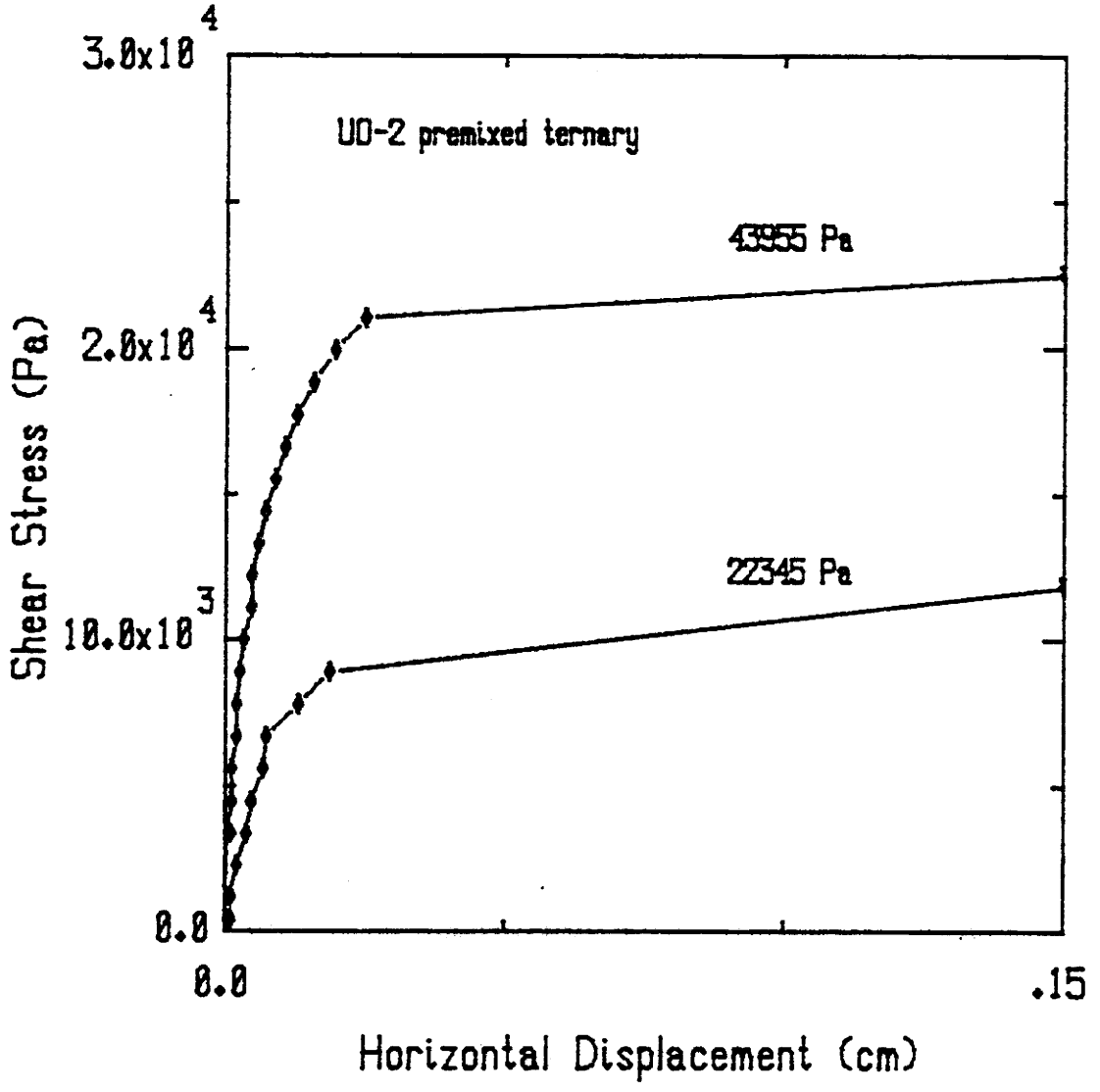

Figure 6.3.3 UO_2 Premixed Ternary Stress-Displacement Behavior

for single fraction UO_2 microspheres was made by graphing the test results for fine, medium and coarse fractions. Displayed in Figure 6.3.4 is the shear stress versus displacement curves for the three fractions, tested separately, at a normal stress of 47560 Pa.

The coarse fraction appears to have the steepest slope of the three in the neighborhood of the origin, which is perhaps indicative of the initial interlocking characteristics of the coarse spheres. The smaller particles, on the other hand, are less influenced by this effect, and resist movement more in relation to the degree of surface-to-surface contact attained. This explains the occurrence of a steeper slope for the fine fraction UO_2 than for the medium fraction UO_2.

In addition, the fine fraction is composed of a mixture of comparatively irregular spheroids, some of which are stuck together or broken, and consequently the associated internal friction is higher. This is because the rolling, lifting, and sliding motions associated with the movement of the particles during shear are not in the same direction as the applied force. Hence, the displacement is not achieved as easily.

It can also be seen that the ultimate strength of the fine fraction is higher than the ultimate strength of the medium or coarse fractions. Again, this is due to the increased internal friction exhibited by these small, rather irregular, spheres. From this, one would expect that addition of fine fraction to a medium, coarse mixture would improve the strength characteristics of the

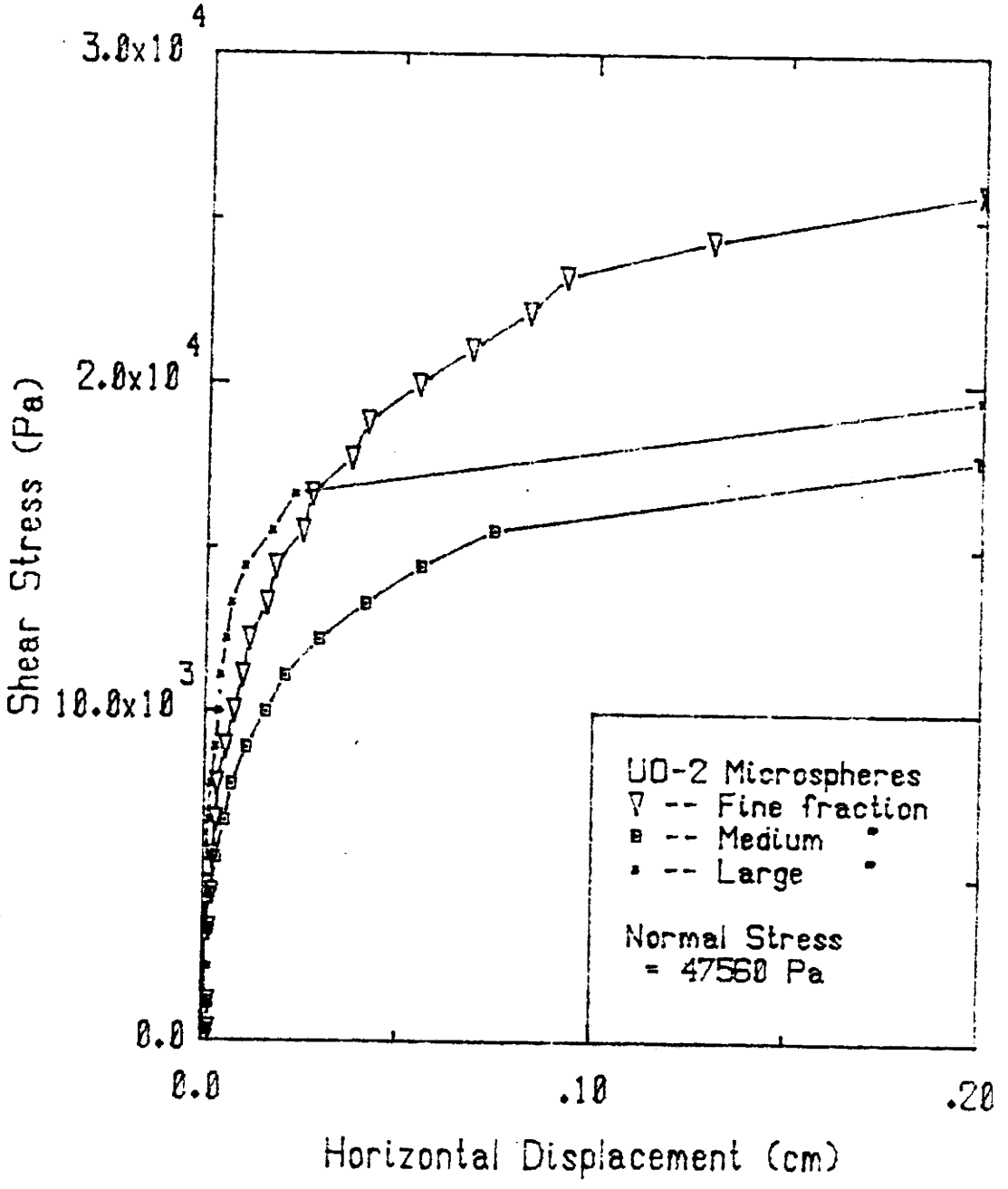

Figure 6.3.4 UO_2 Single Fraction Stress-Displacement Comparison

material.

By referring to Table 5.3.3, one can see that the confidence interval for fine fraction average ultimate shear stress at a normal stress of 47560 Pa, does not include the values which are given as the average for the medium and the coarse fraction. Therefore, a significant difference exists between the results of the fine and those of the coarse and medium. This is not the case when a comparison is made between the coarse and the medium ultimate shear stresses, however, as the confidence interval for the medium fraction includes the average value of the coarse fraction. Thus it is tenable that there might, indeed, be no difference in the ultimate shear stress for these two sizes. At least, without further observations, this is what we must conclude.

Figure 6.3.5 shows another stress-strain comparison. Here, the uniform mixture exhibits a lower ultimate shear stress than the premixed material. Observation of the 95% confidence intervals in Table 5.3.3 for the ternary uniform and the ternary premixed materials show some overlapping with the CI for the ternary uniform including the mean value of the ternary premixed. Therefore, we cannot conclude that there is a significant difference between the two sample means. Hence, it is tenable that the mixing technique had no affect on the outcome of the experiment. More observations are necessary to ascertain whether or not this is, truly, the case.

A comparison of all the different mixtures is presented in

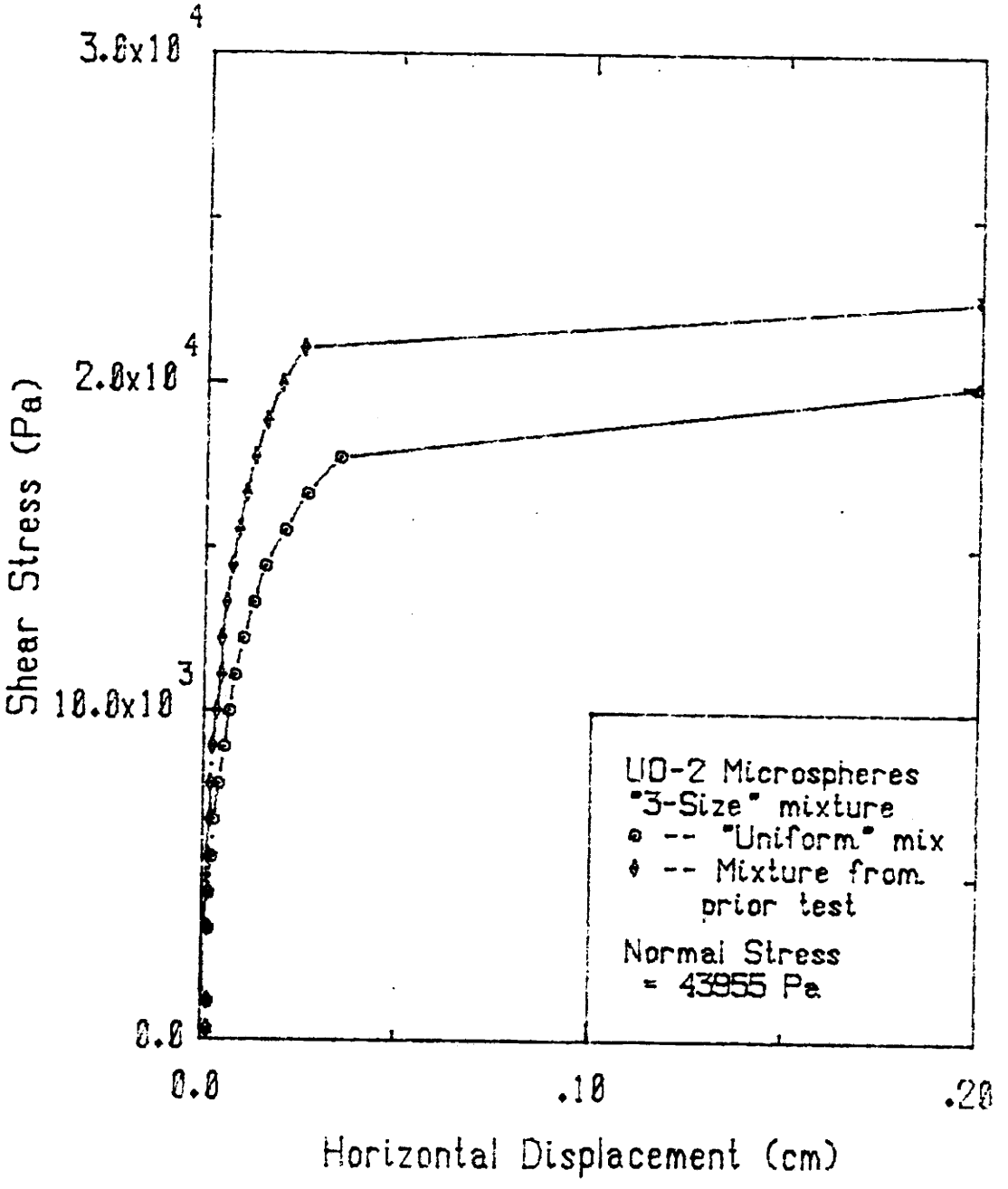

Figure 6.3.5 UO_2 Ternary Fraction Stress-Displacement Comparison

Figure 6.3.6. It appears that the addition of fine fraction to a medium, coarse fraction does indeed result in a higher ultimate shear stress than for either medium or coarse alone. There is a significant difference between the premixed ternary mixture, which includes 22 wt% fines, and either the medium or the coarse fraction ultimate shear strength. Although the comparisons are not at equal normal stresses, it is evident that because the normal stress of the ternary mixture is lower than that of the single fractions, the significance would hold if the normal stresses were equal. This is true if we assume that the ultimate shear strength for the premixed ternary will continue to increase with increasing normal stress.

The "unloading" curves shown in Figures 5.3.9 and 5.3.10 show what appears to be the effects of "strain hardening". Strain hardening is a condition exhibited by some metals which is typified by increased resistance to further displacement after the metal has been strained beyond its elastic limit, unloaded and subsequently subjected to more stress.

A similar behavior is indicated by the UO_2 medium and coarse fractions. As indicated in the figures, there is a tendency for the displacement to resume at a higher shear stress after unloading.

6.3.2 Friction Angle for UO_2 Microspheres

No independent data were available for comparison with our experimental observations. The only comparison possible was with

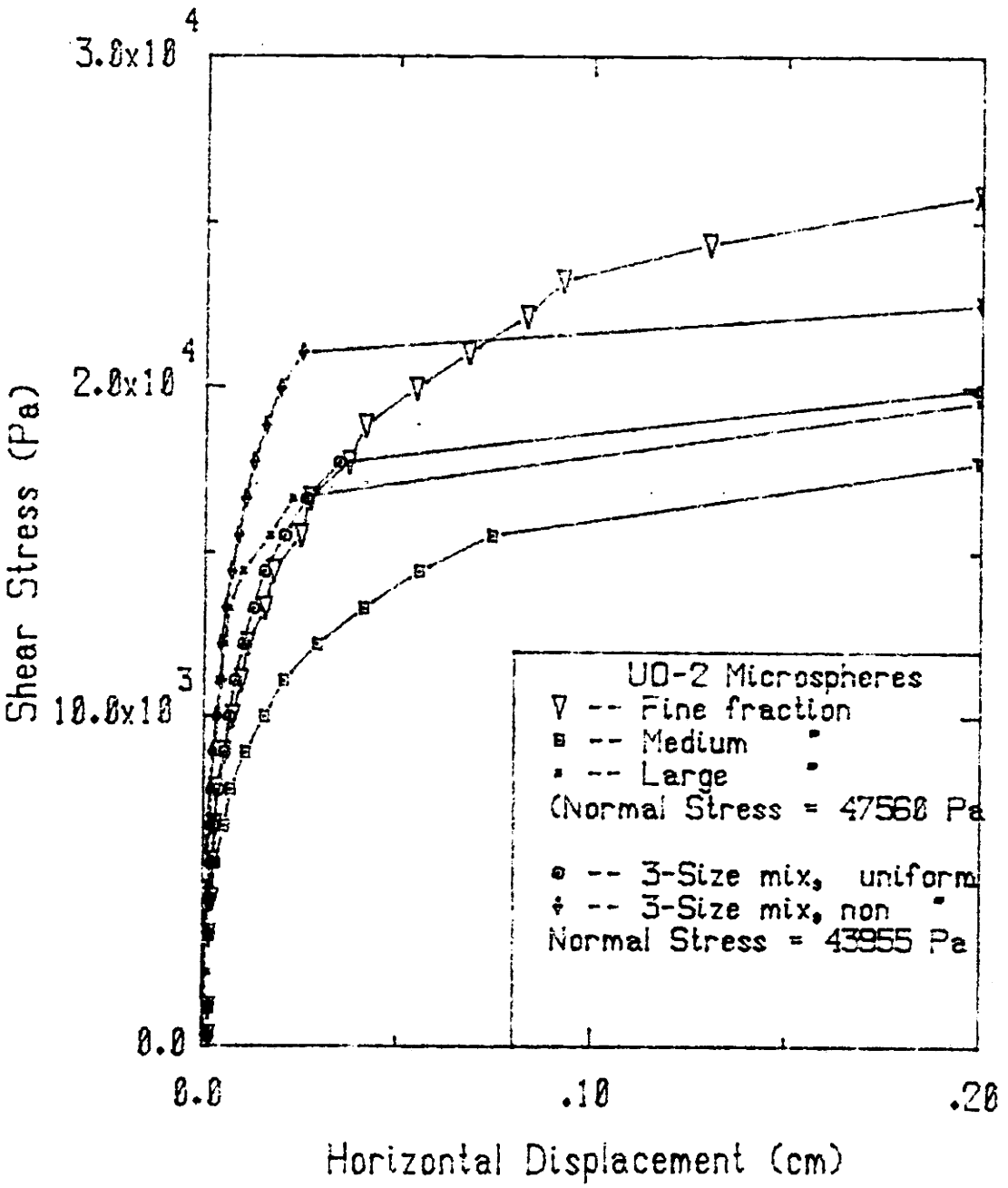

Figure 6.3.6 UO_2 Stress-Displacement Comparison (All Materials)

our angle of repose measurements. These compare favorably.

Friction angles for different regressions of the data were given in Table 5.3.4 which also lists the associated curve fitting parameters. Two materials for which the angle of repose was obtained are the coarse fraction UO_2 and the premixed ternary UO_2. For these, the friction angles calculated from the polar regression, which should compare favorably with the angle of repose measurements, were 22.69^{o}, and 27.29^{o},respectively, for the two materials. (See section 6.2.2 for a discussion of which regression should be used.)

The results of the angle of repose experiment with the coarse fraction, listed in Table 5.3.5, indicate an average value of 25.23^{o}. The friction angle for this fraction is within the 95% confidence interval of the average angle of repose. Therefore, the coarse fraction UO_2 friction angle compares favorably with the associated angle of repose measurement. To determine actual statistical significance, the test with independent samples should be employed as indicated in Appendix A.

However, the angle of repose measurements for the ternary mixture, depicted in Table 5.3.6, appears to show a significant difference from the friction angle measurement. This may be due to the relatively few number of experiments performed with this fraction. In addition, there was an inherent variability due to the random nature of the mixing, which would make the measurement inconsistent.

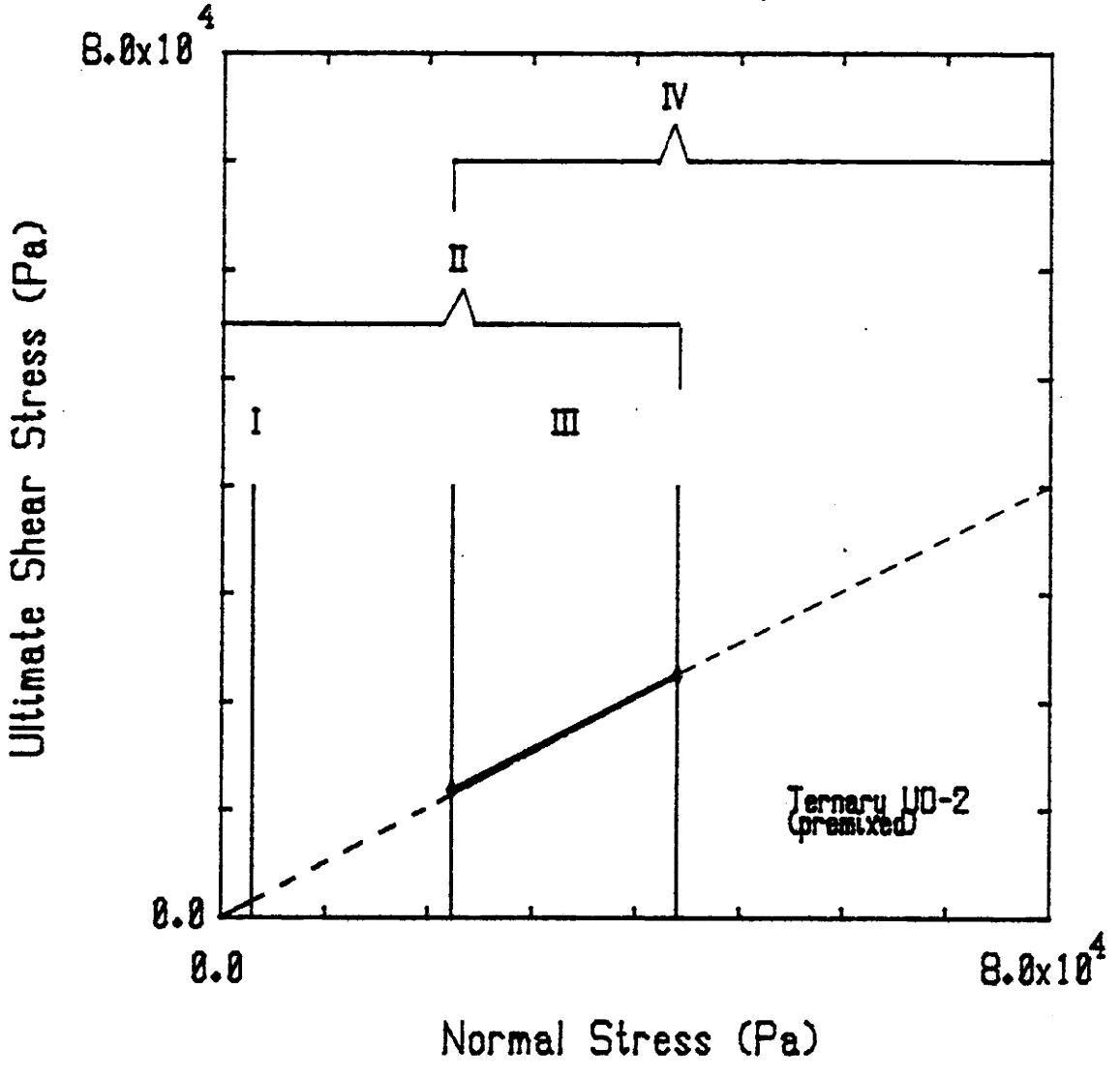

Figure 6.3.7 UO_2 Friction Angle Approximation Regions

Figure 6.3.7 shows the regions of approximation for the friction angle for premixed ternary UO_2. Region I is best approximated by the angle of repose value and is arbitrarily close to the origin. Region II, which extends from the origin through the experimental results, represents a domain over which the polar regression value is acceptable. The observed data are in region III and are best approximated by the linear regression of these values. Region IV represents extrapolation beyond the range of observations and is best approximated by the latest information available, namely the extrapolated linear regression from Region III.

The polar and linear regressions for the ternary case are shown in Figure 6.3.8 where an extrapolation of each curve has been made to a point corresponding to a maximum normal stress of 6.0×10^7 Pa. This represents a practical value produced in operating conditions during mechanical loadings such as thermal transients. The polar extrapolation predicts an ultimate shear stress which is 1.32 MPa (1.32×10^6 Pa) higher than the ultimate shear stress predicted by the linear extrapolation, approximately a 4.4% difference.

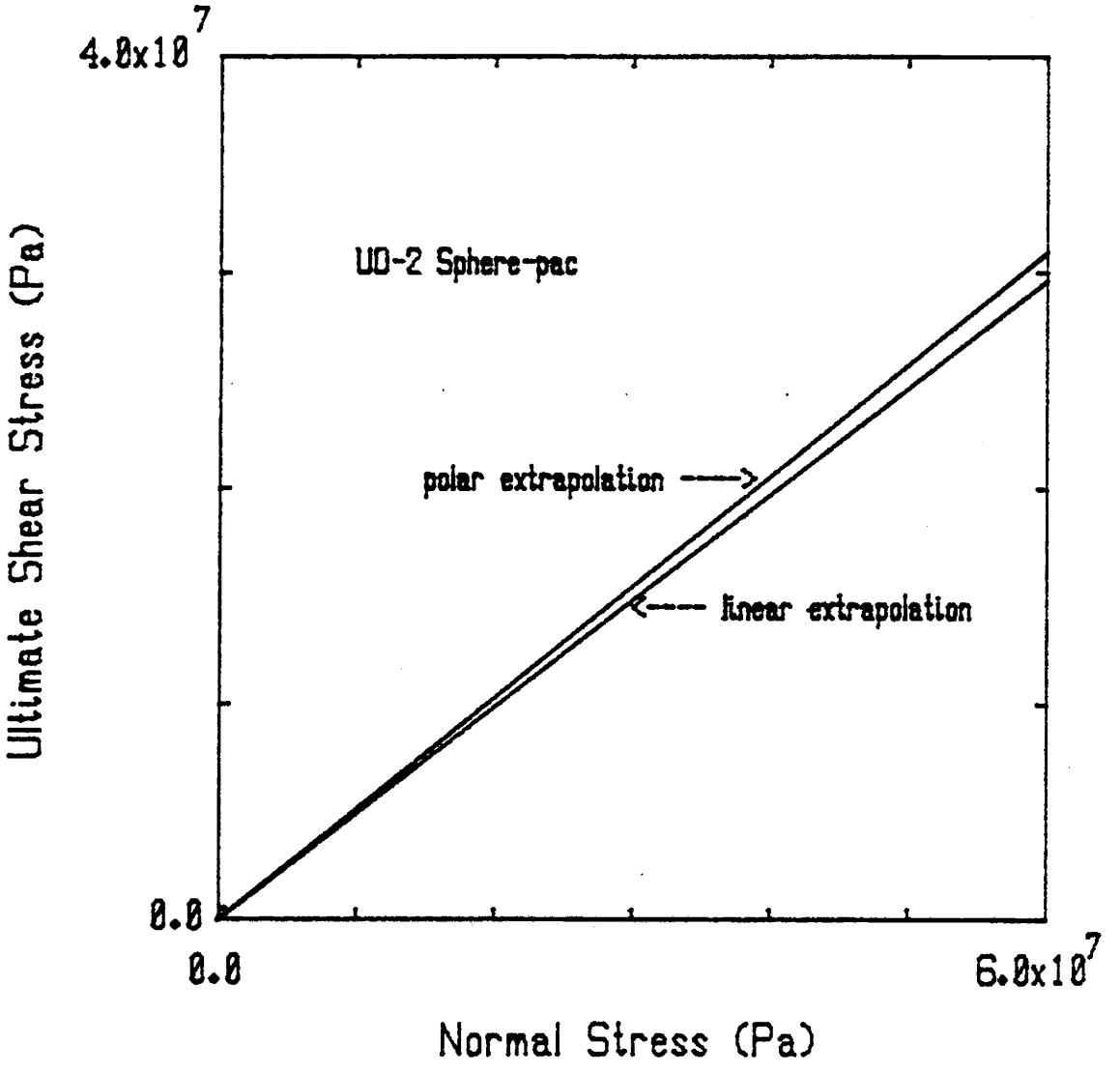

Figure 6.3.8 Potential Error with Polar Extrapolation of UO_2 Data

7. SUMMARY AND SUGGESTIONS FOR FUTURE WORK

7.1 The Current Experiment

Since the present generation of reactor fuels may not be well suited to extended burnup applications, current studies are underway to evaluate alternative fuel materials. Sphere-pac fuel is one of the candidates.

As part of the continuous effort to evaluate this alternative, the present experiment was conducted to ascertain one of the important parameters required in modeling the mechanical behavior. This parameter is the friction angle, Φ_{CV}, which indicates the behavior of a curve relating the stress at which a material yields to the normal (compressive) stress state of the material. The Mohr-Coulomb equation was introduced as the criterion for evaluating this parameter.

To determine the friction angle, we exploited the experience of the soils scientists and their success with the direct shear test. The design and fabrication of the mechanism employed in the direct shear test was discussed and the procedures for performing the experiment were explained.

The design of the experimental apparatus proved to be important. The soils science mechanism could not be used, because it was too bulky. Another smaller apparatus had to be constructed

which would conform to the special radioactive nature of the sample to be studied.

Initial tests were performed using a non-radioactive substance, alumina microspheres, to determine the overall feasibility of the operation. These tests produced data which compared favorably to independent results for the same material using another independent test. The friction angle measured by a triaxial test gave a value for the friction angle of 18.50^{o}. Our apparatus showed a value of 18.11^{o} using the same extrapolation method employed with the triaxial data, and 15.38^{o} using another, intuitively appealing, method.

Once it was determined that the testing of UO_2 should be done, more experiments were performed using three sizes of UO_2 microspheres. Tests were conducted for fine, medium, coarse, and ternary (three-size) samples. The results were also compared with an experiment which determined the angle of repose for the material. The angle of repose measurement compared favorably for a single fraction sample, but unfavorably for a ternary sample. This disparity was possibly due to the inherent problems associated with mixing the three-size mixture consistently for each sample.

Other information was collected concerning the stress-strain behavior of the material. Of particular interest was the observation of what appeared to be strain hardening of the material during unloading tests that were performed for the medium and coarse fraction.

7.2 Pros and Cons of Direct Shear Testing

There are some drawbacks to this type of shear test:

a. The area of the sample changes as the test progresses.

b. The actual failure surface is not a plane, as is assumed or as was intended from the way the shear box was constructed, nor is the shearing stress uniformly distributed over the "failure" surface, as is also assumed.

c. The test uses a small sample, with the result that preparation errors become relatively important.

However, there are some advantages in utilizing this type of test:

a. The triaxial test is relatively, much more difficult to perform and interpret.

b. The size of the sample makes it less time consuming to perform.

c. With the use of square sample boxes, the reduction

in area during the test can be easily accounted for.

We did not use a square sample box in our experiment to compensate for the change in the area of the sample. However, this was negligible compared to measurement errors associated with the scale reading. This and other improvements are included in the following section concerning future work.

7.3 Suggestions for Future Work

a. Improvement of the measurement accuracy of the scale and the incorporation of vertical displacement measurement capability into the experiment to allow study of dilatancy. (Also the incorporation of a square chamber dimension instead of the circular one used in the current experiment would reduce errors by allowing easy calculation of the change in area as the sample is displaced.)

b. Adaptation of the device to allow measurements to be recorded with a chart recorder connected to strain gauge devices. (A continuous record of the behavior of the material would be accomplished in this manner.)

c. Accumulation of data at lower normal stresses as well as at much higher normal stresses. (This would provide a more accurate appraisal of the behavior of the material over a broader range of loadings.)

d. Development of consistent mixing techniques for samples of ternary UO_2. (Perhaps neutron or X-radiography could be employed to observe the packing of samples subjected to different mixing schemes. This would allow a more complete study to be done of the stress-strain behavior for a desired mixture of particle sizes.)

e. Additional unloading tests to ascertain the degree of strain hardening associated with stressed UO_2 sphere-pac material.

f. Remote operation of the test device in an elevated temperature environment to determine the effect of temperature on shear characteristics.

g. Use of the direct shear device with other materials, such as the Vipac material, closely akin to sphere-pac but irregular in shape.

h. Arrange the experiment to obtain better statistics through random sampling and more observations.

All of the above suggestions represent additional work that would prove helpful in obtaining needed information about the mechanical behavior of nuclear reactor fuels. This would further the effort presently underway to obtain safe, economic, and clean power utilizing the nuclear option.

REFERENCES

1. D. R. Olander, Fundamental Aspects of Nuclear Reactor Fuel Elements, Technical Information Center, Office of Public Affairs, ERDA, 1976.

2. Exxon Nuclear Company, Pacific Northwest Laboratory, and Consumers Power Company, "Fuel Performance Improvement Program, Quarterly/Annual Progress Report," (COO-4066-13, UC-78), October, 1978 to September, 1979.

3. C. M. Cox, D. R. Cuneo, and E. J. Manthos, "Performance of Sphere-Pac and Pelletized $(U,Pu)O_2$ During Severe Overpower Transients," ANS Topical Meeting on Fast Reactor Fuel Element Technology, New Orleans, April 1971.

4. D. A. Collins and R. Hargreaves, "A Model for Fission Gas Behavior in UO_2 Fuel for the Advanced Gas Reactor and Steam Generating Heavy Water Reactor," Proceedings of International Conference on Physical Metallurgy of Reactor Fuel Elements, Berkeley, U.K., September, 1973.

5. M. Ades and K. L. Peddicord, "Modeling of the Thermal and Mechanical Behavior of LMFBR Fuel Elements, Part I - Oxide Fuels," OSU-EIR-31, March 1978.

6. H. Matzke and C. Ronchi, "Experimental Determination and Interpretation of Microscopic Swelling and Gas Release in Fast Reactor Fuels," Proceeding of the International Conference on Physical Metallurgy of Reactor Fuel Elements, Berkeley, U.K., September, 1973.

7. M. A. Azarfar, A Methodology For Safeguards Evaluation And Its Application To Mixed Oxide Fuel Fabrication, Ph.D. Dissertation, Oregon State University, 1982.

8. T. L. George, A Model for the Mechanical Behavior of Mixed Carbide Sphere Pac Fuel Pins, Ph.D. Dissertation, Oregon State University, December, 1982.

9. R. H. G. Parry, ed., Stress-Strain Behavior of Soils, Proceedings of the Roscoe Memorial Symposium, Cambridge University, March 29-31, 1971.

10. M. E. Harr, Mechanics of Particulate Media, A Probabilistic Approach, McGraw-Hill International Book Company, New York, 1977.

11. K. H. Roscoe, A. N. Schofield, and C. P. Wroth, "On the Yielding of Soils," Geotechnique, Vol. 8, No. 1: 22-53, March, 1958

12. J. C. Williams, ed., The Packing of Solid Particles, Chapman and Hall Ltd., London, 1968.

13. K. H. Roscoe, A. N. Schofield, and A. Thurairajah, "Yielding of Soils in States Wetter than Critical," Geotechnique, vol. 13, no. 3, September, 1963.

14. American National Standards, "Standard Method for Direct Shear Test of Soils Under Consolidated Drained Conditions," ANSI/ASTM D 3080 - 72 (Reapproved 1979), pp. 468- 471., 1979.

15. K. L. Peddicord and B. Nassersharif, "Fuel Clad Mechanical Interaction of Sphere-Pac Fuel," to be published.

16. G. W. Snedicor and W. G. Cochran, Statistical Methods, The Iowa State University Press, Ames, Iowa, 1980.

17. B. Nassersharif, "HI-PLOT Plotting and Regression Routine," Describing Function Theory as Applied to Thermal and Neutronic Problems, Ph.D. Dissertation, Oregon State University, to be completed December, 1982.

APPENDICES

APPENDIX A

Statistics Review and Error Analysis Techniques

A.1 Statistics

A.1.1 Introduction

Some basic statistical concepts will be presented which will permit an understanding of the significance of the experimental observations. Only the rudimentary parts of statistics will be covered to allow the reader to follow what has been accomplished in the statistical analysis.

The methods of statistics are useful to the experimenter in that they provide techniques whereby data obtained by repetitive observation can be interpreted and analyzed (A-1). In performing the direct shear test repetitively, many measurements are taken for a sample of particles whose shear characteristics are to be determined. The sample of particles is only a small part of all of the available material of like composition. The total amount of material of the same composition is termed the "population", and the "sample" is that portion of the population for which measurements are made.

The sample is used in order to obtain "estimates" of the characteristics of the population. In order that the sample reliably represent the true nature of the population, it should be a "random sample". In other words, the sample should be chosen in such a manner that it has the same probability of being chosen as any other sample. We use the word "statistics" to describe the

numerical quantities which characterize the population and are obtained from the sample observations.

A.1.2 Descriptive Statistics

There are basically two methods of presenting results of experimental observations in the form of statistics (A-2). These are "descriptive statistics" and "inferential statistics." Descriptive statistics are presented in the form of graphs, tables, and bar diagrams, while inferential statistics provide actual inferences about the population of interest based on the information obtained from the sample.

In descriptive statistics, a measurement may have the following form

$$X_1, X_2, X_3, \ldots, X_n$$

where X_1 is the first sample value, X_2 is the second sample value, and X_n is the n^{th} sample value obtained from an experimental observation.

An especially useful statistic obtained from a set of sample values is the arithmetic average or "mean" of the sample observations, defined by

$$\bar{X} = \frac{\sum_{1}^{n} X_i}{n} \qquad (A.1.1)$$

This statistic represents a measure of location of the population mean. Other measures of location are the median and the mode. The median is the value for which half of the observations are below and half are above. The mode represents the most frequent observation. If the mean is approximately equal to the median, we say that the sample observations show a "symmetric" distribution with respect to the mean. On the other hand, if the median is very different from the mean, we say that the sample observations are not symmetric, but are "skewed".

Another useful statistic is the sample "variance" defined as

$$s^2 = \frac{\sum_{1}^{n} (X_i - \bar{X})^2}{n - 1} \qquad (A.1.2)$$

where s^2 is the sample variance, X_i is the sample observation, $\bar{X}$ is the sample mean, and n is the sample size. While this relation provides a definition of the sample variance, a more useful "calculating formula" is derived by expanding the squared term in Equation A.1.2 to obtain the following

$$s^2 = \frac{\sum_{1}^{n} x_i^2 - (\sum_{1}^{n} x_i)^2/n}{n - 1} \qquad (A.1.3)$$

The variance is a "measure of variability" of the measurements within the population. Another measure of variability is the "range". The range is the largest value observed minus the smallest value observed. In an attempt to put variability back into the original units of the sample observations, the "standard deviation" was devised. This is defined as simply the square root of the variance or

$$s = \sqrt{s^2} \qquad (A.1.4)$$

A.1.3 Inferential Statistics

Suppose, for a moment, that we assume a finite population, say 20 tons of UO_2 sphere-pac fuel, exists. We would like to measure the ultimate shear strength of this material at a specific normal (compressive) stress. If we somehow could measure the ultimate shear stress of <u>each</u> sample for <u>all</u> of the material we could obtain the "true" population mean by

$$\mu = \frac{\sum_{1}^{N} \tau_i}{N} \qquad (A.1.5)$$

where μ is the "true" population mean, τ_i, the ultimate shear stress for the sample "i" and N, the total number of samples in the population.

However, this would be inconvenient to say the least, and therefore, we rely on only a few sample observations to give us an idea of what the true population average is. The problem, here, is the validity of our estimate. How good is our sample estimate of the true population mean? This is one of the questions that inferential statistics attempts to answer.

If we take a few sample observations and calculate the sample mean, we get a number. If we were to do this again with more of the material, we would obtain another sample mean. We would not expect these two numbers to be the same. In fact, these statistics (the mean ultimate shear values) are random variables. As such, they have an associated probability distribution which describes their behavior. If the sample size is large or the population has a "normal distribution", we say that the distribution of the mean ultimate shear values is also normal. We have assumed a normal population for our experiment. A normal distribution has the following functional form:

$$f(X) = \frac{1}{\sqrt{2\pi}\sigma_X} \exp\left\{-1/2\left[(\bar{X} - \mu/\sigma_{\bar{X}})^2\right]\right\} \qquad (A.1.6)$$

where $\bar{X}$ is the sample mean, μ is the population mean, and $\sigma_{\bar{X}}$ is the population "standard error of the mean."

If we know the population mean and "standard error", we can calculate the probability that we will obtain an average ultimate shear value greater than a specified value for a given sample size, n. First we calculate the "standard error of the mean" as

$$\sigma_{\bar{X}} = \frac{\sigma_{sd}}{\sqrt{n}} \qquad (A.1.7)$$

where σ_{sd} is the known population standard deviation.

This value tells how much the means differ from sample to sample. It is evident from this expression that as the size of the sample increases, the amount of deviation from the population mean should be less. This is in line with what we would expect.

If Equation A.1.6 is transformed into the "standard normal" distribution with $\mu = 0$ and $\sigma_{\bar{X}} = 1$, we can determine the probability of getting a larger value of average ultimate shear than a given specific value. This is simply the area under the standard normal distribution curve from the "normalized value" for our given specific value out to infinity. This is because the total area under the curve must necessarily be 1.0. The "normalized value" is

obtained by

$$z = \frac{\bar{X} - \mu}{\sigma_{\bar{X}}} \qquad (A.1.8)$$

where $\bar{X}$ is the sample mean, μ is the true population average, and $\sigma_{\bar{X}}$ is the standard error of the mean given is Equation A.1.7. This "z-value" is termed the "standard normal variate" or "standard normal deviate" and is used as a test statistic for populations where the standard deviation is known or can be readily determined.

Tables of standard normal deviates can be found in most statistics texts. They represent the number of standard deviations from the mean for a standard normal curve. For example, the probability that our average ultimate shear stress would be greater than 1 standard deviation ($z = 1.0$) from the known population mean is found in the tables to be about 0.32.

We have shown that a probability can be assigned to the occurrence of a given range of average ultimate shear values, once we know the population average. We can similarly specify an interval in which we would expect the true population average to be, once we know an average ultimate shear from sampling. This is done using the concept of "confidence intervals."

The average value obtained from a set of observations is a "point" estimate of the true average value of a population. A confidence interval represents an "interval" estimate. Thus, we can

say that 95 times out of 100 in repeated sampling, we would expect the following interval to contain the true population mean

$$(\bar{X} - 1.96\sigma_{\bar{X}} < \bar{X} < \bar{X} + 1.96\sigma_{\bar{X}}) \qquad (A.1.9)$$

where the interval (-1.96, 1.96) represents the portion of the standard normal curve which contains 95% of the total area. Another way to say this, is that 5% of the time in repeated sampling, the interval found using Equation A.1.9 will not include the true average value of the population.

The problem in our experiment was that we did not know the value of the population standard deviation, and hence could not use the z-values to determine our 95% confidence intervals. Consequently it was necessary to employ the "t distribution" as the probability distribution for our sample means.

The t distribution uses an estimate, $s_{\bar{X}}$, for the population standard error of the mean, where $s_{\bar{X}}$ is found by substituting the sample standard deviation, s, for σ_{sd} in Equation A.1.7. The t statistic is calculated the same way as the z-value except that the $s_{\bar{X}}$, replaces the $\sigma_{\bar{X}}$. That is,

$$t = \frac{\bar{X} - \mu}{s_{\bar{X}}} \qquad (A.1.10)$$

The shape of the t distribution is nearly the same as that of the normal distribution. For large values of sample size it looks very much like a normal distribution. For smaller sample sizes (usually less than 30) the curve is "flatter" and more "spread out" than that of the standard normal distribution. Hence, more deviation from the mean is required to produce the same confidence interval.

To use the t tables, which list the probabilities of obtaining a larger value of deviation from the mean than the t value, the number of "degrees of freedom" must be known. This is the size of the sample minus 1. For example, if a 95% confidence interval is desired, the true mean should be contained in 95% of the following intervals in repeated sampling with a sample size of 3:

$$(\bar{X} - 4.303\ s_{\bar{X}} < \bar{X} < \bar{X} + 4.303\ s_{\bar{X}}) \qquad (A.1.11)$$

So, if we run a series of tests, calculate the average value of the desired measurement, find the standard deviation, and calculate the estimate of the standard error of the mean, we can determine the 95% confidence interval associated with this average value. This is what was done with the shear stress values determined for the alumina and the UO_2 materials used in this experiment. To determine

the "significance" of a measurement it is necessary to use what is known as "hypothesis testing."

A.1.4 Hypothesis Testing

If you are interested in testing some hypothesis about the true mean of the population, your hypothesis is that this true mean, μ, has some specific value. On the basis of what you observe in your experimental sampling, you decide whether or not this is likely.

Thus, you construct a hypothesis test in the following manner (A-2):

a. State the null and alternate hypothesis
b. State the desired confidence level
c. State the test statistic and its distribution
d. Set up a rejection region
e. Calculate the value of the test statistic based on sample information
f. Draw conclusions

For example, suppose we want to determine if there exists a significant difference between the ultimate shear stress for fine fraction UO_2 and that for the coarse fraction (see Table 5.3.3). We would perform the following hypothesis test using the procedure outlined above:

a. H_o: $\mu_1 - \mu_2 = 0$
   H_a: $\mu_1 - \mu_2 \neq 0$

The first, or "null" hypothesis states that there appears to be no difference between the two population means. The alternate hypothesis states that there is a significant difference between the two population means.

b. 95% confidence level

c. The test statistic used will be for the hypothesis test with independent samples given by

$$t = \frac{(\bar{X}_1 - \bar{X}_2) - (\mu_1 - \mu_2)}{S_{\bar{X}_1 - \bar{X}_2}} \qquad (A.1.12)$$

where,

$$S^2_{\bar{X}_1 - \bar{X}_2} = \frac{\text{pooled } S^2 (n_1 + n_2)}{n_1 n_2} \qquad (A.1.13)$$

and

$$\text{pooled } S^2 = \frac{(n_1 - 1)S_1^2 + (n_2 - 1)S_2^2}{n_1 + n_2 - 2} \qquad (A.1.14)$$

Here, $\bar{X}_1$ and $\bar{X}_2$ correspond to the fine and coarse samples respectively. Similar correspondence exists for the sample standard deviation, S and the sample size, n.

d. For the rejection region corresponding to a confidence level of 95%, we check the t tables with $n_1 + n_2 - 2$ degrees of freedom (df = 4). We find that our

rejection region is composed of the absolute values of t greater than 2.776.

e. To calculate the value of the test statistic using Equations A.1.12 through A.1.14 we need some values from Table 5.3.3. These are given below

Sample 1	Sample 2	
$n_1 = 3$	$n_2 = 3$	test runs
$\bar{X}_1 = 25828$	$\bar{X}_2 = 19571$	Pa
$S_1 = 637.4$	$S_2 = 1686$	Pa

From these values we calculate a value of t equal to 6.01.

f. Conclusion: Reject the null hypothesis. In other words, the average ultimate shear stress determined for the fine fraction is significantly higher than the ultimate shear stress determined for the coarse fraction at the 95% confidence level. This is because our calculated value of the test statistic, 6.01, is greater than 2.776, which puts it in the rejection region for our test.

The hypothesis test is an effective tool for evaluating the significance of data from experimental observation.

A.2 Error Analysis

There were several sources of measurement error in this experiment. These are listed below:

Measured value	Accuracy
Normal force	$\pm$ 4.9 x 10^{-4} Newtons
Tangential force	$\pm$ 2.22 Newtons
Chamber diameter	$\pm$ .0025 cm

To evaluate the error associated with our calculation of ϕ_{CV} using the polar regression method, we first give the determining equation as

$$\phi_{CV} = \arctan(a) \qquad (A.2.1)$$

where a is the slope of the polar regression curve obtained by "least squares" methods. The value of a was calculated with the following equation:

$$a = \frac{\sum_{i}^{n} \sigma_i \bar{\tau}_i}{\sum_{i}^{n} \sigma_i^2} \qquad (A.2.2)$$

where $\bar{\tau}_i$ is the average ultimate shear stress given by the following expression

$$\bar{\tau}_i = \frac{1}{K_i} \sum_{1}^{K_i} \tau_{ki} \qquad (A.2.3)$$

K_i is the number of experiments in the sample and τ_{ki} is the ultimate shear stress for the k^{th} experiment in the i^{th} lot. $\bar{\tau}_i$ is the mean value of the τ_k's for a given constant normal stress σ_i.

The individual ultimate shear stresses in each lot are given by

$$\tau_{ki} = \frac{S_{ki}}{A} \qquad (A.2.4)$$

So,

$$\bar{\tau}_i = \frac{1}{AK_i} \sum_{1}^{K_i} S_{ki} \qquad (A.2.5)$$

where A is the nominal area of the shearing plane and the S_{ki}'s are the individual scale readings indicating the tangential force.

The normal stresses for each lot are calculated from the measured normal force, N_i by,

$$\sigma_i = \frac{N_i}{A} \qquad (A.2.6)$$

Inserting Equations A.2.5 and A.2.6 into Equation A.2.2 gives

$$a = \frac{\sum_{1}^{n} \frac{N_i}{A} \frac{1}{AK_i} \sum_{1}^{K_i} S_{ki}}{\sum_{1}^{n} \frac{N_i^2}{A^2}} \qquad (A.2.7)$$

or, upon canceling terms,

$$a = \frac{\sum_{1}^{n} \frac{N_i}{K_i} \sum_{1}^{K_i} S_{ki}}{\sum_{1}^{n} N_i^2} \qquad (A.2.8)$$

Substituting into A.2.1 gives

$$\phi = \arctan \frac{\sum_{1}^{n} \frac{N_i}{K_i} \sum_{1}^{K_i} S_{ki}}{\sum_{1}^{n} N_i^2} \qquad (A.2.9)$$

We now have the friction angle, ϕ (CV subscript dropped) in terms of the measured values only, and the propagation of errors analysis can proceed. The error propagated in the calculation of ϕ is related to the variance of the measured values and is determined by (A-3):

$$\text{var}(\phi) = \sum_{1}^{n} \left[\text{var}(N_i) \left(\frac{\partial \phi}{\partial N_i} \right)^2 \right] + \sum_{1}^{n} \left[\text{var}(\bar{S}_i) \left(\frac{\partial \phi}{\partial \bar{S}_i} \right)^2 \right] \qquad \text{(A.2.10)}$$

where we have inserted the variance of the average ultimate shear stresses instead of the variance of the individual shear stresses since

$$\text{var}(\bar{S}_i) = \frac{1}{K_i} \text{var}(S_{ki}) \qquad \text{(A.2.11)}$$

and

$$\bar{S}_i = \frac{1}{K_i} \sum_{1}^{K_i} S_{ki}$$

Equation A.2.10 can be simplified somewhat by making some approximations. Since

$$\text{var}(N_i) \approx \left(\frac{N_i}{3} \right)^2 = 2.67 \times 10^{-8} \qquad \text{(A.2.12)}$$

which is negligible compared to the variance of the average ultimate shear stresses and

$$\left(\frac{\partial \phi}{\partial N_i} \right)^2 << \left(\frac{\partial \phi}{\partial \bar{S}_i} \right)^2 \qquad \text{(A.2.13)}$$

we can consider the first term on the right hand side of Equation A.2.10 negligible. Hence, the expression for the variance of the friction angle becomes

$$\mathrm{var}(\phi) = \sum_{1}^{n} \left[\mathrm{var}(\bar{S}_i) \left(\frac{\partial \phi}{\partial \bar{S}_i} \right)^2 \right] \qquad \text{(A.2.14)}$$

Thus, the variance of ϕ is reduced to a dependence on the average scale reading and becomes much simpler to evaluate.

The partial derivative in Equation A.2.14 can be evaluated using the following expression for the derivative of the arctangent:

$$\frac{\partial \phi}{\partial \bar{S}_i} = \frac{1}{1+u^2} \frac{du}{d\bar{S}_i} \qquad \text{(A.2.15)}$$

where,

$$u = \frac{\sum_{1}^{n} N_i \bar{S}_i}{\sum_{1}^{n} N_i^2} \qquad \text{(A.2.16)}$$

So,

$$\frac{du}{d\bar{S}_i} \cong \frac{N_i}{\sum_{1}^{n} N_i^2} \qquad \text{(A.2.17)}$$

When Equations A.2.16 and A.2.17 are substituted into Eq. A.2.15, and the result is substituted into Eq. A.2.14, we get

$$\text{var}(\phi) = \sum_{1} \frac{n\ \text{var}(\bar{S}_i)\left[\ N_i\ \left(\sum_{1}^{n} N_i^2\right)\right]^2}{\left[\left(\sum_{1}^{n} N_i^2\right)^2 + \left(\sum_{1}^{n} N_i \bar{S}_i\right)^2\right]^2} \qquad \text{(A.2.18)}$$

We now have an expression for the variance of the friction angle in terms of the variance of the average scale readings at ultimate strength and the associated normal force. Since, several tests were done at each level of normal force, the total propagated error can be evaluated by using the actual, observed variance of the scale readings in the calculation of the $\text{var}(\bar{S}_i)$.

When the actual, observed variance was employed, the variance in the friction angle for alumina was determined to be 4.65×10^{-5} (units of radians squared). Thus, two standard deviations are $.781^{o}$. The reported value of ϕ is therefore

$$\phi_{CV} = 18.11^{o} \pm .781^{o}$$

The measurement error contribution can be approximated by assuming that the measurement accuracy of the scale represents an interval of plus or minus three standard deviations from the mean value. If this is the case, we have

$$\text{var}(S_{ki}) = \left(\frac{\Delta S}{3}\right)^2 = \text{constant} \qquad \text{(A.2.19)}$$

where ΔS is the scale accuracy ($\pm$ 2.22 Newtons). Using this as the variance, Equation A.2.18 can be evaluated (using Table 5.2.4) to give the variance due to the measurement error contribution as 1.32×10^{-5} (radians squared). This gives a "two standard deviation value" of $.416^{o}$. The reported value of ϕ considering only scale measurement errors becomes

$$\phi_{CV} = 18.11^{o} \pm .416^{o}$$

This gives a relative total error of 4.31%. When only the measurement contribution is considered, the relative error is 2.30%.

If we assume the same relative errors for the linear extrapolation, we get the following reported values for two standard deviations:

$\phi_{CV} = 15.38^{o} \pm .663^{o}$ (total errors propagated)

$\phi_{CV} = 15.38^{o} \pm .354^{o}$ (only measurement errors propagated)

A similar analysis of the UO_2 data (using Table 5.3.3) gives the results shown in Tables A.2.1 and A.2.2.

Table A.2.1

Propagated Errors in Uranium Dioxide Friction Angle Calculation (Polar)

Material	Friction Angle	Total Error (2 Standard Deviations)	Measurement Contribution (2 Std. Dev's.)
Fine	28.50^{o}	$\pm .685^{o}$	$\pm .679^{o}$
Medium	20.97^{o}	$\pm 1.14^{o}$	$\pm .694^{o}$
Coarse	22.69^{o}	$\pm 1.64^{o}$	$\pm .679^{o}$
Uniform Ternary	22.40^{o}	$\pm 1.38^{o}$	$\pm .789^{o}$
Premixed Ternary	27.29^{o}	$\pm .676^{o}$	$\pm .670^{o}$

Table A.2.2

Propagated Errors in Uranium Dioxide Friction Angle Calculation (Linear)

Material	Friction Angle	Total Error (2 Standard Deviations)	Measurement Contribution (2 Std. Dev's.)
Fine	------	-------	-------
Medium	17.80^{o}	$\pm .964^{o}$	$\pm .589^{o}$
Coarse	20.78^{o}	$\pm 1.50^{o}$	$\pm .621^{o}$
Uniform Ternary	------	-------	-------
Premixed Ternary	26.28^{o}	$\pm .651^{o}$	$\pm .645^{o}$

APPENDIX A REFERENCES

A-1. J. L. Hodges, Jr. and E. L. Lehmann, Basic Concepts of Probability and Statistics, Holden-Day Incorporated, San Francisco, 1964.

A-2. G. W. Snedecor and W. G. Cochran, Statistical Methods, The Iowa State University Press, Ames, Iowa, 1980.

A-3. A. M. Mood, F. A. Graybill, and D. C. Boes, Introduction to the Theory of Statistics, McGraw-Hill Inc., 1963.

APPENDIX B

Direct Shear Test Procedure for Alumina Microspheres

Alumina Direct Shear Test Procedure:

1. Set all set and gap screws to flush position.

2. Align chambers and insert alignment pins.

3. Fill shear box with approximately 60 ml of sample material. Cover sample with paper disk.

4. Place on vibrator.

5. Secure apparatus and vibrate for 60 seconds.

6. Perform shear test:

   a. Load piston with known weight.
   b. Set gap (.05 cm). Check with gauge.
   c. Attach dial indicator.
   d. Tighten set screws against piston.
   e. Back off gap set bolts several turns.
   f. Recheck gap.
   g. Note dial indicator reading.
   h. Connect scale between ratchet and shear box.
   i. Remove alignment pins.
   j. Note scale reading.

k. Apply force with ratchet.

l. Record scale and dial readings.

m. Repeat k. until failure.

7. Clean up and repeat a number of times for statistics.

These procedures were adopted from initial trial run 18 August, 1982 in room C-130, Radiation Center, Oregon State University, Corvallis, Oregon.

APPENDIX C

Direct Shear Test Procedure for Uranium Dioxide Microspheres

Uranium Dioxide Direct Shear Test Procedure:

1. Dress with lab coat, two pair of gloves, finger rings, and film badge, and make sure sash is kept down on hood at all times.

2. Check equipment.

3. Display procedures on hood: separate sheets.

4. Set all set and gap screws to flush position.

5. Align chambers.

6. Place paper "doughnut" over top of cylinder and tape edges.

7. Weigh sample in container.

8. With the hood sash down fill the shear box with approximately 50 ml of sample using taped 1000ml Erlenmeyer flask and funnel arrangement or 125 ml flask storage container.

9. Wait approximately 15 seconds before removing flask from "doughnut" to allow residual settling.

10. Weigh empty sample container.

11. After about 15 seconds remove "doughnut".

12. Insert paper disk and aluminum piston.

13. Place entire assembly on vibrator.

14. Secure apparatus and vibrate for 1 minute at 60 hertz and amplitude setting of 50.

15. Perform shear test:

a. Load cylinder with known weight.
b. Set gap (larger than largest particle size).
c. Connect scale and dial indicator.
d. Visually note dial indicator reading.
e. Tighten set screws against piston.
f. Back off gap set bolts several turns.
g. Recheck gap.
h. Remove alignment pins.
i. Survey gloves.

j. Note scale and dial indicator reading.

k. Apply force with ratchet.

l. Survey gloves.

m. Record scale and dial readings.

n. Repeat k. until failure.

16. Clean up and containment:

a. Remove dial indicator, weight, and scale.

b. Thread bolts back in to just touch the bottom box.

c. Put clips on gap set bolts and knocker on top of piston.

d. Feed strings through bucket.

e. Place bucket over assembly.

f. Tape securely.

g. Attach clamps to pan/bucket interface at opposite positions and tape upper clamp handles to bucket.

h. Feed strings through funnel.

i. Place funnel over bucket.

j. Feed strings through rubber funnel cork.

k. Insert rubber cork into funnel.

l. Tape funnel/bucket interface securely.

m. Pull strings to lift upper shearing assembly.

n. While holding the assembly 2 or 3 inches above the material, move knocker up and down with string, tapping the assembly approximately 10 times.

o. Let particles settle about 15 seconds.

p. Remove tape from the funnel/bucket connection.

q. Place box in position for receiving top assembly.

r. Remove funnel plus assembly.

s. Place over metal tray and lower the assembly into the tray.

t. Remove strings from the funnel and reposition funnel over the bucket.

u. Relocate metal tray so that it is out of the way.

v. Tape the funnel to the bucket again.

w. Place the 1000 ml Erlenmeyer flask over the funnel and tape securely.

x. Invert entire assembly onto stand.

y. Vibrate 2 minutes at 60 hz. and 80 amplitude.

z. While vibrating, tap the entire assembly vigorously, starting at the top and working down. Pay special attention to jarring the "pouring side" of the assembly.

aa. Remove flask and tape the funnel opening.

ab. Cover the flask opening with the glass funnel/tube assembly and tape securely. Also, place a piece of tape over the end of the glass funnel/tube assembly and place back in the storage cave.

ac. Return the entire direct shear assembly to the original upright position. Tap the assembly to cause settling of any residual spheres to the bottom of the assembly or to taped surfaces.

ad. Prepare suitable quantities of Kimwipes with alcohol for cleaning bucket and funnel.

ae. Remove the tape from both the funnel and the

bucket (keep hood down).

af. Place funnel and bucket on stands for later use.

ag. Remove the clips from the upper box assembly.

ah. Clean the assembly with Kimwipes and alcohol.

17. Return to step 1 for repeat of procedure.

These procedures were adopted from a trial run on 8 October 1982 in room C-130, Radiation Center, Oregon State University, Corvallis, Oregon.